universität wien

DIPLOMARBEIT / DIPLOMA THESIS

Titel der Diplomarbeit / Title of the Diploma Thesis

„Delineation of internal landslide structures using Electrical Resistivity Tomography and geotechnical investigations – case study Hofermühle, Lower Austria“

verfasst von / submitted by

Christina Karl

angestrebter akademischer Grad / in partial fulfilment of the requirements for the degree of

Magistra der Naturwissenschaften (Mag. rer. nat.)

Wien, 2018 / Vienna, 2018

Studienkennzahl lt. Studienblatt / degree programme code as it appears on the student record sheet:	A 190 456 412
Studienrichtung lt. Studienblatt / degree programme as it appears on the student record sheet:	Lehramtsstudium UF Geographie und Wirtschaftskunde UF Physik
Betreut von / Supervisor:	Univ.-Prof. Dipl.-Geogr. Dr. Thomas Glade

Erklärung

Hiermit versichere ich,

- dass ich die vorliegende Diplomarbeit selbstständig verfasst, andere als die angegebenen Quellen und Hilfsmittel nicht benutzt und mich auch sonst keiner unerlaubter Hilfe bedient habe,
- dass ich dieses Diplomarbeitsthema bisher weder im In- noch im Ausland in irgendeiner Form als Prüfungsarbeit vorgelegt habe
- und dass diese Arbeit mit der vom Begutachter beurteilten Arbeit vollständig übereinstimmt.

Wien, am 18. Mai 2018 Christina Karl

Acknowledgements

I received support from so many people in writing this thesis and I would like to convey my gratefulness to all these people.

I would like to express my sincere gratitude to my supervisor Dr. Thomas Glade for providing his invaluable guidance throughout the course of this project while always allowing me to realize my own ideas.

I would like to specially thank Dr. Adrian Flores-Orozco for the time he took to answer so many of my questions. Thank you for guiding me through the complex world of Geophysics and for constantly motivating me to work harder.

Special thanks to Margherita Johanna Stumvoll for the many interesting and enriching conversations and for her great support with ArcMap.

Also, I would like to thank Dr. Robert Peticzka for his critical advice. Thank you, Christa Hermann for your endless support in the laboratory.

To all people who supported me in the field, thank you.

To all relatives and friends who shared their support in one way or the other throughout my studies, thank you.

Above all, thank you Josef for the countless times you could have done other things but stayed with me to write this thesis.

Table of Contents

List of Figures

List of Tables

Zusammenfassung

Große Teile Niederösterreichs sind häufig von gravitativen Massenbewegungen betroffen. Besonders die Flysch Zone, eine geologische Einheit, die sich durch die Voralpen Niederösterreichs streckt, ist anfällig für Rutschungen. Die mächtigen Verwitterungsdecken aus feinkörnigem Material sind besonders störanfällig für Regenfälle. Aufgrund Mächtigkeit der Verwitterungsdecken nehmen Rutschungen oftmals eine beträchtliche Größe an. Die Hofermühl Rutschung in Konradsheim bei Waidhofen an der Ybbs ist daher nur eine von vielen Rutschungen in dem Gebiet. Es handelt sich um eine komplexe Rotationsrutschung mit mehreren Rutschflächen, die ungefähr eine Fläche von 50.000 m^2 einnimmt. Ausgelöst erstmal vor 35 Jahren, kam es im Jahr 2013 zu einer Reaktivierung. Seither zeichnet sich die Rutschung durch geringe Bewegungsraten (entlang der Abrisskante sowie am darüberliegenden Hang) aus.

Obwohl viele Ursachen für Hangrutschungen ihren Ursprung im Untergrund nehmen, ist über den Untergrund der Hofermühl Rutschung wenig bekannt. Die folgende Arbeit präsentiert daher die Ergebnisse der ersten Untergrunduntersuchungen an der Hofermühl Rutschung. Im Rahmen der Arbeit wurden sowohl direkte, als auch indirekte Methoden zur Erkundung des Untergrundes angewandt. Entlang des Hangs wurden sechs parallele ERT Profile aufgenommen, um die räumliche Verteilung elektrischer Eigenschaften des Untergrunds zu erkunden. Drei DPH Tests zur Analyse des mechanischen Eindringwiderstands des Bodens wurden durchgeführt. An einem Standort wurde eine Bohrung durchgeführt, welche Aufschluss über die Art des Materials, die Korngrößenverteilung, Wassergehalt und die elektrolytische Leitfähigkeit gibt.

Anhand der erhobenen Daten wurden Untergrundstrukturen des Hangs abgeleitet. Der Fokus lag dabei auf der Beschreibung der Art des Materials und dessen Verteilung, Unterschieden in hydrologischen Bedingungen sowie der Identifizierung von Schichtgrenzen, insbesondere der Festgesteinsgrenze sowie potentieller Rutschflächen. Auf Basis der Ergebnisse wurden zudem zwei Modelle zur Interpretation des Untergrundes erstellt.

Aufgrund von Unsicherheiten bezüglich der Interpretation der indirekten Daten (ERT und DPH) im Zusammenhang mit einem Mangel an direkten Daten (PD) lässt sich der Untergrund der Hofermühl Rutschung momentan nur in groben Zügen beschreiben. Genaue und sichere Aussagen in Bezug auf Wassergehalt und Schichtgrenzen sowie der Verteilung von Materialien sind zu diesem Zeitpunkt nicht möglich. Die Ergebnisse lassen des Weiteren den Schluss zu, dass die Analyse von hydrologischen Bedingungen im Untergrund alleine aufgrund von ERT Daten in tönigen Böden, wie im Untersuchungsgebiet vorgefunden wurden, nicht möglich ist. Im Fall der Hofermühl Rutschung ist davon auszugehen, dass der hohe Tongehalt im Untergrund einen erheblichen Beitrag zur Gesamtleitfähigkeit im Untergrund beiträgt und dadurch Variationen im Wassergehalt nicht notwendigerweise anhand der ERT Bilder bestimmt werden können. Die ERT Bilder wurden deswegen vor allem in Hinblick auf den Tongehalt interpretiert.

Die Erkenntnisse über den Aufbau des Untergrundes der Hofermühl Rutschung legen den Schluss nahe, dass weitere Rutschungen am Hang ein erhebliches Ausmaß erreichen könnten, da große Mengen an feinkörnigem Material vorliegen. Um Vorhersagen über die Entwicklung der Hangstabilität sowie über das potentielle Ausmaß weiterer Rutschungen am Standort treffen zu können, sind daher noch weitere Untersuchungen notwendig.

Abstract

Large parts of Lower Austria are frequently affected by landslides. The Flysch zone, a geologic unit that stretches through the alpine foothills of Lower Austria, is particularly susceptible to landslides. The thick layers of weathered and fine-grained flysch that have developed are easily disturbed through rainfalls and extensive slides are common. Situated in Konradsheim in Waidhofen/Ybbs, the Hofermühle-landslide is therefore one of many slides in this area. It is a slow moving, shallow, complex rotational landslide with several different sliding planes and affects an area of around 50.000 m². Initiated around 35 years ago, it has been reactivated in 2013. Subtle signs of movement around the crown of the landslide as well as the adjacent slope, indicate that further landslide events are likely.

Little is known about the subsurface, even though common causes of landslides originate in ground. The following thesis presents the first subsurface exploration of the adjacent slope to the landslide. A combination of direct and indirect techniques was applied for the subsurface investigation. Six parallel ERT profiles were recorded along the slope to measure the electrical resistivity of the ground. Three DPH tests were conducted to investigate the grounds resistance to penetration and Percussion Drilling was deployed at one location on the slope, providing ground truth information on particle size distribution, fluid conductivity and water content.

Based on the measured variation in subsurface properties, subsurface structures were delineated. The focus was on the identification of materials involved and their distribution, the exploration of variation in hydrological conditions, and, the identification of boundaries, specifically the bedrock as well as pre-existing failure surfaces. Two possible subsurface-models were delineated, presenting the data obtained by different methods in an integrative form.

Limitations for the description of subsurface structures result from ambiguity in the interpretation of indirect data related to a lack of direct data for validation. Therefore, the subsurface of the Hofermühle-landslide can only be described in general terms. A detailed description of subsurface structures is not possible at this point. Furthermore, the evidence suggests that Electrical Resistivity Tomography is not suitable to identify variations

hydrological conditions, as the correlation between saturation and the electrical resistivity may be masked by surface conductivity of clay. The variation in the resistivity images may thus be more indicative of varying material properties, particularly the clay content.

The evidence suggests that landslide hazard on the slope is significant. Not only is further movement likely, but also the amount of material on the slope that may be activated in the future is considerable, posing a risk to the building at the foot of the slope. Ultimately, further analyses are required to link subsurface conditions to dynamic changes of slope stability and make reliable predictions about the potential magnitude of future landslide events at the site.

1 Introduction

Landslides shape the appearance of the earth's surface, particularly in mountainous and coastal areas. They are complex phenomena and their study draws on many different disciplines. Starting from intensive, site-specific analyses of individual landslides, including conventional geotechnical analysis site investigations and mapping, landslide research has progressed to regional-scale analyses, including landslide inventories or hazard and susceptibility assessments (Keefer & Larsen, 2007, p. 1136). The following thesis presents the case study of the Hofermühle-landslide in Lower Austria/Austria. It focuses on the subsurface exploration of a slope endangered to landslides. In the first chapter, background information is provided. An overview of the current state of research at the site is given and the research interest is introduced. The aim of the study and relating research questions are derived. Lastly, the thesis outline is presented.

1.1 Background and Problem Statement

Mountainous terrain, the geologic setting, long lasting and heavy rainfalls, rapid snowmelts as well as land use make large parts of Lower Austria highly susceptible to landslides (Schweigl & Hervás, 2009, p. 7). Specifically, the Flysch zone, which stretches through Gresten, Scheibbs and Waidhofen an der Ybbs is affected (Petschko, Glade, Bell, Schweigl, & Pomaroli, 2010, p. 278; Schwenk, Spendlingwimmer, & Salzer, 1992, p. 589). In this area, thick layers of weathered, unconsolidated rock and soil have developed and extensive slides are common (Lotter & Haberle, 2013, p. 14). Although human lives are rarely endangered by slides in Lower Austria, landslides frequently cause damage to towns and infrastructure (Schwenk et al., 1992, p. 598). These socio-economic costs of landslides are expected to rise in the next decades as the population increases and urban areas and infrastructure expand (Keefer & Larsen, 2007, p. 1136). Interestingly, parts of the costs are man-made since humans often play an important role in the causation of landslides in Lower Austria (Schwenk et al., 1992, p. 599). The already high costs of landslides and their potential to increase emphasise the need for better landslide risk mitigation measures and a better understanding of the causation and triggering of landsides in Lower Austria. While the “basic physical factors governing the initiation of landslides – the interactions among material strength, gravitational stress, external forces, and pore-fluid pressure has been well understood, it is still difficult to predict just where and when a landslide will occur” (Keefer & Larsen, 2007, p. 1136). Such knowledge however is crucial for landslide risk assessment. Therefore, the Province of Lower Austria has launched the project “NoeSLIDE - Monitoring unterschiedlicher Typen gravitativer Massenbewegungen in Niederösterreich”. The project aims at providing long-time measurement series to better correlate landslide events with triggering factors as well as the improvement of landslide investigation and monitoring methods. Currently, six landslides are investigated and/or monitored. One research location is the Hofermühle-landslide in Waidhofen/Ybbs.

1.2 Current State of Research at the Site

The Hofermühle-landslide is a slow moving, shallow, complex rotational landslide with several different sliding planes, affecting an area of around 50.000 m^2. According to residents, the initial movement took place approximately 35 years ago and was reactivated in 2013 after heavy rainfalls, that are considered the trigger of the movement. Investigations of the Hofermühle-landslide until this date focused on the description of movement events and their extent and the identification of landslide features and damaged structures. Landslide dynamics are investigated by periodic GNSS measurements of reference points, laser scanning and tachometric measurements. An automated weather station records temperature, precipitation, air pressure and radiation.

1.3 Research Interest

The extent of landslides nearby and the morphology of the slope suggest that further movement-processes are very likely, making it an ideal location for the analysis of the pre-event phase of the landslide disaster cycle (Perrone, Lapenna, & Piscitelli, 2014, p. 129). Furthermore, it is expected that further landslide processes might damage the building on the toe of the slope. Yet, information about the subsurface of the landslide and adjacent slope, i.e. on the geological and hydrological setting, as required for risk assessment (Perrone et al., 2014, p. 129), is scarce.

1.4 Aims

This thesis aims at characterizing the subsurface of the Hofermühle landslide, particularly to variations in the textural parameters by a combination of Electrical Resistivity Tomography (ERT), Percussion Drilling (PD) and Dynamic Probing Heavy (DPH). The goal is to delineate subsurface structures (materials involved, their extend and thickness, discontinuities (bedrock, sliding plane, water saturated areas in the ground) of the landslide from the variation in physical properties (i.e. resistivity, particle size, penetration resistance). Based on the information obtained, a model for the subsurface may be established.

1.5 Hypotheses and Research Questions

The thesis examines the following hypothesis:

From the variation of the parameters electrical resistivity, penetration resistance, particle size, water content, subsurface structures, materials involved, their extend and thickness, boundaries and discontinuities such as potential failure surfaces, water saturated areas and the bedrock can be delineated.

The hypothesis is assessed through the following research questions:

What information about subsurface structures can be obtained through each Percussion Drilling, Dynamic Probing Heavy and Electrical Resistivity Tomography?

The opportunities that individual methods offer for the exploration of landslides vary greatly. Different methods provide information on specific parameters and in various formats and scales. Each method has specific benefits and limitations for the exploration of landslides. This way, the various methods allow the exploration of different aspects of a landslide. Hence, one question of this study addresses the potential of each individual method for the subsurface exploration of the Hofermühle-landslide.

What information about subsurface structures can be obtained through the combination of Percussion Drilling, Dynamic Probing Heavy and Electrical Resistivity Tomography?

Sub-questions:

To what extent can direct data from PD be used to validate indirect data as obtained through DPH and ERT?

To what extent can DPH and ERT be used to extrapolate data obtained through PD?

It is generally assumed that the combined application of different methods leads to a more comprehensive understanding of a slope, as the weaknesses of individual methods may be overcome (Perrone et al., 2014, p. 129). A more complete and realistic interpretation of subsurface structures may be obtained. Specifically, the interpretation of results obtained by indirect methods may become more accurate if validated through direct data. Conversely, the informational value of direct methods, like drilling, is often limited to the vicinity of the location. Methods providing indirect, yet 2-dimensional data, like ERT, may be used to extrapolate data obtained by direct methods. Therefore, one research question concerns the correlation between the individual methods and assesses the potential of a combined approach.

What subsurface model can be established from data obtained through PD, DPH and ERT?

Lastly, the thesis will attempt an interpretation of the measurement results in an integrated form and attempt to delineate models for the subsurface of the landslide.

1.6 Thesis Outline

Chapter 2 introduces the reader to the fundamentals of landslide description and analysis by terms, definitions and classifications and presents the basic physical principles that govern the initiation of a landslide and landslide dynamics. Furthermore, common causes of landslides are considered. Chapter 3 gives an overview of methods that are frequently applied for the investigation of landslides. The methods applied in the study are explained in detail. Chapter 4 introduces the historic and environmental setting of the study site and discusses typical causes of landslides as well as promoting factors in the study area. Chapter 5 presents the methodological approach and gives detailed information on each individual step of the investigation. In chapter 6, the results are presented, and a first interpretation is provided. In chapter 7, the results are discussed, whereby the research questions are addressed.

2 Fundamentals of Landslide Description and Analysis

Landslides are only one of many actors of geomorphological change. While their influence on geomorphology in flat areas is negligible, it is considerable in mountainous and coastal areas. By transporting material downwards, they contribute to the levelling of the landscape and consequently change the appearance of the surface of the earth (Clague & Stead, 2012, p. 10; Crozier, 1986, p. 4).
Research on landslides has been a dynamic discipline in the last couple of decades. From definitions and classifications systems, to investigation and monitoring methods nothing has remained unchanged. Today, landslide research is a complex undertaking that draws on many different disciplines.

The following chapter gives an overview on central ideas on landslides in the academic discourse. It begins with providing essential landslide vocabulary by introducing terms, definitions, and classifications used to describe and categorize landslides. Next, it presents the basic physical principles that describe landslide dynamics. The major factors leading to the infrequent event of a landslide are briefly outlined. In addition, a few basic concepts of stability and instability are considered. Thereby, evaluation methods for slope stability are presented and common concepts to distinguish between slopes of varying stability are discussed. A short overview on factors influencing slope stability is provided. Lastly, the chapter introduces common techniques for the investigation of landslides (and landslide hazards). In this context, landslide investigation techniques relevant in this study are explained in more detail.

2.1 The Multitude of Landside Definitions: An Overview

The term landslide is used as an inclusive term for a range of slope processes, encompassing rapid rockfalls as well as slides that unfold so slowly as to be imperceptible to the human eye. Other than the term "landslide" suggests, landslides are not restricted to a specific type of movement and they can occur underwater as well. In the light of this ambiguity, some scholars, for example Varnes (1978), Crozier (1986) and, most recently, Shanmugam and

Wang (2015) have advocated for the use of another, more precise term for landslides. However, their arguments could not convince the rest of the scientific community and "landslide" continues to be widely used in English-speaking academia. Consequently, any definition of "landslide" in a paper must be as precise as possible and capture the commonalities of the various processes commonly associated with the term landslide.

A well known and probably the most concise definition is by Cruden (1991, p. 28): a landslide is "the movement of a mass of rock, earth or debris down a slope". This definition has become very popular in academia as it has been promoted by the UNESCO Working Party on World Landslide Inventory (WP/WLI, 1993). Likewise, Clague and Stead (2012, p. 1) define landslides as "the downslope movement of earth materials under the influence of gravity". Although not as clear about the material involved as Cruden (1991), the definition by Clague and Stead (2012, p. 1) acknowledges gravity as the driving force behind landslides. In another attempt of defining landslides, Clague (2013, p. 595) pays more attention to the materials involved and defines landslides as "the failure and movement of a mass of rock, soil or artificial fill under the influence of gravity". While recognizing a possible human impact in the definition by including "artificial fill", the definition does not limit landslides to slopes and, therefore, does not adequately distinguish landslides from other geomorphological processes, typically excluded from landslides, such as subsidence. A more particularized definition which specifically addresses the distinction of landslides from other geomorphological processes is given by Crozier (1999), who defines landslides as "the downward or outward movement of a mass of slope forming material under the influence of gravity, occurring on discrete boundaries and taking place initially without the aid of water as a transportational agent".

As these definitions show, landslides are distinguished from other geomorphological processes mostly through the fact that they involve movement of material down a slope.

2.2 Classification Systems for Landslides

Classifications play an essential role in the perception and communication of scientific problems. They stipulate a controlled vocabulary, thus helping to organize and communicate research findings as well as putting things in context. As pointed out by Crozier (1986, p. 3), "classification is a powerful process in the transfer of ideas: classifications institutionalize concepts and are therefore both valuable and dangerous".

2.2.1 Commonalities and Differences of Classification Systems

A classification of landslides was often shaped by a certain perspective, or served a specific interest in research, as observed by Crozier (1986). For example, landslide classification can be approached from the perspective of landslides as a process or of landslides as a hazard to humans. Besides, landslides are complex phenomena, each defined by a unique interplay of factors, like causes, materials or modes of movement. Depending on the perspective, a classification might differ.

Against this backdrop, it comes as no surprise that scholars have drawn up numerous classifications for landsides in the past. Early attempts of classifying landslides come from Sharpe (1938), Varnes (1958; 1978) , Hutchinson (1968) as well as Crozier (1978). Cruden and Varnes (1996) as well as Dikau, Brunsden, Schrott and Ibsen followed in 1996. In 2014, Hungr, Leroueil, and Picarelli published a review and update of the Varnes classification, however it is not yet certain how this update will be received by the academic community.

Commonly, landslides are categorized according to several discriminating attributes that appear significant in the context of a specific research interest or perspective. A few attributes that have been used and continue to be used to describe landslides include the type of movement, the kind of material, the geographic location, as well as the degree of potential hazard (Crozier, 1986, p. 8).

Referring to the growing number of classifications in landslide studies at that time, Crozier (1986, p. 3) argued that classifications run the danger of losing their purpose, that is providing explicit and unambiguous terminology. Eventually, the UNESCO Working Party on World Landslide Inventory (WP/WLI, 1993) promoted a standardization of terms used in the context of landslides. In response, Dikau (1996) as well as Cruden and Varnes (1996) respectively established classifications and updates of older classifications which meet the suggestions of the UNESCO Working Party on World Landslide Inventory.

2.2.2 The Classification of Landslides of Cruden and Varnes (1996)

The classification of Cruden and Varnes (1996) is the most popular in the English-speaking world. With only a few corrections and additions, the classification broadly follows the one Varnes developed in 1978. Cruden and Varnes (1996) suggest a set of descriptive attributes for the classification of landslides. Their chief criteria (attributes) used to categorize landslides are the type of movement (primarily) and the kind of material (secondarily) (Cruden & Varnes, 1996, p. 49). Other attributes for characterizing a landslide are the state and distribution of activity, the style and rate of movement, as well as the water content of the landslide mass. These seven categories are the basis for both categorizing and naming a landslide. They can be combined in a preferred order to formulate a descriptive name which in turn indicates the type of landslide (Cruden & Varnes, 1996, p. 4). The more information about a landslide is available, the more elaborate its name will be. For instance, a landslide may be described in the following way: reactivated, composite, extremely rapid, dry rockfall-debris flow. Figure 1 gives an overview on the main landslide types described by their type of movement and the materials involved. In Table 1, all descriptors are listed. To help produce controlled vocabulary in research, Cruden and Varnes (1996, p. 7) additionally developed a nomenclature for observable features in an idealized landslide. The nomenclature is presented in Appendix A. Additional Information.

Type of Movement

The type of movement is of such high importance to the authors because it largely determines measures of responding to the landslide. However, it can sometimes be hard to identify. Numerous landslides exhibit complex movement patterns so that no single type of movement would adequately describe the nature of the landslide. In such cases, Cruden and Varnes (1996) suggest ascribing several types of movement to a landslide, preferably in a way that the sequence of types of movement in the name indicates the sequence of movements in the landslide. The main types of movements as defined by Cruden and Varnes (1996) are falls, slides, flows, topples, and spreads.

A *fall* happens when material detaches along a surface and then “descends mainly through the air by falling, bouncing, or rolling”. Falls only happen on steep slopes. Thus, they can be “very rapid to extremely rapid”. During a fall, “little or no shear displacement takes place”. (Cruden & Varnes, 1996, p. 23)

In a *topple,* material moves out of a slope by rotating forward “about a point or axis below the center of gravity of the displaced mass”. “Topples range from extremely slow to extremely rapid”. (Cruden & Varnes, 1996, p. 24)

Sliding describes the “downslope movement of soil or rock occurring dominantly on surfaces of rupture or on relatively thin zones of intense shear strain”. Usually, “the volume of displacing material enlarges from an area of local failure”. (Cruden & Varnes, 1996, p. 27)

A *spread* is the “extension of a cohesive soil or rock mass combined with a general subsidence of the fractured mass of cohesive material into softer, underlying material” (Cruden & Varnes, 1996, p. 34).

A *flow* denotes the “spatially continuous movement in which surfaces of shear are short lived, closely spaced and not usually preserved”. The graduation to slides depends on the “water content, mobility and evolution of the movement”. (Cruden & Varnes, 1996, p. 38)

Materials

Three categories are used to distinguish between materials involved in the landslide process: rock, earth and debris. Rock is defined as a hard and intact mass. Earth and debris are both defined as soil, which is an aggregate of solid particles of minerals and rocks. The distinction between the two is made by comparing grain size fractions. If 20 % to 80 % of the particles are larger than two millimeters, the material will be defined as debris. If, on the other hand, 80 % or more of the particles are smaller than 2 mm, the material will be defined as earth. (Cruden & Varnes, 1996, pp. 21–22)

State of Activity

The state of activity describes in which phase a landslide currently is. If there is movement, the landslide may be termed active, whereas an inactive landslide has not moved for more than one seasonal cycle. (Cruden & Varnes, 1996, pp. 12–14)

Rate of Movement

The rate of movement indicates how much a landslide is moving in a given time span and is further used to estimate the associated risk for humans and infrastructure. It ranges from extremely slow to extremely rapid. (Cruden & Varnes, 1996, pp. 17–20)

Water Content

A qualitative assessment of the water content in the displaced mass may help to form assumptions on the water content before the displacement (Cruden & Varnes, 1996, pp. 20–21).

Style of Activity

The style of activity describes in which way different movements contribute to the landslide. For example, on the one hand, landslides can exhibit different types of movement in different areas at the same time. On the other hand, different types of movement may follow each other in a sequence. (Cruden & Varnes, 1996, pp. 15–17)

Distribution of Activity

The distribution of activity describes which areas of the landslide are active and in what way. For example, movement may be limited to a specific area, or affect a larger area. (Cruden & Varnes, 1996, pp. 14–15)

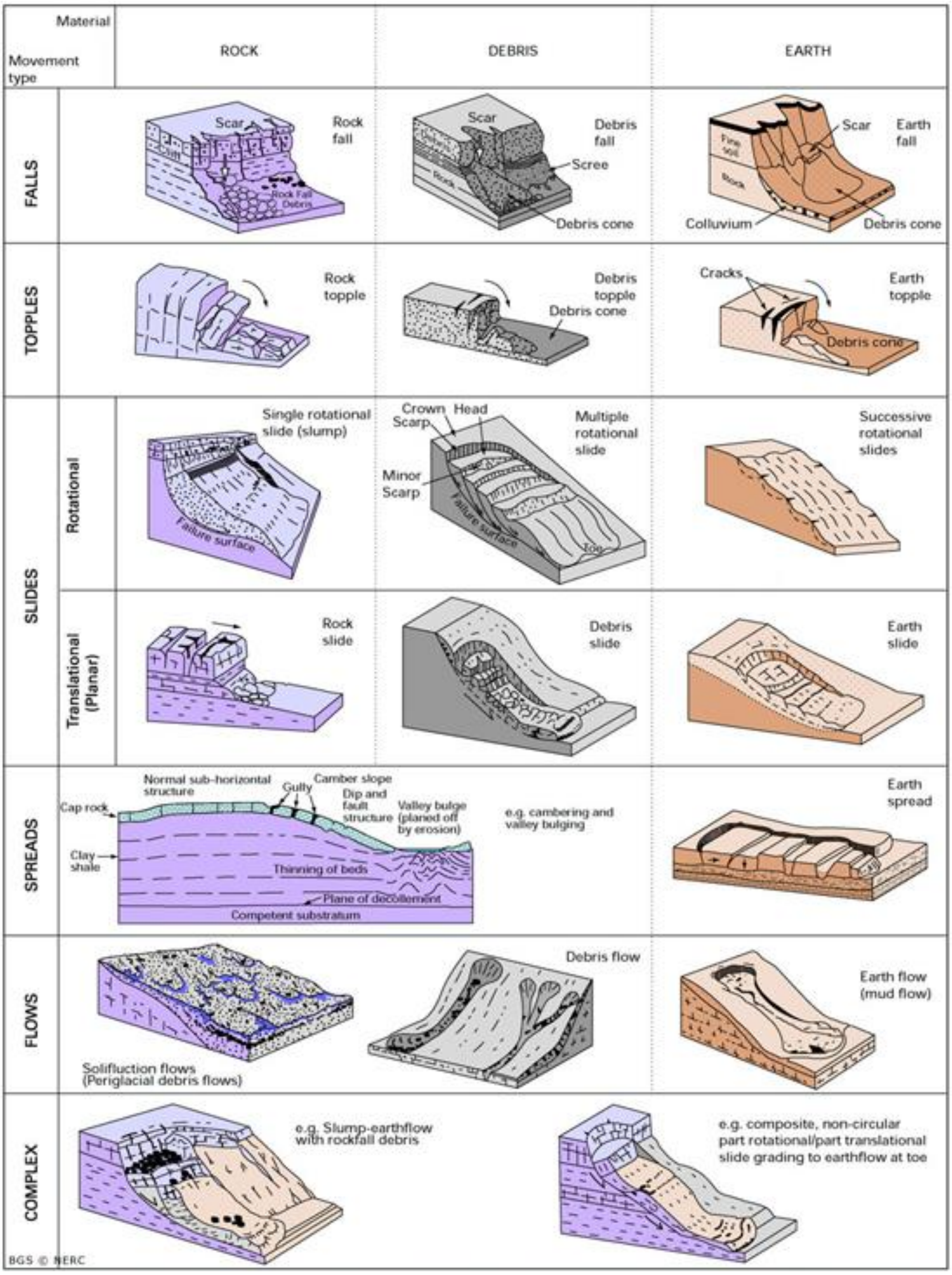

Figure 1. Main types of landslides as characterized by their type of movement and materials involved, after Cruden and Varnes (1996) as cited in BGS (2017)

Table 1. Categories for classifying landslides (Cruden and Varnes 1996)

State of Activity	Distribution of Activity	Style of Activity	Rate of Movement	Water Content	Material	Type of Movement
active	enlarging	complex	extremely slow	dry	rock	fall
reactivated	retrogressing	composite	very slow	moist	soil - debris - earth	topple
suspended	advancing	multiple	slow	wet		slide
inactive - dormant - abandoned - stabilized - relict	widening	successive	moderate	very wet		spread
	confined	single	rapid	-	-	flow
	diminishing		very rapid	-	-	-
	moving		extremely rapid	-	-	-

As can be shown, landslides are complex phenomena. In many cases, they are difficult to categorize. Since a categorization may not always encompass all the characteristics of a certain landslide, it is essential to describe a specific landslide as detailed as possible.

2.3 A Model for Landslide Dynamics

A simple and commonly used model for landslide is a block resting on an inclined plane (represented by the rectangle in Figure 2). In this model, the block represents the mass of the potential landslide while the surface of the inclined plane represents the assumed sliding surface. To accurately describe (and predict) landslide processes, the forces acting on the slopes must be considered.

The first force to be noticed is, of course, the gravitational force $\overrightarrow{F_G}$. It acts on the block, pulling it towards the center of the earth. The gravitational force, also expressed as the weight of the block, can be split into two separate components: one perpendicular to the inclined plane, called the "normal force", and another one parallel to the plane, termed the "downhill force".

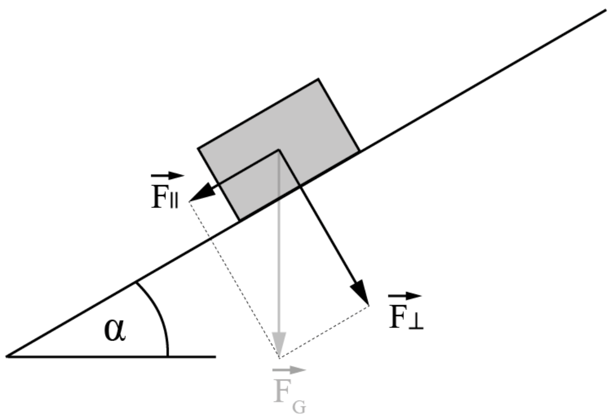

Figure 2. The gravitational force ($\overrightarrow{F_G}$) and its components ($\overrightarrow{F_\parallel}$ and $\overrightarrow{F_\perp}$) acting on the block

As illustrated in Figure 2, the normal $\overrightarrow{F_\perp}$ force is the cosine of the gravitational force. It is represented by:

$$\overrightarrow{F_\perp} = \overrightarrow{F_G} \cdot \cos\alpha \tag{1}$$

$\overrightarrow{F_\perp}$ ... *Normal force* (N)

$\overrightarrow{F_G}$ ... *Gravitational force* (N)

α ... *slope angle* (°)

The downhill force $\overrightarrow{F_{\parallel}}$, on the other hand, is represented by the sinus of the gravitational force:

$$\overrightarrow{F_{\parallel}} = \overrightarrow{F_G} \cdot \sin \alpha \tag{2}$$

$\overrightarrow{F_{\parallel}} \ldots Downhill\ force\ (N)$

The block does not sink into the plane because the force $\overrightarrow{F_N}^*$ of the plane acts on the block and balances the normal force. It acts perpendicular to the plane but in opposite direction to the normal force $\overrightarrow{F_N}$. Considering only these forces, the residual force acting on the block is the downhill force $\overrightarrow{F_{\parallel}}$ and the block accelerates down the plane. Assuming the block is at rest, there must be other forces balancing the downhill force. For most slopes, it is a combination of both frictional forces and cohesive forces that resist movement (until a certain threshold).

The frictional force $\overrightarrow{F_f}$ results from the interlocking of surfaces due to irregularities. It acts opposite to the net applied force and can be expressed as:

$$\left|\overrightarrow{F_f}\right| \leq \mu \cdot \left|\overrightarrow{F_{\perp}}\right| \tag{3}$$

$\mu \ldots coefficient\ of\ friction\ (empirical\ property, dimensionless)$

It follows that the bigger the slope angle α, the bigger the downhill force $\overrightarrow{F_{\parallel}}$ will be (Figure 3) and consequently the bigger the resisting forces must be to balance the downhill force (Crozier, 1986, p. 41).

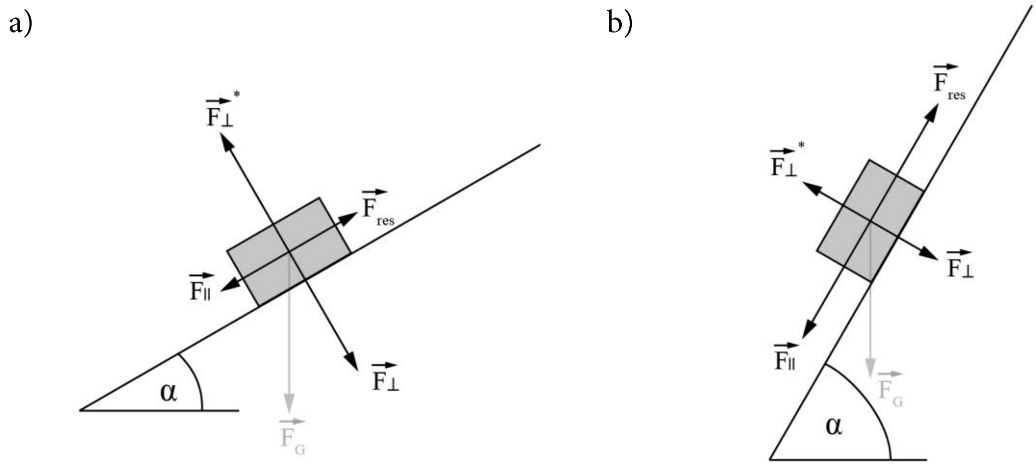

Figure 3. Forces and force components acting on a block on an inclined plane at rest at different slope angles. The slope angle in a) is smaller than in b). Consequently, the downhill force $\overrightarrow{F_{\parallel}}$ in a) is smaller than in b), whereas the normal force $\overrightarrow{F_{\perp}}$ is bigger in a) than in b). Resisting forces in b) must be bigger than in a) to balance the downhill force $\overrightarrow{F_{\parallel}}$.

The frictional force $\overrightarrow{F_f}$ may take any value from zero up to a maximum value $\mu \cdot \left|\overrightarrow{F_{\perp}}\right|$. Past this threshold of maximum value, a slab of soil will start accelerating downwards. In the static case (cohesion ignored), the frictional force $\overrightarrow{F_f}$ will always balance the net applied force on the block, preventing movement. In other words, there is a threshold angle ϕ (the angle of friction) before which a body of a mass m (kg) resting on an inclined plane will start sliding. It is defined as (De Blasio, 2011, p. 27):

$$\tan \phi = \frac{mg \sin \phi}{mg \cos \phi} = \mu \qquad (4)$$

$m \dots mass\ resting\ on\ an\ inclined\ plane\ (e.g.\ of\ the\ slab\ of\ soil)\ (kg)$

$\phi \dots threshold\ angle\ (°)$

Some soils, such as clayey soils, exhibit cohesive behavior. Cohesion c in natural soils derives from electrostatic bonds between clay and silt particles and makes the particles or molecules stick together. Other than friction, cohesion is independent of the applied normal force $\overrightarrow{F_{\perp}}$. (De Blasio, 2011, p. 31)

The total resistive force $\overrightarrow{F_{res}}$ of a slab of cohesive-frictional soil with constant thickness resting on a plane inclined with angle α is then the sum of the frictional and cohesive contributions and is expressed as follows (De Blasio, 2011, p. 31):

$$\overrightarrow{F_{res}} = mg \cos \alpha \, tan\phi + cWL \tag{5}$$

$\overrightarrow{F_{res}} \ldots resistive\ force\ (N)$

$\alpha \ldots slope\ angle\ (°)$

$W \ldots width\ of\ the\ slab\ (m)$

$L \ldots length\ of\ the\ slab\ (m)$

$c \ldots cohesion$ (Pa)

As the mass m of the slab of soil is (De Blasio, 2011, p. 31):

$$m = \rho DWL \cos \alpha \tag{6}$$

$D \ldots vertical\ projection\ of\ the\ thickness\ D'\ (m), wherby\ D' = D \cos \alpha$

$\rho \ldots density\ of\ the\ body \left(\frac{kg}{m^3}\right)$

The total resistive force $\overrightarrow{F_{res}}$ can be written as (De Blasio, 2011, p. 31):

$$\overrightarrow{F_{res}} = \rho g D W L \cos^2 \alpha \tan \phi + cWL \tag{7}$$

or

$$\overrightarrow{F_{res}} = \sigma W L \tan \phi + cWL \tag{8}$$

In the context of landslides, it is common to not only express dynamics in terms of forces, but in terms of stresses and strengths. Stress is defined as the internal force that neighbouring particles of a body exert on each other when the body is subjected to an external force. It is expressed as a ratio between the external force to the area it acts upon. Its unit is Pascal (Pa). In a landslide, the stress is composed of normal stress σ and shear stress τ. The normal stress σ is the normal force component of the gravitational force $\overrightarrow{F_G}$ divided by the surface area in contact. The shear stress τ is the parallel component of the gravitational force $\overrightarrow{F_G}$, divided by the surface area in contact. (De Blasio, 2011, p. 25):

For a given body of soil or rock with a thickness of $D' = D \cos \alpha$, where D is the vertical projection of the thickness, normal stress σ and shear stress τ can then be expressed as (De Blasio, 2011, p. 25):

$$\sigma = \frac{\overrightarrow{\vec{F}_{\perp}}}{A} = \frac{\rho g D' A \cos \alpha}{A} = \rho g D' \cos \alpha = \rho g D \cos^2 \alpha \tag{9}$$

$$\tau = \frac{\overrightarrow{F_{\parallel}}}{A} = \frac{\rho g D' A \sin \alpha}{A} = \rho g D' \sin \alpha = \rho g D \sin \alpha \cos \alpha \tag{10}$$

$\overrightarrow{\vec{F}_{\perp}} \ldots Normal\ force\ (N)$

$\overrightarrow{F_{\parallel}} \ldots Downhill\ force\ (N)$

$A \ldots area\ of\ the\ surface\ in\ contact\ (m^2)$

$g \ldots gravity \sim 9{,}81 \left(\frac{m}{s^2}\right)$

$\alpha \ldots slope\ angle\ (°)$

$\rho g D' A \ldots magnitude\ of\ the\ weight\ force\ (N)$

Strength on the other hand is defined as the maximum stress a body can withstand before failure or plastic deformation (De Blasio, 2011, p. 25). The strength of the body can be expressed in terms of the type of stress it withstands. As an example, "shear strength" is the ability of a body to withstand shear. Shear strength, in its simplest form, is expressed by the Coulomb-Terzaghi shear strength equation (Crozier, 1986, p. 40) that is commonly used to calculate shear strength of slope forming material:

$$s = c + (\sigma - u) \cdot tan\ \phi \tag{11}$$

or

$$s = c + \left(\frac{W}{A}\ cos\ \beta - u\right) \cdot\ tan\ \phi \tag{12}$$

$s \ldots shear\ strength\ (Pa)$

$c \ldots cohesion\ with\ respect\ to\ effective\ normal\ stress\ (N)$

$\sigma \ldots total\ normal\ stress\ (Pa)$

$u \ldots porewater\ pressure\ (Pa)$

$W \ldots weight\ of\ material\ (N)$

$A \ldots area\ of\ shear\ plane\ (m^2)$

$\beta \ldots angle\ of\ surface\ of\ rupture\ or\ shear\ plane\ (°)$

The Coulomb-Terzaghi shear strength equation links the shear strength of a slope forming material to the sum of the normal stress (σ) and cohesion (c). The pore-water pressure is also considered in the equation.

As has been shown, the forces acting on a slope can be modelled by a block resting on an inclined plane. Although a situation in real life is much more complex, the physical principles introduced in this section are the basis for a first assessment of the stability of a given slope (see section 2.4).

2.4 The Concept of Slope Stability and Instability

A landslide is a relatively rare event for the individual slope. Most "slopes are stable or at least marginally stable for most of the time" and "an actual landslide represents a transient condition infrequently attained by the slope" (Crozier, 1986, p. 38).

The analysis of slope stability draws on the analysis of the forces and stresses that act on a slope. In general, stability is a matter of equilibrium between forces in the slope that promote landslides and forces that resist landslides. As long as these forces are balanced, a slope will remain stable. (Ishibashi & Hazarika, 2015, p. 363)
However, every slope is subjected to a range of external influences. Over time they can change the distribution of forces within that slope. Sometimes it happens rapidly, for example during a storm, other times more gradually, for example in the context of climate change. As a result, the stability of a slope may change so that a landslide occurs on a slope that has been stable for long periods of time. Thus, slope stability is no stable quantity and one may never assume that a given slope is 100% safe. A slope that is currently stable may quickly become an unstable slope, with risk of collapsing. (Crozier, 1986, p. 36)

2.4.1 Stability Analysis

A common mean of analyzing slope stability is through a comparison of the promoting and resisting forces by either calculating the ratio of the two or by calculating the difference between the two. The "limiting equilibrium method" is through a quantitative comparison

of the forces that tend to promote movement and those forces that tend to resist movement (Crozier, 1986, p. 39; Ishibashi & Hazarika, 2015, p. 367). Conventionally, this comparison is expressed by the ratio of the magnitude of the shear stress to the magnitude of shear strength, termed "factor of safety". Both being equal in magnitude, the factor of safety takes a value of 1.0. At this point, the soil mass is on the brink of movement. Higher values represent "progressively more stable situations", lower values represent successively unstable situations. (Crozier, 1986, p. 39)
However, the limiting equilibrium method has a major drawback. Because the factor of safety is a ratio, it ignores absolute differences in excess strength. Excess strength must be reduced to zero to make a slope unstable (Glade, Anderson, & Crozier, 2005, p. 44). Thus, spatial variations are better represented by the excess strength instead of the factor of safety (Glade et al., 2005, p. 44). The excess strength – also termed "margin of stability" – is the difference between strength and stress. The margin of stability, together with the magnitude and frequency of external destabilizing forces, offers a valuable framework for distinguishing between slopes of varying stability (Glade et al., 2005, p. 44).

As both methods are based on the analysis of the forces, or stress and strength, respectively, their information value depends on the availability and quality of data. Unfortunately, identifying the stress condition within a slope and, more importantly, the range of external stresses is very challenging in practice (Crozier, 1986, p. 33). Additionally, the accuracy and validity of the findings for the whole slope depend on how homogenous the conditions within a slope are (Crozier, 1986, p. 42). He notes that the values obtained for stability analysis represent "only a minute fraction of the material involved" and such analysis may only be representative for no more than "a point in time and little more than a point in space on the slope in question" (Crozier, 1986, p. 42).

2.4.2 Stability States

Crozier (1986, pp. 32–33) and Glade et al. (2005, pp. 44–45) distinguish between three states of stability. They hinge on the ability of external forces to produce failure at a given margin of stability. Stable slopes are characterized by a margin of stability large enough to withstand the impact of all natural dynamic forces that may destabilize a slope. Marginally stable slope are slopes that are currently not exhibiting movement but are easily disturbed by the influence of dynamic external forces. The actively unstable state, which is probably the easiest to identify, describes slopes that are undergoing continuous or intermittent movement. Their margin of stability is almost zero. (Glade et al., 2005, p. 44)

However, the boundaries between the three categories are rather blurry. Therefore, stability is often represented on a spectrum. One end of the spectrum represents slopes of a high margin of stability and low chances of collapse. The other end of the spectrum represents slopes that are exhibiting landslides. (Glade et al., 2005, p. 44)

Ultimately, slope stability is a measurement of probability for a slope to exhibit landslides and can be interpreted as “the propensity for a slope to undergo morphologically and structurally disruptive landslide processes” (Glade et al., 2005, p. 43).

2.4.3 Factors Influencing Slope Stability

The factors influencing slope stability are diverse. Crozier groups these factors according to the place of operation, their function and their rate of change (Crozier, 1986, pp. 34–35). Glade et al. (2005, pp. 45–46), on the other hand, identify four groups of external factors promoting instability which are also grouped according to their cause: precondition factors, preparatory factors, triggering factors and sustaining factors. Precondition factors – also termed predisposing factors – are static, inherent factors which influence the margin of stability and furthermore act as a catalyst for other dynamic factors to destabilize the slope. Preparatory factors are dynamic factors which reduce the margin of stability over time without initiating movement. Through the action of preparatory factors, the stability of a slope changes from stable to marginally stable. Triggering factors are those initiating movement on a slope, changing its stability state from marginally stable to actively unstable. Factors determining the behavior of an actively unstable slope – for example in terms of duration, rate and form of movement – are called sustaining factors. These factors can be anything from dynamic external factors (e.g. rainfall) to factors influencing the state of the landslide movement or the terrain (e.g. morphology of the slope). (Glade et al., 2005, pp. 45–46)

Factors and causes according to Glade et al. (2005, pp. 45–46) are summarized in Table 2. The causes for landslides in the study area Waidhofen an der Ybbs are considered in section 3.4.

Table 2. Selection of precondition, preparatory, triggering and sustaining factors in landsliding (Dikau & Glade, 2002)

Cause	Preparatory and precondition factors (disposition)	Triggering factors	Sustaining factors
Geology	discontinuity[1] (stratigraphy, cleavage, etc.) Structural discontinuity[1] (e.g. strike and dip, tectonic disturbances) weathering isostasy	earth quake volcanic eruption	rock types discontinuity[1] structural discontinuity[1] (e.g. strike/dip, tectonic disturbances)
Climate	persistent rainfall snow melt freeze-thaw cycles	rainfall[1] (intensity, amount) rapid snow melt	rainfall (intensity, amount)
Soil	weathering geotechnical material properties soil type cycles of soil shrinkage and swelling subterranean erosion (e.g. tunnel erosion)	not applicable	water saturation thickness of the soil

Cause	Preparatory and precondition factors (disposition)	Triggering factors	Sustaining factors
Vegetation	natural change of vegetation (e.g. forest fires, drought)	not applicable	vegetation
Hydrology	thawing of permafrost	rapid change of groundwater table or pore-water pressure	channel roughness onward transport of moving masses
Topography	slope exposure[1] height of slope[1]	not applicable	slope angle[1] curvature[1] depth contour[1]
Anthropogenic	deforestation construction of dams removal of the foot of a slope increase of the load on the upper part of a slope irrigation mining artificially induced movement (e.g. detonation) leaking water pipes	slope cutting[1] undercutting of a slope[1] extra load[1]	construction (control structures) sams river engineering (straightening, increase or decrease in size)
[1]These factors can act as preparatory, triggering or sustaining factors, depending on the stability of the slope.			

As suggested, various factors are involved in a landslide. The cause of a landslide can never be narrowed down to one single factor (Crozier, 1986, p. 38). This can be shown best by the margin of stability. For instance, a potential trigger can only start a landslide when it is big enough to overcome excess strength. In other words, when preparatory factors have already decreased the margin of stability to a minimum, a weaker trigger can start a landslide. Crozier (1986, pp. 37–38) illustrates this idea with a scale balancing four bricks on each side. One side of the scale represents promoting factors, the other one resisting factors. If one brick is added to the side of promoting factors, the balance will be disturbed. The last block triggers the movement but without the other factors (blocks) one block would not have sufficed to trigger movement.

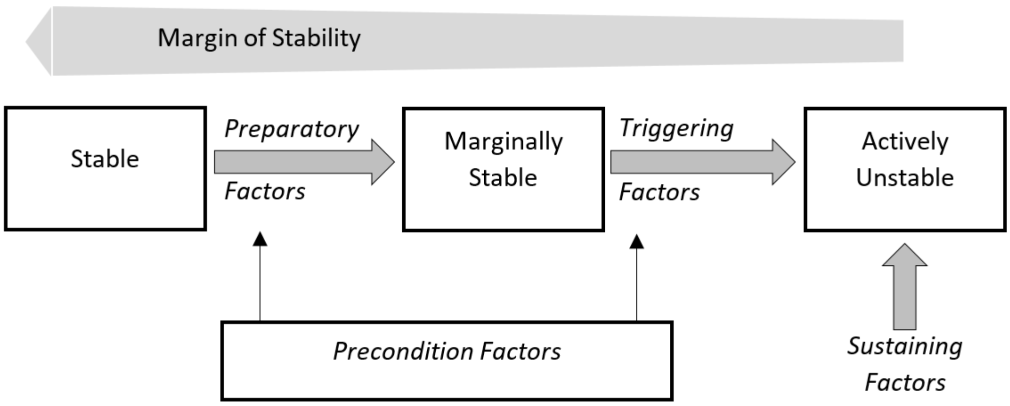

Figure 4. Interplay of factors according to Crozier (1986, p. 38)

2.5 Methods for the Investigation and Monitoring of Landslides

The identification of the conditions and processes that promote slope failure is paramount in order to predict the landslide hazards in a given area. The more information on their relative contribution is available, the more reliable an estimation of slope failure will be. (Highland & Bobrowsky, 2008, p. 46)
To gain information, scientists resort to a variety of methods. They range from traditional geotechnical approaches (e.g. drilling) to geophysical methods and computer modelling. Which method is best suited for the individual investigation depends on the type of landslide as well as the purpose of the investigation. For example, a rockfall requires a different approach than an earth slide. Usually a combination of different methods is applied.

The following chapter gives a general overview on some of the popular techniques for the investigation of landslides or landslide hazards. The methods relevant for this thesis are introduced separately. Thereby, attention is given specifically to geoelectrical measurements. Next to an explanation of the measurement principle, relevant electrical properties and modes of conduction in the subsurface are outlined. Furthermore, the connection between geotechnical properties of rocks and soils and their electrical properties is explored.

2.5.1 Surface Investigation Techniques

Map Analysis and Aerial Reconnaissance

A common first step in the investigation of landslides is the analysis of maps. Topographic maps, geologic maps, hydrologic maps or soil maps help in getting a first overview of the area or site and its environmental setting. They can also give a first idea of factors that promote slope failure. Similarly, aerial imagery – such as photography, satellite, radar, acoustic or infrared – are commonly used to identify characteristic features of a landslide or landscape features such as topography, vegetation, rivers and streams, or settlements and infrastructure. (Highland & Bobrowsky, 2008, p. 46)

Remote Sensing Techniques

Aerial information has become even more valuable to landslide research as new techniques have become available to researchers. Promising remote sensing techniques such as light detection and ranging (LiDAR) or drones have been successfully applied in the investigation of landslides (Rossi et al., 2016; Rossi, Tanteri, Salvatici, & Casagli, 2017). A review of laser techniques in landslide investigation and monitoring is offered by Jaboyedoff et al. (2012). Other common techniques are tachymetry, or electronic distance measurement (EDM).

Field Reconnaissance

More subtle signs of movement might not be visible on maps or images and are better detected in the field – especially when the area is forested or urbanized (Highland & Bobrowsky, 2008, p. 46). Indicators of current and past landslides – such as steps, scarps and cracks in the ground, tilted trees or trees with curved trunks – are best identified in the field. Moreover, field work provides an opportunity to update maps and images or to generate new maps, such as geomorphological or geological maps. The sampling of rocks and soils for laboratory analysis requires fieldwork and can serve as a basis for a more thorough investigation. Field work thus represents a major part of most investigations. (Highland & Bobrowsky, 2008, p. 46)

2.5.2 Subsurface Investigation Techniques

The investigation of the subsurface is particularly important in terms of identifying the conditions and processes that potentially lead to failure, as many of them originate in the subsurface (e.g. geology).

Installation of Instruments in the Ground

Various instruments can be installed in the subsurface in order to estimate forces in the ground. Inclinometers can be set up to measure angles of tilt or changes thereof, extensometers or strain meters can be applied for stress and strain measurements and piezometers for measuring pressures. A simple method for tracking movement is the establishment of control points. (Highland & Bobrowsky, 2008, p. 47)

Drilling

A standardly applied method is drilling. Where possible, drilling is the only way of determining directly the type of materials involved in a landslide as well as their distribution (i.e. stratigraphy). Core borings might reveal information on the geometry or thickness of the landslide mass, as well as the water table or the degree of disruption of the landslide materials (Highland & Bobrowsky, 2008, p. 47). There are several drilling techniques. Popular techniques are Displacement Boring, Wash Boring, Auger Boring, Rotary Drilling, Percussion Drilling, and Continuous Sampling.

Geophysical Methods

Geophysical methods are frequently used for the investigation and monitoring of landslides (Jongmans & Garambois, 2007, p. 3). They include seismic, electrical resistivity, electromagnetic, gravity, ground penetrating radar, and magnetics. Their cost- and time-effectiveness as well as their advanced imaging capacities make them particularly suited for the identification of spatial and temporal variations of physical properties in the subsurface (Jongmans & Garambois, 2007, p. 4). Instead of providing point-information, they provide global information, allowing a 2-dimensional and 3-dimensional interpretation of the subsurface and even 4D time and space imaging (Jongmans & Garambois, 2007, p. 1). Applications of geophysical methods in the context of landslide research include the identification of soil and rock properties as well as their distribution (stratigraphy), the localization of boundaries in the ground (e.g. bedrock, water table, failure surface) or the estimation of the geometry of subsurface structures (Perrone et al., 2014, p. 130).

Nevertheless, geophysical methods have many sources of uncertainty. One challenge is that the data provided by geophysical methods are spatial averages, because the signals traverse the area of investigation from a source to a receiver. As these are limited in number,

geophysical properties are only approximately measured. More importantly, geophysical methods provide only an indirect view into the ground and the properties measured (e.g. electrical resistivity) are usually not the ones of primary interest (as for example, the porosity), but are only related to them. (National Research Council, 2005, p. 108)
As the relation between the measured properties and the ones of primary interest is not exact, there remains a certain ambiguity in the interpretation of the results of geophysical methods, resulting in the need for calibration (Jongmans & Garambois, 2007, p. 4). Consequently, geophysical methods are best applied in combination with traditional methods, like sampling or drilling for validation (Highland & Bobrowsky, 2008, p. 47).

Computer Modelling

Computer modelling is a promising method for the analysis and prediction of landslides (Highland & Bobrowsky, 2008, p. 47). Although computer modelling still has tremendous potential for development, it has been successfully applied to determine the volume of the landslide mass, or track changes in the surface expression or cross section (Highland & Bobrowsky, 2008, p. 47). Computerized terrain analysis and digital terrain modelling appear especially powerful in the context of landslide analysis. Furthermore, computer modelling offers options for performing complex stability analysis and might allow a prediction of future landslide risk, especially when field data is available and can be included in the analysis.

2.6 Percussion Drilling

One method applied in the study is Percussion Drilling (PD), which consists of driving cylindrical sample tubes into the ground, either manually or with a motor. A chain-driven drop weight is repeatedly dropped onto an anvil so that soil pushes into the sample tubes. Drill rods are connected to the sample tubes to drive them into greater depths. The depth that can be achieved in a drilling depends on the soil type as well as the presence of obstacles. Sample tubes are usually one meter long. After every meter, the sample tube is extracted using a hydraulic jack. The diameter of the sample tubes is selected according to the condition of the soil and in descending diameters to reduce cross-contamination. In window sampling, the sample tubes feature a "window" on one side, allowing for instant analysis and soil sampling from the core. Windowless sampling is carried out using conventional sample tubes equipped with an inner plastic liner to facilitate easy removal of the core. Drilling (and sampling) is the only option to obtain direct information on subsurface conditions.

2.7 Dynamic Probing Heavy

Another method applied is Dynamic Probing Heavy (DPH). The purpose of a penetration test is to gain knowledge of the resistance of a soil towards penetration and create a continuous profile of ground resistance with depth. Dynamic Probing may be used to estimate the stratigraphic interfaces or to trace the outlines of objects in the ground. It may also be used to locate soft areas, voids or cavities within the soil. Often dynamic probing is used to interpolate data between boreholes or to supplement information achieved in drillings. (Eißsfeldt, 2011, p. 4)

A cone is attached to a series of one-meter-long steel rods with graduation markings at 100 mm intervals. The rods are driven into the ground by a hammer which is dropped repeatedly onto the rods until the required depth is reached or a refusal is met. The number of blows it takes to drive the cone down each 100 mm ($N_{10}\ values$) increment is recorded.

A quantitative interpretation of results obtained through DPH is controversial due to the effect of skin friction (Khodaparast, Rajabi, & Mohammadi, 2015). The obtained $N_{10}\ values$ contain the tip resistance as well as the surface friction and their contribution to the overall penetration resistance is hard to assess. This is specifically problematic in binding soils or in the investigation of larger depths (Eißsfeldt, 2011, p. 4).

2.8 Geoelectrical Measurements

Several geoelectrical measurements were performed at the Hofermühle-landslide. Geoelectrical measurements are popular in the investigation of landslides. They are particularly attractive for the investigation of landslides and are economically inexpensive way to get an overview of a study site and locate areas that demand closer inspection as they yield 2-dimensional information on subsurface properties. Moreover, geoelectrical measurements have proven successful in reconstructing the geometry of the landslide body, the identification of sliding surfaces between the slide material and the bedrock as well as locating high water content areas (Perrone et al., 2014, p. 129). Geoelectrical measurements encompass a wide range of methods that allow the assessment of various electromagnetic properties of the ground, such as conductivity or chargeability. Table A 3 in Appendix A. Additional Information provides an overview of common geoelectrical techniques.

The measurement of the electromagnetic properties is based on measuring the propagation of natural fields (e.g. self-potential, earth magnetic field), or artificially induced fields (either galvanic through electrodes or via induction (EM measurements)). Electric currents or fields in the ground obey the laws of Maxwell but are influenced by the lithologic properties of the ground, causing a spatial distribution of electrical properties (such as resistivity or chargeability) in the subsurface. (Binley & Kemna, 2005, p. 129)

The relation between structures in the ground and their electrical properties is used to deduce the spatial distribution of structures as well as their geotechnical properties (e.g. type of rock, porosity, water content, etc.). However, the obtained data can be the result of many different situations in the ground, which is why geoelectric measurements are ideally complemented by geological or geotechnical data (Jongmans & Garambois, 2007, p. 4).

2.8.1 Electrical Properties of Subsurface Materials

Geoelectric measurements permit the assessment of electrical properties of the subsurface. Electrical properties commonly analyzed are conductivity (or its reciprocal resistivity) as well as chargeability. The electrical conductivity of materials in the subsurface is the most relevant property influencing the propagation of electromagnetic fields.
The electrical conductivity of natural materials varies of many orders of magnitude, ranging from 10^{-18} Sm^{-1} (diamond) to 10^{-7} Sm^{-1}. Carefully interpreted, the electrical properties of subsurface materials allow the delineation of the variation of related properties, although they are not directly observable through measurements. (Knödel, Krummel, Lange, & Berktold, 1997, pp. 83–91)

Resistance (R) is, according to Ohm's law, defined as the measured voltage divided by the measured current. The unit is Ohm (Ω). Since the geometry and volume of the object are not accounted for, resistance as a property is only assigned to objects. Its reciprocal is called *conductance*.

Resistivity, or *specific resistance,* (most often represented using ρ*)* on the other hand is the resistance per unit volume (see Figure 5). It is thus a property of materials. When considering a current passing through a unit cube of material, resistivity is defined as the voltage (V/m) measured across the unit's cube length divided by the current passing through the cross-sectional area (A/m^2). The resulting unit is Ohm-m (Ωm). Its reciprocal is called *conductivity.*

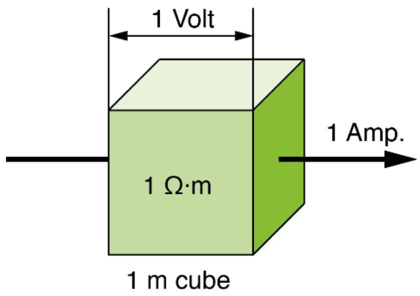

Figure 5. Illustration of the definition of resistivity (resistance per unit volume)

$$\rho = R \cdot \frac{A}{L} \tag{13}$$

$R \ldots resistance\ of\ the\ body\ (\Omega)$

$A \ldots cross\ section\ of\ the\ body\ (m^2)$

$L \ldots length\ of\ the\ body\ (m)$

The *conductivity,* or *specific conductance,* of a given material (most often represented using σ) has the unit Siemens per meter $\left(\frac{S}{m}\right)$ and is the inverse resistivity of that material:

$$\sigma = \frac{1}{\rho} \tag{14}$$

2.8.2 Paths of Conduction in the Subsurface

There are several ways in which an electric current can flow in the subsurface. First, there is conduction via a lattice (e.g. atomic lattice, as in metals), second, there is electrolytic conduction through ions (as for example in many fluids) and third there is conduction on the interface of two materials (e.g. rock matrix and pore water). As pure materials are rarely found in the subsurface, most materials encountered are a mixture of more than one phase (solid, liquid, gas), and the general resistivity is due to different mechanisms of conduction (Friedman, 2005; Knödel et al., 1997, p. 86). Depending on the material, one mode of conduction may prevail. (Knödel et al., 1997, pp. 83–91; Ward, 1990, p. 150)

In pure metals and semiconductor materials, the charge carriers of the electric current – electrons and electron-hole pairs – move through the atomic lattice. In pure metals, the electrons can move freely, which is why metals are good conductors for the electric current. Therefore, metals are easily distinguished from other materials in electric surveys due to their low resistivity with values around $10^{-8}\ \Omega m$. In semiconductors – such as metallic ore minerals – the electrons are somewhat limited in number and restricted in their movement as they can only move when they receive a sufficiently large amount of external energy (e.g. heat). The limited number and mobility of charge carriers gives semiconductors a higher and more variable resistivity than metals. In rocks and rock forming minerals like silicates and carbonites, this mode of conduction is negligible since the electrons are fixed to the atomic lattice (Ward, 1990, p. 148). Thus, rocks are generally considered insulators. Their conductivity ranges from $10^{-14} to\ 10^{-10} Sm^{-1}$ (Knödel et al., 1997, p. 84).

Another way in which an electric current can flow through the subsurface is through the interface between the rock and pore waters. This type of conduction is characteristic of clay minerals. In clays, a double layer of exchange cations is formed: one is fixed to the clay surface and the other, called diffuse layer, lies adjacent to the fixed layer. The diffuse layer contains cations that can move freely under the influence of an electric field and thus add to the charge carriers available in the rock specimen. (Knödel et al., 1997, p. 85; Ward, 1990, p. 150). All minerals exhibit this characteristic to a certain degree, but it is most pronounced in clays. Therefore, rocks containing clay are characterized by an abnormally high conductivity (Ward, 1990, p. 150).

The most common mode of conduction in near surface rocks and soils is electrolytic conduction through ions in the pore water, taking place in connected pores, cracks, fractures, faults and along boundaries and shear zones (Ward, 1990, p. 148).
The ions in the pore water result from the disassociation of salts – for example in water and they can move easily through the liquid under an electric field. The presence of water (containing dissolved ions) helps to increase the conductivity of otherwise non-conductive materials. Isolated water voids in any given non-conductive material will not increase conductivity – however a thin and connected layer of fluid within a rock or body of soil already increases the conductivity dramatically (Knödel et al., 1997, p. 84).
In a solution of dissolved salts, each ion carries a definite quantity of charge. The more ions are available in a solution, the more charge can be carried altogether by that solution (Ward, 1990, p. 148). The temperature of the pore water also plays an important role. By increasing the temperature of a fluid (e.g. the pore water of rocks), its viscosity is increased and the ions in the fluid become more mobile (Ward, 1990, p. 149).

2.8.3 Conductivity of Rocks

Most rocks and rock forming minerals are considered isolators, since the electrons are fixed to the atomic lattice. Their conductivity ranges from $10^{-14} to\ 10^{-10} Sm^{-1}$ (see Figure 6). Oxides, Sulphides and Graphite are exceptions. (Ward, 1990, p. 148)
Typical values for resistivity of rocks and rock forming minerals are listed in Figure 6. However, rocks near the surface are rugged and their porosity is generally high so that these spaces can be filled with water or clay minerals which all help to increase the conductivity of the rock. The conductivity of a rock thus depends largely on the conductivity of the pore water and its distribution within the rock. (Knödel et al., 1997, p. 84) A detailed description of the electrical properties of rocks is by Schön (2015).

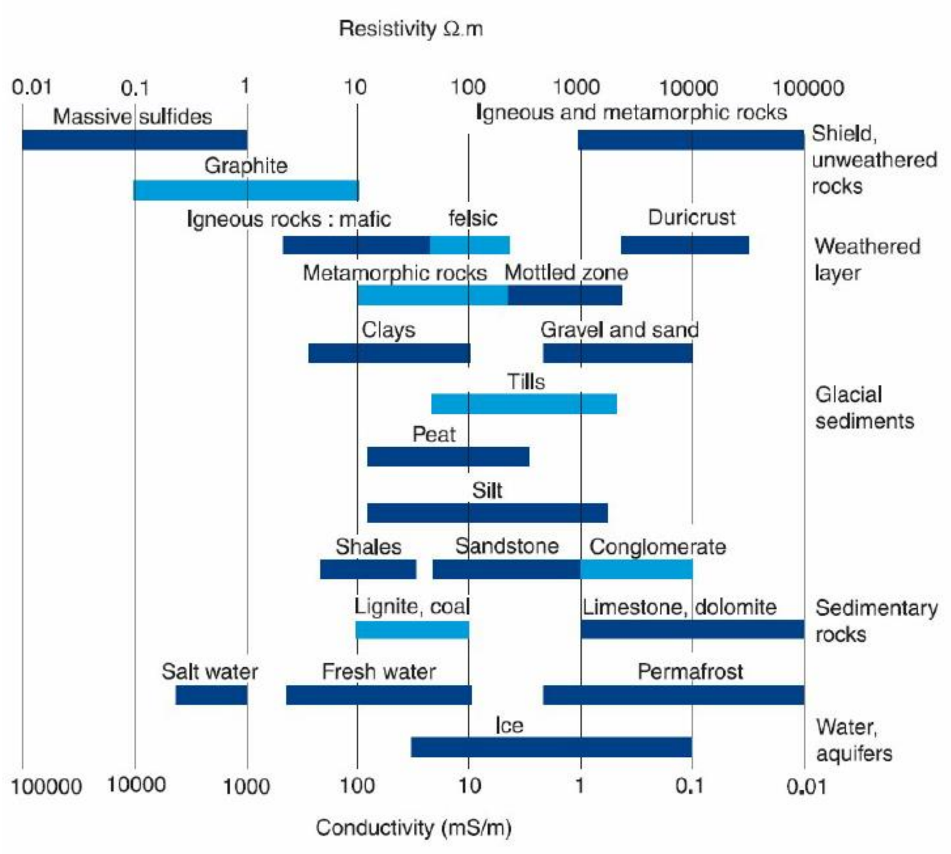

Figure 6. Typical ranges of conductivities of earth materials (Fargier et al., 2012, p. 268; Palacky, 1988, p. 55)

How many pores a rock has and what geometry they have greatly influences the conductivity of a rock. The porosity ϕ is defined as the ratio between the measured volume of water to the measured volume of rock (the fractured volume of water) in a saturated rock (Ward, 1990, p. 148):

$$\phi = \frac{V_e}{V_r} \tag{15}$$

V_e ... $measured\ volume\ of\ water\ (m^3)$

V_r ... $measured\ volume\ of\ rock\ (m^3)$

For rocks containing little or no dead-end pore volume, V_e can be approximated as the product of the length of the electrolyte paths (L_e) and the cross-sectional area of the electrolyte paths (A_e) (Ward, 1990, p. 148):

$$V_e = L_e A_e \tag{16}$$

$L_e \ldots length\ of\ the\ electrolyte\ paths\ (m)$

$A_e \ldots area\ of\ the\ electrolyte\ paths\ (m^2)$

As the electric current in a rock largely flows through the pore waters and not through the silicate framework of the rock, the resistivity of a rock can be expressed as (Ward, 1990, p. 148):

$$R = \rho_e \frac{L_e}{A_e} \tag{17}$$

The conductivity of saturated and partially saturated clay-free sediments is described in a good approximation by Archie's law (Archie, 1942):

$$\sigma_r = \frac{\phi^m}{a} \cdot \sigma_w \cdot S^n \tag{18}$$

and for the resistivity:

$$\rho_{\mathrm{r}} = \frac{a}{\phi^m} \cdot \rho_w \cdot S^{-n} \tag{19}$$

$\sigma_{\mathrm{r}} \ldots conductivity\ of\ the\ sediment\ \left(\frac{S}{m}\right)$

$\rho_{\mathrm{r}} \ldots resistivity\ of\ the\ sediment\ (\Omega m)$

σ_w ... $ionic\ conductivity\ of\ the\ pore\ water\ \left(\frac{S}{m}\right)$

ρ_w ... $resistivity\ of\ the\ pore\ water\ (\Omega m)$

ϕ ... $porosity\ (m^3)$

m ... $cementation\ exponent$ (dimensionless)

a ... $proportionality\ factor$ (dimensionless)

S ... $saturation\ level\ (dimensionless)$

n ... $saturation\ exponent\ (dimensionless)$

The general form of Archie's law (as cited in Ward, 1990, p. 148) is written for rocks with no clay content:

$$F = \frac{\rho_r}{\rho_w} = a\phi^{-m} \tag{20}$$

ρ_r ... $resistivity\ of\ the\ rock\ (\Omega m)$

F ... $formation\ resistivity\ factor\ (dimensionless)$

The numerical values for m vary between 1,40 and 2,20 whereas those for a span from 0,6 to 1,0. For different rocks, different formation factors can be used to adequately link resistivity and porosity. (Ward, 1990, p. 148)

Archie's law might be extended by one term to include surface conduction, as to be valid for rocks containing a considerable amount of clay (Ward, 1990, p. 150):

$$\sigma_0 = \sigma_e + \sigma_f \tag{21}$$

σ_0 ... $conductivity\ of\ the\ material\ \left(\frac{S}{m}\right)$

$\sigma_e \ldots conductivity\ due\ to\ electrolytic\ conduction$ (as in Archie's law for rocks devoid of clay) $\left(\frac{S}{m}\right)$

$\sigma_f \ldots conductivity\ due\ to\ surface\ conduction\ \left(\frac{S}{m}\right)$

In addition to the pore volume in a rock specimen, the geometry of the pores – or the texture of a rock – determines its resistivity (Ward, 1990, p. 149). As Ward (1990, p. 149) notes, the particle size also has an effect on resistivity. For example, a well sorted sandstone has large void spaces and is relatively conductive, while a basalt contains much unconnected pore spaces and does not conduct electric currents as well as a sandstone (Ward, 1990, p. 149).

Various geological processes change the texture and composition of a rock. Generally, geological processes will decrease the resistivity of rocks (Ward, 1990, p. 149).

2.8.4 Conductivity of Soils

The conductivity of soils is more complicated than that of rocks. It is related to several factors, most importantly the nature of the soil composition (i.e. particle size distribution, mineralogy), the soil structure (i.e. porosity, pore size distribution, connectivity), the water content and the temperature (Bai, Kong, & Guo, 2013). Because the water in the soil is the only conductive of the three phases composing the soil (solid, liquid and gas), the water content is most significant to determine the conductivity of a soil (Friedman, 2005, pp. 47–48). As Fukue, Minato, Horibe, and Taya, (1999, as cited in Bai et al., 2013) found, the electrical resistivity decreased when water content increased. Thus, the electrical conductivity depends largely on the amount of water in the pores. Accordingly, properties such as volumetric fraction of the three phases present in a soil as well as the conductivity of the soil solution are the dominant factors determining the conductivity of a soil (Friedman, 2005, pp. 47–48). The amount of water, however, depends mostly on the structures of the soil, i.e. the void distribution, the geometry of pores, the connectivity of the pores and the porosity (Friedman, 2005, pp. 47–48). Their influence on conductivity is therefore indirect only. Since temperature can excite and change the viscosity of a liquid and consequently its conductivity, temperature change can affect the conductivity of a soil as well (Bai et al., 2013). Complementary to this, Auerswald, Simon and Stanjek (2001) concluded that the amount of water and its conductivity are of considerable importance, but demonstrated that clay content is equally significant. In a multiple regression they found that volumetric clay content, electrical conductivity of soil solution, and logarithmic water content accounted for 84% of the variation in resistivity at a ratio of 1 : 0.8 : 0.4.

Other but less significant properties are particle shape and orientation, particle-size distribution, cation exchange capacity, wettability and environmental factors like ionic strength and cation composition (Friedman, 2005, pp. 47–48).

Considering the studies cited above, it can be expected that the electrical conductivity varies between soil types as their properties, which influence electrical conductivity, differ.

2.8.5 Measuring Electrical Properties

After introducing the relevant properties and analysing their dependence on the properties of subsurface materials, this section will focus on the measurement of resistivity.

In direct-current methods, an artificial stationary electromagnetic field is generated in the ground using two electrodes that are firmly attached to the ground (Knödel et al., 1997, p. 122), allowing an electric current to flow from one electrode to the other (see Figure 7). These electrodes are commonly referred to as “transmitter electrodes”. Depending on the electric properties of the subsurface, the current can be strong or weak. So as not to measure the ground resistance of the transmitter electrodes, a potential difference is measured with two other electrodes (the “receiver electrodes”) that have a high resistance (Knödel et al., 1997, p. 122) (Figure 7). This arrangement of four electrodes is commonly applied in direct-current measurements, however, the specific outline of the electrodes may vary (Knödel et al., 1997, p. 122).

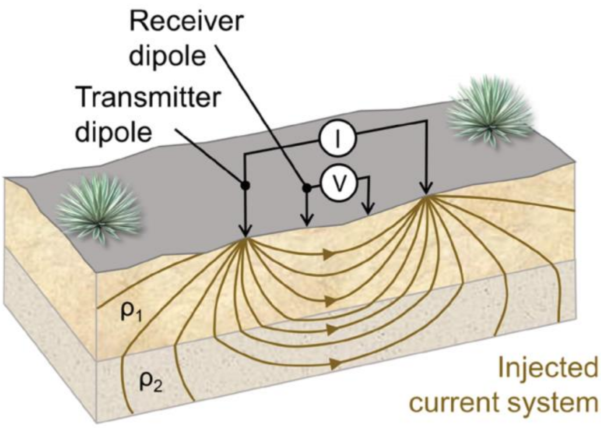

Figure 7. Schematic image of a four-point measurement (Bücker et al., 2017, p. 282)

The measurement provides information on the apparent electrical properties (e.g. resistivity) of specific points of the subsurface. While the apparent electrical properties are not representative of the true resistivity of any structure in the ground, they vary spatially and can be diagnostic of subsurface structures (Ward, 1990, p. 156). To assess these spatial changes, the set-up is altered or simply moved. Inverse methods may then be applied to create an image of the subsurface (Binley & Kemna, 2005, pp. 130–131).

The Electric Field between Two Electrodes

When a potential between two electrodes in the ground exists, an electric field is generated and current flows between these two electrodes. In a homogenous ground, the potential lines of the electric field take the form of half-spheres around the electrodes and the electric current flows along lines perpendicular to the potential. (Ward, 1990, pp. 155–156)

The distribution of the potential- and current-lines is illustrated in Figure 8.

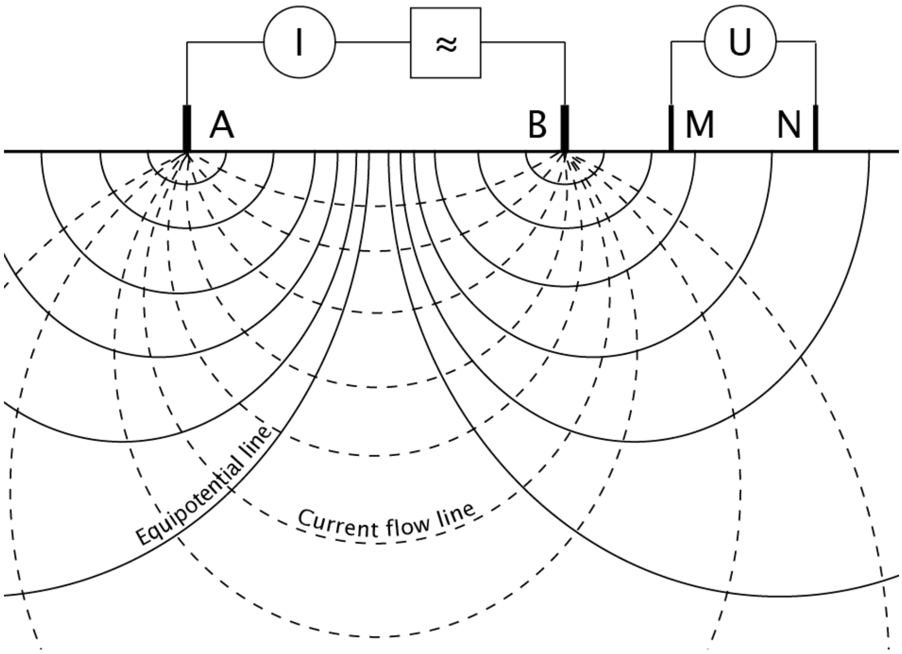

Figure 8: Distribution of current and potential lines in a homogenous half space

Supposing the current flows from A to B, the potential V_A measured at P_M (see Figure 8) is calculated as follows (Ward, 1990, p. 156):

$$V_{P_1} = \frac{I\rho}{2\pi}\left[\frac{1}{r_1} - \frac{1}{r_2}\right] \tag{22}$$

I ... $current$ (A)

ρ ... $resistivity$ (Ωm)

r_1 ... $distance$ $between$ A and M

r_2 ... $distance$ $between$ M and B

In practice, a potential difference is measured instead of a potential. For a setting as illustrated in Figure 8, the potential difference between P_1 and P_2 can be written as (Ward, 1990, p. 156):

$$\Delta V = \frac{I\rho}{2\pi}\left[\frac{1}{r_1} - \frac{1}{r_2} - \frac{1}{r_3} + \frac{1}{r_4}\right] \tag{23}$$

r_3 … $distance\ between\ B$ and $N\ (m)$

r_4 … $distance\ between\ A$ and $N\ (m)$

Type of Current/Voltage Use

Originally, direct current was for geoelectric measurements. However, a low frequency alternating current is better suited as many problems related to direct current (i.e. noise) can be minimized and nowadays alternating current is usually employed in geoelectric measurements. The current is either in the form of a low-frequency alternating current or in the form of a square wave current, where the current is switched on and off in regular intervals. (Ward, 1990, p. 155) The ratio of the voltage to the current is called the impedance of the earth (Ward, 1990, p. 154). From the impedance, the apparent resistivity of the subsurface can be calculated (Binley & Kemna, 2005, p. 130).

The Apparent Resistivity

Since the electrical resistivity is the most commonly investigated property and the most relevant for this study, the following section will illustrate the principle of apparent electrical properties and their relation to subsurface structures on the basis of the apparent resistivity. For a homogenous subsurface the electrical properties are assumed to be spatially constant. The resistivity of a homogenous half space is then (Ward, 1990, p. 156):

$$\rho = \frac{\Delta V}{I} \cdot K \tag{23}$$

K is the so-called geometric factor which depends on the geometry of the array used. A measurement of resistivity will, in this case, provide the true value for resistivity as written in equation (23).

In an inhomogeneous or anisotropic ground, as is usually encountered in the field, the resistivity (as well as other electrical properties) will vary spatially. A measurement for resistivity is not necessarily representative of the true resistivity of any structure in the ground; rather, it corresponds to an equivalent homogenous isotropic half space that would generate the same result in the measurement. The apparent resistivity, however, varies systematically if measurements are taken at different locations or for different depths and thus can be indicative of subsurface structures. (Ward, 1990, p. 156)

Instead of using equation (23), the apparent resistivity (Ωm) is written as (Ward 1990:156):

$$\rho_a = \frac{\Delta V}{I} \cdot K \tag{24}$$

The apparent resistivity ρ_a of an n-layered earth is then (see Ward 1990:157):

$$\rho_a = K\frac{V}{I} = \frac{\rho_1}{2\pi}\int_0^\infty k_{123\ldots n}(\lambda)[J_0(\lambda r_1 - J_0(\lambda r_2) - J_0(\lambda r_3) + J_0(\lambda r_4)]d\lambda \tag{25}$$

Effect of Terrain Topography on Resistivity Measurements

Many geoelectrical measurement systems are made for the investigation of flat terrain, yet numerous resistivity measurements are made on irregular terrain. The effects of topography on resistivity measurements can be considerable. Topographic features change the pattern of the equipotential surfaces and current lines and might introduce anomalies to the data that might lead to inaccurate interpretations of the ground. (Bhattacharya & Shalivahan, 2016) A valley for example can produce a resistivity low while a hill can produce a resistivity high (Ward, 1990, p. 178).

Electrode Configurations

Multiple electrode configurations for geoelectric surveys exist which differ in the configuration of the electrodes (see Figure 9). Each configuration has its strengths and limitations. The suitability of a specific set-up depends on: the problem that is to be solved, the potential spatial variability of electrical properties, equipment availability, and data processing capabilities (Binley & Kemna, 2005, p. 135). For example, the Wenner- and Schlumberger-arrays have a good vertical resolution and are best suited for the investigation of horizontally layered ground. On the other hand, Pole-Dipole or Dipole-Dipole arrays feature a good resolution in the lateral direction and are better suited to detect steeply inclined structures such as tectonic disturbances or escarpments (Knödel et al., 1997, pp. 134–135).

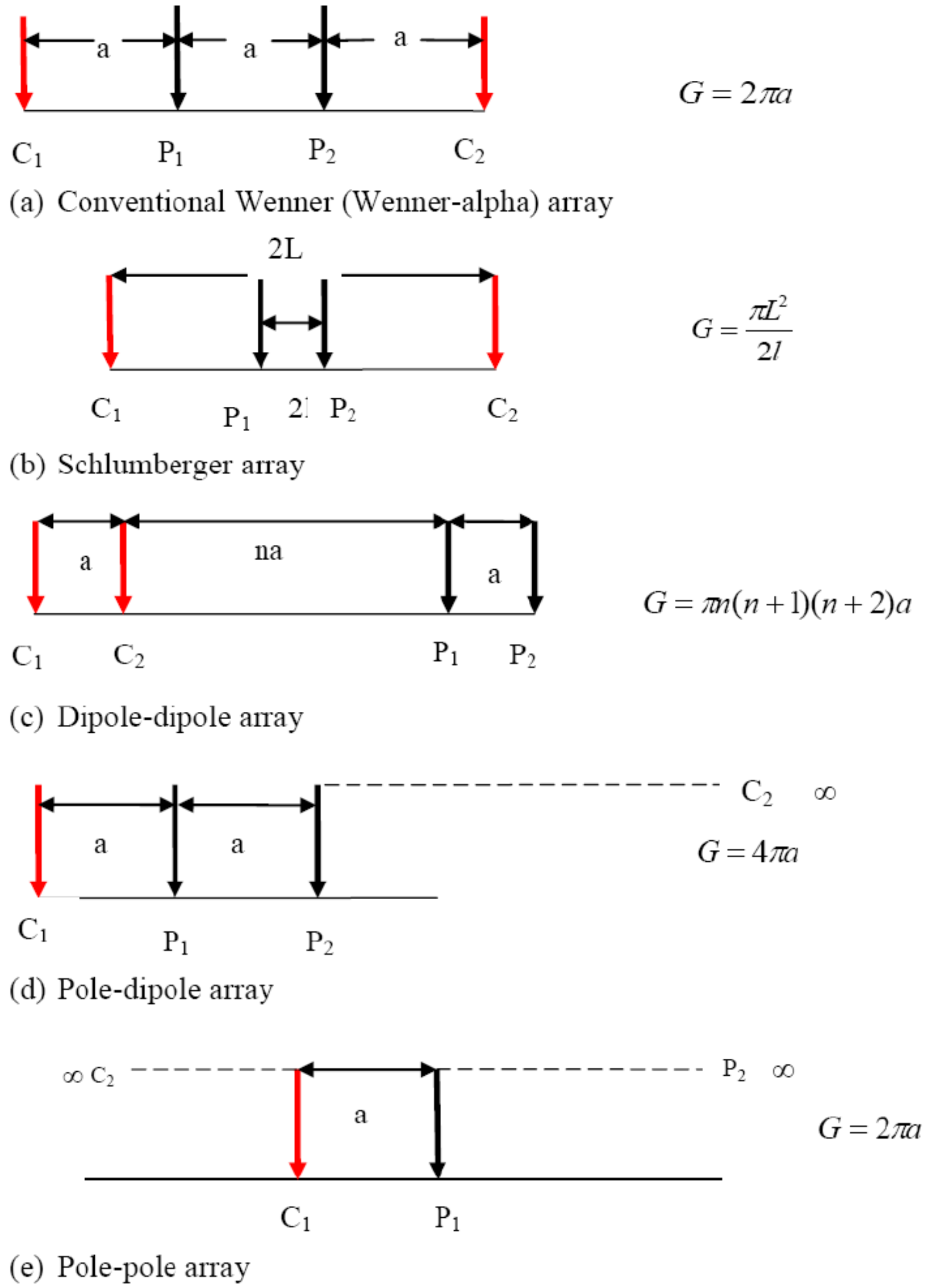

Figure 9. Commonly used electrode configurations (Aizebeokhai, 2011)

Survey Configurations

Geoelectrical measurements may be applied for soundings or profiling or a combination of both (Ward, 1990, pp. 156–165). In vertical electrical sounding, the variations of the electrical properties with depth in a specific location are investigated (vertical changes in apparent resistivity). The space between the electrodes is progressively increased but centered around a fixed point, permitting the current to permeate larger depths. A sounding curve can be generated by plotting the (apparent) resistivity against the depth (Binley & Kemna, 2005, p. 136). In (surface) profiling on the other hand, lateral variations in the electric properties of the ground are of interest. Therefore, the whole array is moved along a surface transect while maintaining a fixed distance between the electrodes (Bücker et al., 2017, p. 282).

The two basic modes are combined in surface imaging to obtain a 2-D or 3-D image of the subsurface (Binley & Kemna, 2005, p. 137). "A surface image survey is carried out by acquiring profiles along transects using different electrode spacing" (Binley & Kemna, 2005, p. 137). Three-dimensional surveys may be conducted by measurements with increased electrode spacing along parallel transects or by using a 2-D grid of electrodes (Binley & Kemna, 2005, p. 137).

Modelling of Data

Geoelectric measurements provide a set of data on the apparent electrical properties of the subsurface. A data set might be plotted to create a pseudo section (for profiling) to illustrate the measurement results (Figure 11). However, a pseudo section is merely a way of plotting the data. It does not yield information on the actual structure of the ground or its distribution of electrical properties. Thus, inverse methods may be applied to estimate the true values and distribution of electrical properties from the observed measurements. Thereby, a mathematical framework or physical theory is used to calculate from measurement results the causal factors that produced them. In science, this approach is called the "inverse problem", since the causes are estimated from the results. The opposite is called the forward problem, in which the outcome of a cause is calculated (Figure 10). Inverse methods thus provide information on properties we cannot directly observe. (Binley & Kemna, 2005, pp. 143–150)

However, it is not possible to determine the actual distribution of electrical properties from the data set because multiple (if not infinite) situations exist that would produce the same outcome within a certain level of uncertainty. Furthermore, the data collection itself is incomplete and inconsistent. The challenge of electrical surveys is not to find a model for the collected data, but one model that is of practical relevance and adequately explains the obtained data. Therefore, the model search needs to be restricted systematically, for example by defining certain model characteristics. Since the inversion is not likely to yield exact results, data misfits and an errors need to be accounted for. (Binley & Kemna, 2005, p. 144) Figure 11 shows a pseudosection of the apparent resistivity in comparison to the calculated inverse model.

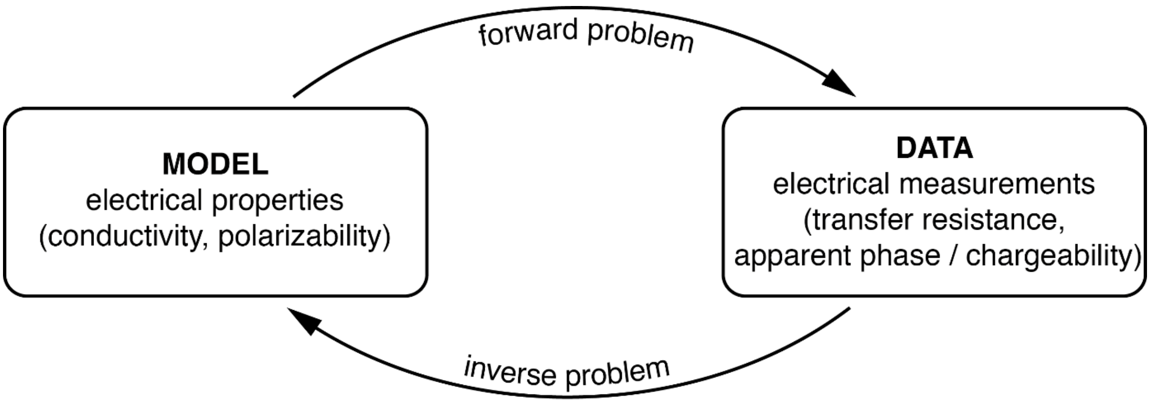

Figure 10. Illustration of the forward and inverse problem for geoelectrical surveys (illustration after (Binley & Kemna, 2005, p. 144)).

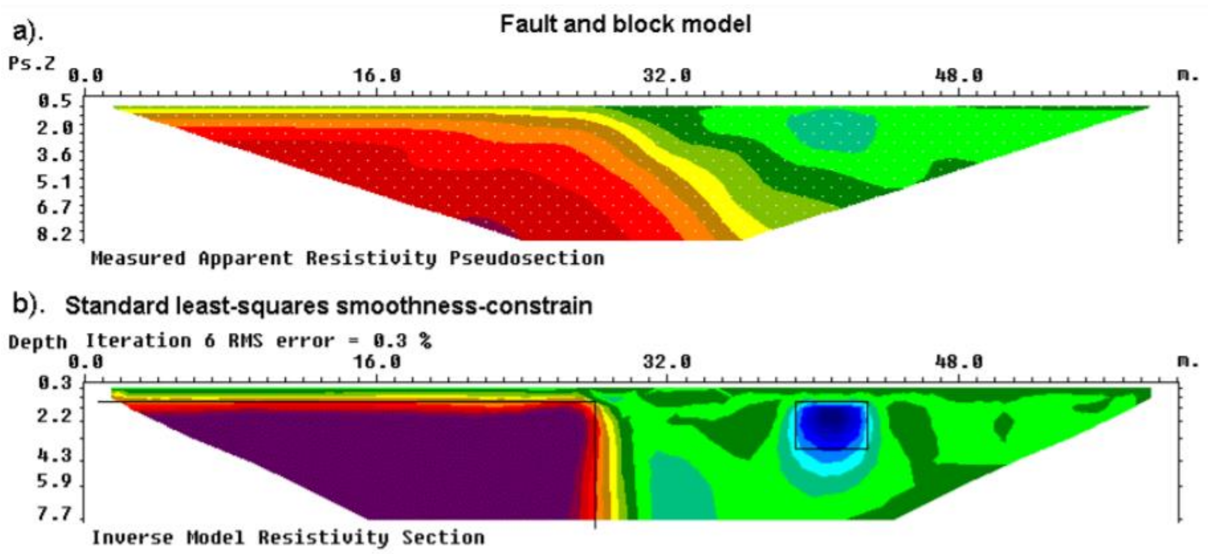

Figure 11. Measured Apparent Resistivity Pseudosection (a) in comparison to the Inverse Model Resistivity Section (Loke, 1999, p. 21).

3 Historic and Environmental Setting

Waidhofen an der Ybbs is highly susceptible to landslides. This is due to a complex interplay of various criteria. The following chapter first introduces the study area and study site. Then the time course of landslide events on the study site is briefly outlined. Since the environmental setting of an area is often helpful in explaining the likelihood of landslides, the study site is characterized in terms of the key environmental factors: climate, lithology, prevailing soils, hydrology and land use. Last, typical causes of landslides as well as promoting factors, as have been recorded in several inventories, in the study area are discussed.

3.1 Study Site

The studied landslide is in Konradsheim in the alpine foothills in the south-western district Waidhofen an der Ybbs of the province Lower Austria (Austria) approximately 5 km east of the identically named municipality Waidhofen an der Ybbs. Figure 12 provides a map of the study site. Rolling to mountainous terrain with moderate slopes and altitudes up to 1.115 m above sea level characterize the area. Generally, the terrain becomes steeper and rockier from north to south. The study site lies in a west-east trending valley at an elevation of around 550 m to 570 m above sea level on a south facing slope with a slope angle of 13° (23 %). It covers an area of approximately 50.000 m^2. The study site is accessible via the road "Redtenbachstraße" in the south or via a smaller approach road ("Krojerlehen") to the adjacent property in the east of the slope. At the western flank of the landslide body lies a small creek (Figure 12). In the north and east, the landslide is surrounded by pastures, while the southern boundary is marked by a small forest. Figure 13 provides photographs of the study site.

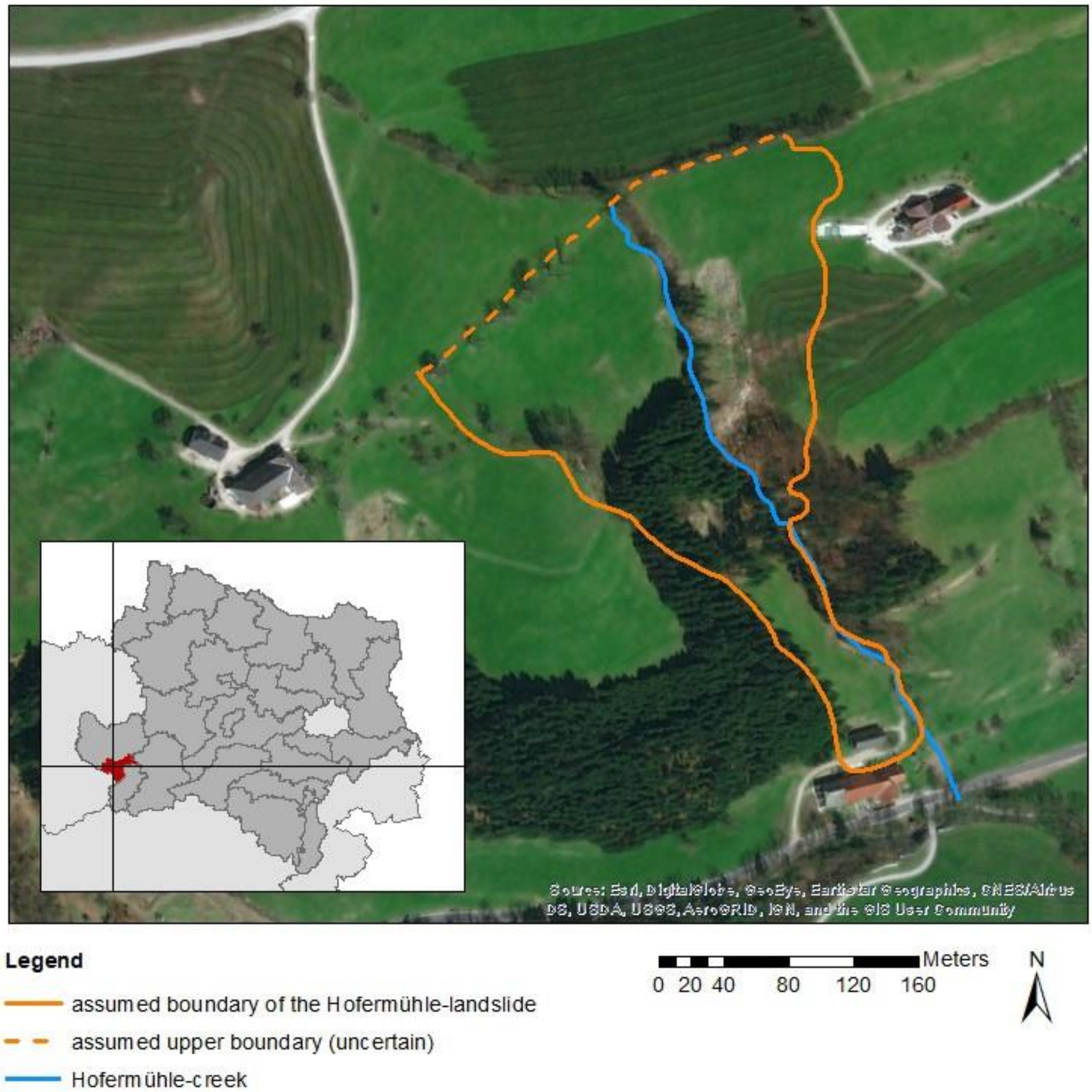

Figure 12. Location and vicinity map of the study site; data source (location map): Land Niederösterreich; data source vicinity map: Esri, Digital Globe, GeoEye, Earthstar Geographics, CNES/Airbus DS, USDA, USGS, AstroGRID, IGN, and the GIS User Community

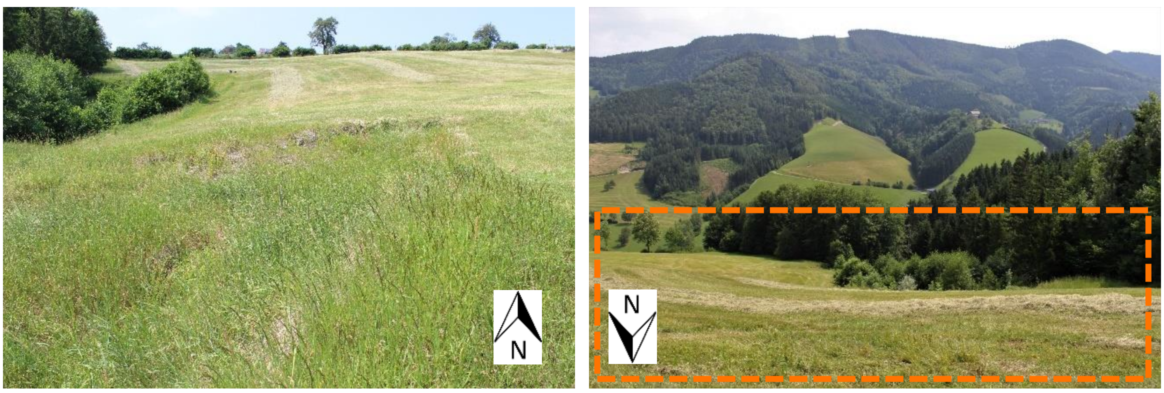

Figure 13. Overview of the study site. Left: northwards; Right: southwards, the orange square marks the study site

3.2 Previous Movements

Detailed information on previous movements and mitigation measures at the Hofermühle landslide were recorded by Sausgruber (2013, 2016). According to residents, the initial movement took place in 1978, on the orographic right of the creek “Hofermühlbach”. As a response, drainages were installed in order to prevent further movement. In 2011, a rotational slide occurred on the other side of the creek (orographic left), creating a drop of two meters in the terrain in the course of one to two weeks. Parts of the forest were removed afterwards. In 2013, the landslide was reactivated after heavy rainfall on April 19th, which are believed to have triggered the slide. This conclusion was supported by the observation that the lower part of the landslide was water saturated, featuring a pasty to liquid consistency. Movement rates of up to 20 meters per hour were recorded. To protect the building on the foot of the hill from damage, a dam was constructed so that material coming down the hill would be deflected. (Sausgruber, 2013, p. 2)
The hollows above the crown (564 m above sea level to 574 m above sea level) grew deeper from 2013 to 2016 and, most notably, the crown increased in that time as well, as Sausgruber (2016) observed. The landslide has also affected a forestry road (535 m above sea level), which is reported to have been sinking (Sausgruber, 2016). Sausgruber (2016) furthermore noted water logging in numerous hollows in and around the landslide.

The descriptions presented above, the digital elevation model as well as the conditions on the site indicate that the landslide is of the type presented in Figure 14. It shows the typical location of a landslide in a soil mantled landscape, which features a similar morphology as the study site. The landslide investigated seems to progressively erode material from higher locations of the slope.

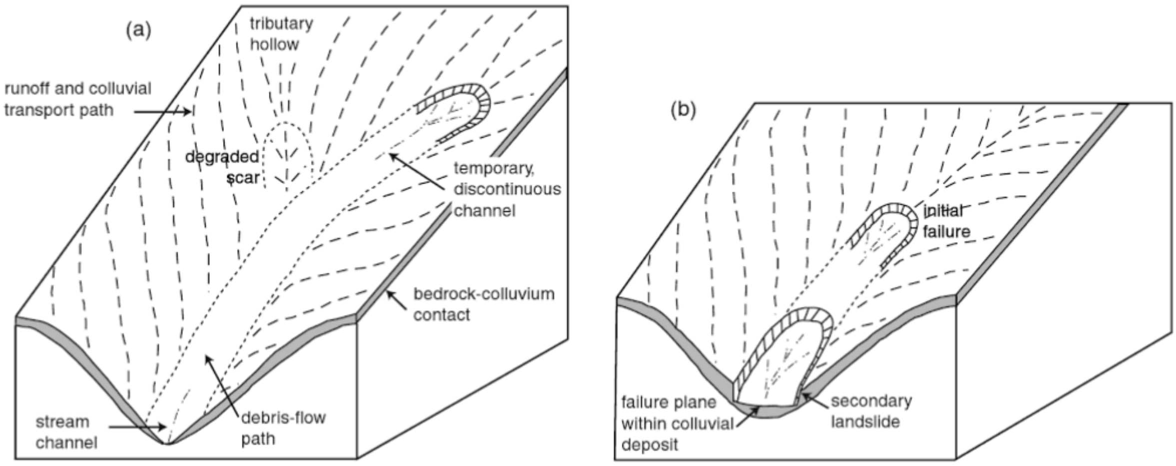

Figure 14. Conceptual sketch of typical landslide locations in soil-mantled landscapes. (a) Debris flow coming out of a topographic hollow. (b) Debris flow originating in a topographic hollow that gives rise to further landslides downslope (Lu & Godt, 2013, p. 41)

3.3 Environmental Setting

By stating "the past is the key to the future", (Highland & Bobrowsky, 2008, p. 46) point out that "future slope failure could occur as a result of the same geologic, geomorphic, and hydrologic situations that led to past and present failures". Consequently, environmental conditions such as climate, topography, morphology, hydrology, lithology and land use determine the spatial distribution of landslides and play a big role in explaining the cause of a landslide event. While the lithological and geological setting can be considered constant over long periods of time, the climatic and morphological settings and land use are more variable and exorable due to humans (Reichenbach, Busca, Mondini, & Rossi, 2014, p. 1).

3.3.1 Climatic Setting

The causal relationship between climatic conditions on the one hand, and landslides on the other hand has been explored in various studies (Borgatti & Soldati, 2010; Dikau & Schrott, 1999; Gassner, Promper, Beguería, & Glade, 2015; Jakob & Lambert, 2009; Sidle, 2007), most often in the context of climate change. While the correlation between climatic conditions and landslides is not as clear-cut as popular views might suggest (Flageollet, Maquaire, Martin, & Weber, 1999), research has provided ample support that specifically the factors precipitation and temperature, although never being the sole cause, play an important role in triggering landslides. There are numerous ways in which climatic conditions influence the landslide probability. In principle, climate dictates “the degree of weathering, the availability of moisture, and the type and structure of vegetation” (Lu & Godt, 2013, p. 13). To provide information on climatic conditions, the following section relies on data from the standard reference period 1981–2010 that has been provided from the Central Institute for Meteorology and Geodynamics of Austria (ZAMG, n.d.) The climate station most relevant for the study site is in Waidhofen an der Ybbs (47°57’28.08”N, 14°47’3.84”E), around 5,3 km away from the landslide.

The climate of Waidhofen an der Ybbs is characterized by four distinct seasons, moderate temperatures and high rates of precipitation year-round. In the most widely used climate-classification, the Köppen-Geiger Classification (see Kottek, Grieser, Beck, Rudolf, & Rubel, 2006), it is categorized as a Cfb-Climate. This describes a warm temperate fully humid climate with mean temperatures ranging from 18 °C to -3 °C in the coldest months, warm summers (T mean max < 22 °C) and at least four months with mean temperatures over 10 °C (Kottek et al., 2006).

Figure 15 provides a climate chart for the town of Waidhofen an der Ybbs. The average yearly temperature in Waidhofen an der Ybbs is 8.5 °C in the standard reference period 1981–2010, albeit temperatures vary greatly between seasons and during the day. Consequently, the average daily temperatures range from -1.5 °C in January, usually the coldest month, to 18.5 °C in July, typically the hottest month of the year. The average minima and maxima range from -4.5 °C (minimum in January) to 37.9 °C (maximum in July). The absolute minimum recorded temperature in the standard reference period 1981–2010 is -25.8 °C, whereas the absolute maximum temperature is 37.9 °C. The temperature variation denotes a pronounced seasonal pattern. On average, 50 days of summer (T > 25 °C) juxtapose 99 freezing days (T < 0.0°C). (ZAMG, n.d.)

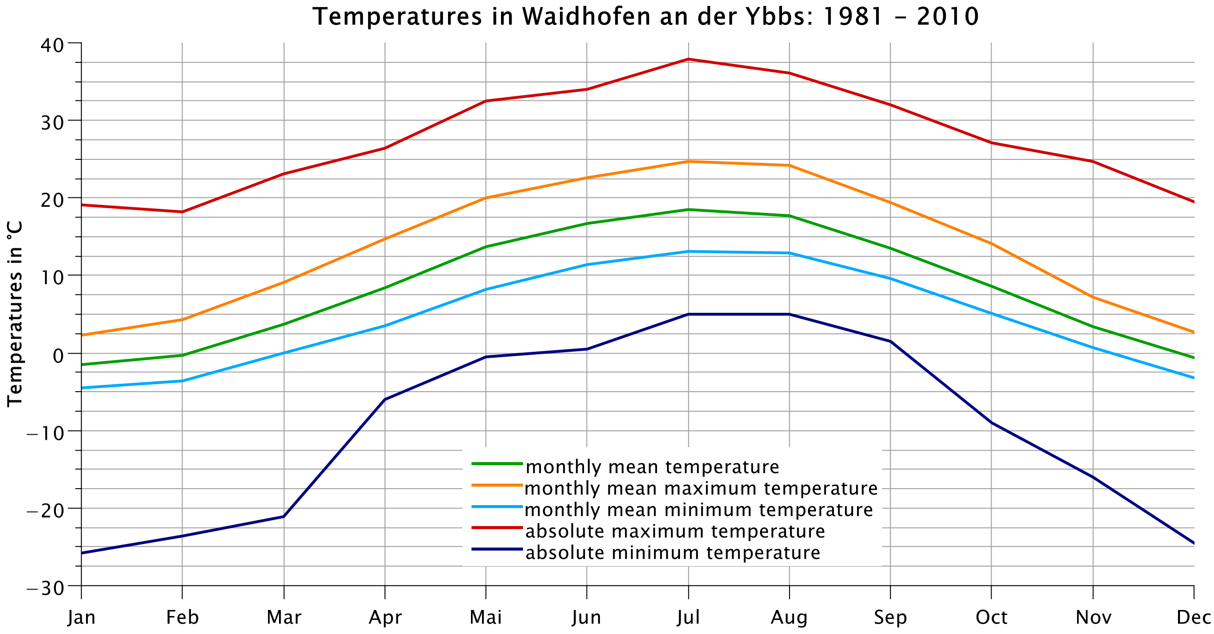

Figure 15. Mean monthly temperatures in Waidhofen an der Ybbs (data source: ZAMG, n.d.)

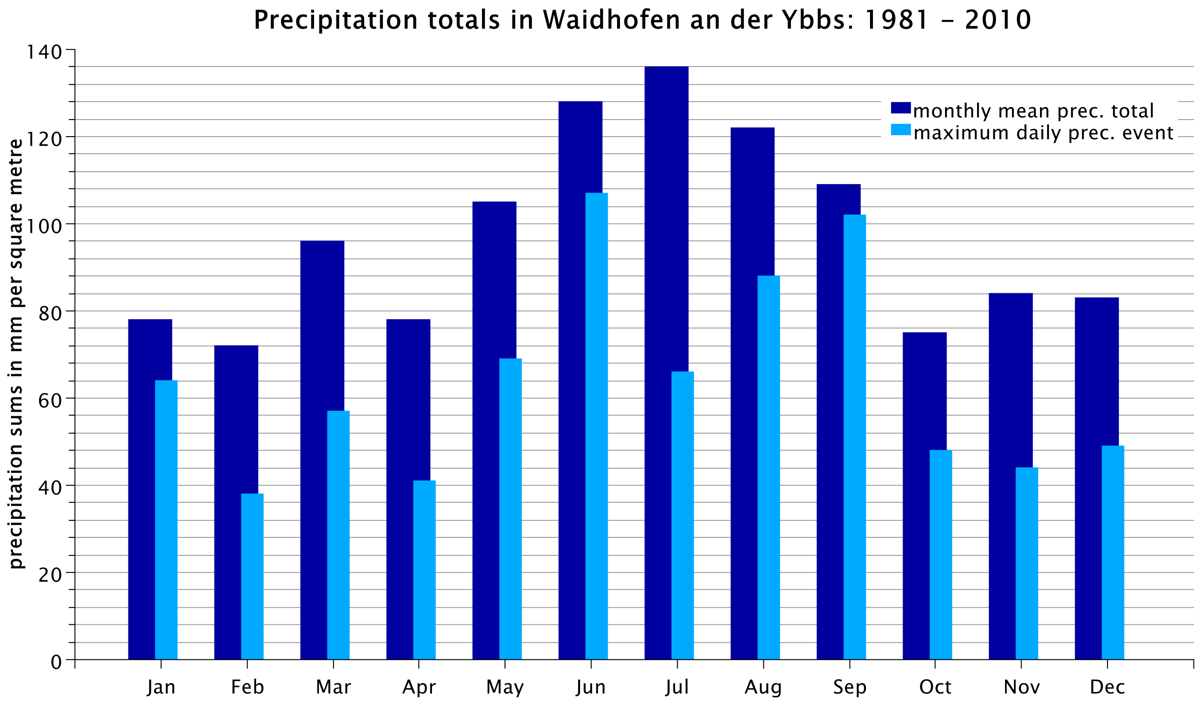

Figure 16. Precipitation in Waidhofen an der Ybbs in the standard reference period 1981–2010 (data source: ZAMG, n.d.)

With an overall mean of 1.165 mm a year. Waidhofen an der Ybbs has a humid climate. Figure 16 shows the monthly precipitation totals in the standard reference period 1981–2010. A precipitation concentration index (PCI) (as applied in Patel & Shete, 2015) of approximately 8.7 indicates uniform precipitation over the year, with peaks from May to September. During this time, monthly mean precipitation sums typically exceed 100 mm. Likewise, heavy precipitation events tend to occur during this time span. The record for daily precipitation in the standard reference period from 1981 to 2010 is 107 mm per square meter. The driest months, although still fairly humid, are January, February, April and October with monthly mean precipitation totals between 70 mm and 80 mm. From November to April, a major part of precipitation falls as snow. In the standard reference period 1981–2010 around 1.360 mm of snow fell during a year, most of it from December to February. (ZAMG, n.d.)

In the face of climate change, variables such as temperatures and precipitation are expected to change for this area within the next hundred years (Gassner et al., 2015, p. 430). Consecutively, the mean annual air temperature is considered to rise by 2.2 °C. In the scenarios applied, precipitation is projected to decrease by 11 %, however, heavy rainfall events are estimated to become more frequent (Loibl et al., 2007).

3.3.2 Hydrologic Setting

The hydrologic setting describes the movement of water in a given area (infiltration, evaporation, runoff, precipitation, transpiration, and ground water flow) and is controlled by other environmental factors, most of all climate and geology. In slopes, water movement is highly dynamic (either liquid or vapour), making it the most common physical mechanism that influences the spatial and temporal distribution of stress conditions in a slope and, consequently, landslide occurrence (Lu & Godt, 2013, p. 13).

The landslide lies in the catchment area of the north-easterly flowing “Redtenbach”-creek, that meets another creek (“Waidhofenbach”) approximately 4 km east of the slope, and eventually flows into the Ybbs river (BMNT, 2018), which has a catchment area of approximately 507 km² and an average runoff of 20 m³/s in the standard reference period 1981–2010 (BMNT, 2015, p. 23). In Ybbs an der Donau, approximately 40 km north-east of

Kondradsheim, the Ybbs enters the Danube. It is further located above the border of two groundwater bodies, namely the groundwater body of the Flysch zone in the north and the groundwater body of the Northern Calcareous Alps in the south (BMNT, 2018). The slides (see 3.2) are located around the channel of the Hofermühl-creek, which transports loose material down the valley bottom and further into the Redtenbach. The channel is deepest in the middle section of the slope (Sausgruber, 2013, p. 2). It features only low water levels. Since the slide from 2013 blocked the channel, the water infiltrates the slide mass. This is reinforced by drainages, which lead water into the channel, but are above the location where water seeps into the sliding mass. Therefore it can be assumed that water infiltrates into the sliding mass and slope. (Sausgruber, 2013, p. 5)

3.3.3 Geologic Setting

The geologic environment is a crucial factor in determining the landslide hazard of a given area. It consists of "the type of rock (igneous, sedimentary, or metamorphic), stratigraphy, structure (bedding, folding, and faulting), defects (joints and sheared and crush zones), and weathering" (Clague & Stead, 2012, p. 134). As suggested by Clague and Stead (2012, p. 134) the geologic underpinning strongly correlates with the likelihood and mechanisms of landsliding and influences landslide activity in several ways. First, tectonics might increase the likelihood of landslides through disruption, fissuring as well as the disintegration of rock formations.

Faults or chasms that lie parallel to the slope as well as integrated layers of marls or clays, which promote the formation of water-impermeable horizons or sliding planes, are further risk factors. The weathering of rocks affects their disintegration by reducing their strength and rigidity and so promotes landslides. (Schwenk et al. (1992)

Second, geology also affects landsliding by its effect on the hydrogeology and the extent of potential rupture surfaces in rock and soil (Ohlmacher, 2000, p. 10).

Waidhofen an der Ybbs is underlaid by a complex geology. Although relatively small in size, four major geological units meet in the district, namely the Helvetikum, the Penninikum, the Oberostalpin and the Molasse. The geological map of Lower Austria furthermore introduces the Quaternary as a separate unit. In Waidhofen an der Ybbs these units are represented mostly by the Rhenodanubian Flysch (Penninikum), composed of alternating layers of marls, clays, and sandstones, the Klippen zones (Helvetikum), outcrops of morphologically prominent marls and limestones, the Northern Calcareous Alps (Oberostalpin), carbonates that form rugged and steep terrain, and the Molasse, a body of clastic sediments, deposits and debris from the Alps (Wessely et al., 2006, pp. 16–19). All units are involved in landsliding (Petschko et al., 2010, p. 278) but the Flysch zone and Klippen zone are especially prone to landslides (Figure 17).

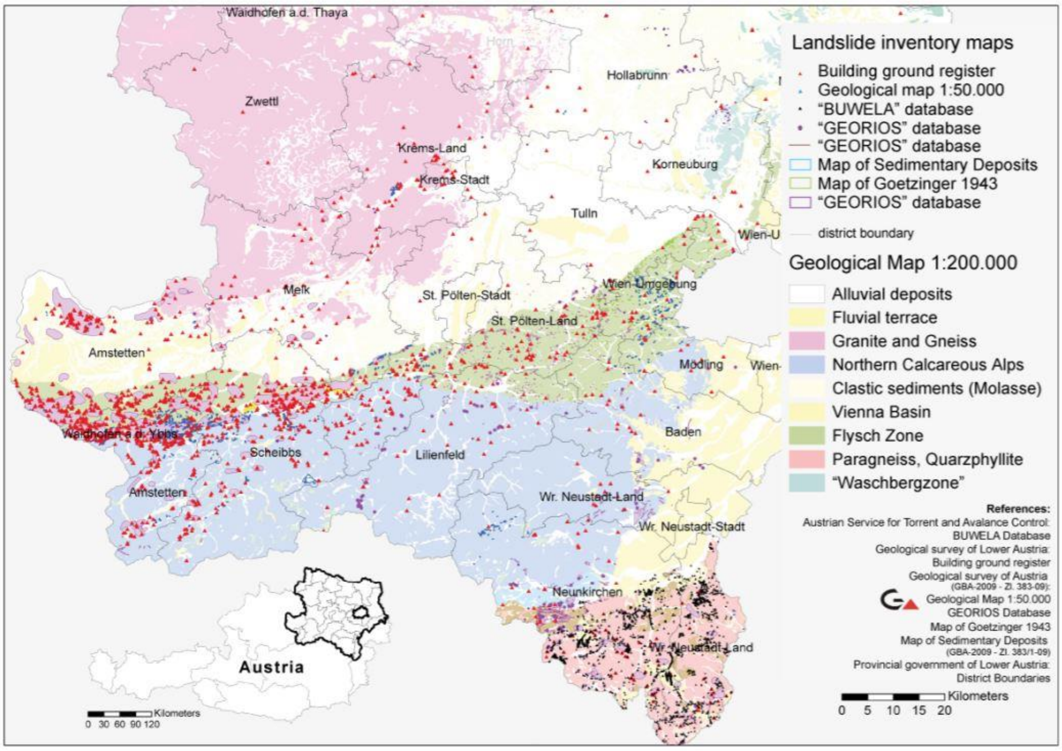

Figure 17. Spatial distribution of mapped landslides, geology and available landslide inventories for Lower Austria (Bell et al., 2011)

The Penninikum: Rhenodanubian Flysch

The Rhenodanubian flysch of the Penninikum is a deep sea sediment consisting of alternating layers of marls, clays, and sandstones, that were deposited from the late Lower-Cretaceous to the early Upper-Eocene through turbidity currents when the Penninic ocean disappeared (Schuster et al., 2015, pp. 33–34; Wessely et al., 2006, pp. 85–86). This makes it a part of the Penninic nappe. Sedimentary structures – such as sedimentary layering, current marks and trace fossils – are largely preserved in these rocks (Schuster et al., 2015, p. 34). It extends from the river Rhine to the Danube and forms rolling to mountainous terrain with gentle slopes and deep soils due to its easy weathering (Schnabel et al., 2002, p. 34; Wessely et al., 2006, p. 17). In Waidhofen an der Ybbs it is represented by the so called "Hauptflyschdecke" as well as the "Nördliche Randzone" (Wessely et al., 2006, p. 87) which take up the northern part of the district.

The (Ultra-)Helvetikum – Grestener Klippen Zone and Hauptklippen Zone

The Klippen zones of the Ultrahelvetikum refer to a group of morphologically prominent rocks from the Jura, mostly marls and limestones, that rise above the Rhenodanubian flysch (Schuster et al., 2015, p. 29; Wessely et al., 2006, pp. 18, 85, 95–97). These rocks come from the Helvetic shelf as well as the southern continental edge of the European plate. In large parts, the Rhenodanubian flysch is thrust over these rocks, but in the south they surface as a narrow band between the Rhenodanubian flysch and the Northern Calcareous Alps and are visible through Neustift, Konradsheim, Waidhofen an der Ybbs, Scheibbs and Traisen (Schnabel et al., 2002, p. 33). Wessely et al. (2006, p. 97) furthermore mention two local types of rock: The "Konradsheimer Klippen" and the "Konradsheimer Konglomerat". The former is comprised of a "feindetritisch" section and a calcareous limy, coarse and clastic section. The latter is a brownish to greyish massive rock made up of calcareous components of different sizes and roundness. Embedded in the "Konradsheimer Konglomerat" are chips of dark grey and greenish-grey marls which were deposited in more recent times (Wessely et al., 2006, p. 97).

The Molasse – Inneralpine Molasse

Embedded in the Grestener Klippen zones are sections of the Inneralpine Molasse, sediments from both the Alps and the Bohemian Mass that were deposited in the Upper Eocene to the Oligocene. When the Alps formed, these rocks were transported north from their origin to their current position (Schnabel et al., 2002, p. 28). They are comprised of clay marls as well as sandstones (Schnabel et al., 2002, p. 7). The Molasse is characteristic for its flat morphology that stands out between the Flysch zone in the north and the Klippen zones in the south (Schnabel et al., 2002, p. 7).

The Oberostalpin – Northern Calcareous Alps

The Northern Calcareous Alps of the Oberostalpin dominate the southern part of the district. They are marine sediments made up of layers of carbonate rocks such as limes and dolomites that were deposited in different sedimentation areas from the Perm to the Paleocene (Wessely et al., 2006, p. 105). During the formation of the Alps these sediments were separated from their basis and largely deformed to form nappes of compressed and folded layers of rock (Schnabel et al., 2002, p. 36). From this unit only the Bajuvarikum, consisting of the Frankenfelser, the Lunzer and the Sulzbach nappe surface in Waidhofen an der Ybbs (Wessely et al., 2006, p. 105).

Quaternary

The geologic map of Lower Austria furthermore introduces the Quaternary as a separate unit, although strictly speaking it is not a tectonic unit like the others mentioned, but rather used as a collective term referring to visible marks of processes of erosion, deposition, translocation and glaciation during and after the genesis of the Alps (Wessely et al., 2006, p. 235).

Geology in the Closer Perimeter of the Study Site

The study site in Konradsheim is situated in a transition zone of these geological units. From north to south are rocks of the Rhenodanubian flysch, followed by a narrow band of rocks from the Klippen zone and, eventually, rocks from the Northern Calcareous Alps. The sediments from the Molasse, as well as the Quaternary are scattered through the region. The rocks present on the analyzed slope are weathered sandstones and marls as well as clays (Sausgruber, 2013, p. 2, 2016). The sandstones and marls form rocky rips at the lower part of the slope, which have a dip of 35°W – NW (Sausgruber, 2013, p. 2).

3.3.4 Soils

Soils themselves are the result of a range of environmental factors such as geology, climate or vegetation and pedogenic processes. As such, they influence the spatial distribution of landslides. Specifically, the type of material and its mechanical properties are decisive for the landslide risk. For instance, clayey soils and fine textured soils in general behave very differently than non-clayey soils or coarse textured soils. They have a higher capacity to hold water and are largely impermeable to water, promoting the formation of a sliding plane (Sidle, Pearce, & O'Loughlin, 1985, as cited in Kitutu, Muwanga, Poesen, & Deckers, 2009, p. 611).
Thus, certain soil characteristics may be used to assess the landslide risk (Zung, Sorenson, & Winthers, 2009, p. 1) as well as the possible mode of failure.

As recorded in the Digital Soil Map of Austria "eBOD" (BFW, 2007), typical soils in Waidhofen an der Ybbs are Cambrisols (specifically Felsbraunerde and Lockersediment-Braunerde), Plastosols, Gleysols, and Planosols. In the northern part of the district, Cambrisols, Gleyosols and Planosols are common. In the southern part of the district, information on soils is scarce, since the area is densely forested and soils under forests are not examined. Typical soils are most likely to be Cambrisols and Rendzina soils. In the western part of the district, where the study site is located, Cambrisols, as well as Planosols prevail. The soil type indicated for the study site is Cambrisol (felsic Cambrisol) with spatially differing soil properties. Included in Appendix A. Additional Information are three soil profiles from locations which are in close vicinity to the study site. Profile A indicates a loose sediment with three horizons on a bedrock consisting of gravel and smaller alluvial materials. Profile B and C show very similar types of soil, namely a clayey rocky brown earth made up of four horizons. The original rock is siliceous flysch and weathered sandstone. In general, rocks like like clay, clay marl, clay slate, marl slate, or lime marls tend to develop thick layers of weathered rock and soils, since they weather very easily when exposed (Schwenk et al., 1992, pp. 620–621).

As various soil samples have shown (Schwenk et al., 1992, p. 622), soils in the study area are heterogeneous. Most of the time, different soil types are intertwined, not extending over larger areas and remaining fragmentary. This is mostly due to the diversity of the bedrock (featuring different types of rocks) as well as the permanent motion of soils that develop on slopes. In the Flysch and Klippen zone, cohesive and slightly cohesive soils are common, many of them containing loamy or fine-sandy layers, sands, coarse sands or scattered layers of rock debris. (Schwenk et al., 1992, p. 622)

3.3.5 Land Use and Land Cover

Land use has a major impact on soil stability. As Promper, Puissant, Malet, and Glade (2014, p. 1) propose, land cover on the one hand acts as predisposing factor and on the other hand controls the number of elements at risk. In Waidhofen an der Ybbs, forests and cultivated grasslands are the most dominant types of land use. Except for single farmhouses or scattered settlements, residential as well as industrial areas and other types of infrastructure are concentrated in the valley bottoms and take a smaller share of the area. In accordance with this, only little land is cultivated (Promper et al., 2014).

The study site itself is covered and surrounded by cultivated grasslands in the north and east, and very small mixed forests in the west and south. Near the study site are conifer forests as well as mixed forests (BMNT, 2018).

3.4 Landslide Hazards in the Study Area

Landslides are a common hazard throughout large parts of the province of Lower Austria (Schwenk et al., 1992, p. 598) but are most frequent in the alpine and pre-alpine regions (see Figure 18). Numerous factors are involved in the process of landsliding in the study area.

Within Lower Austria, the district of Waidhofen an der Ybbs is particularly prone to landslides (Petschko et al., 2010, p. 278). In 2010 Petschko et al. counted 691 landslides in total in their inventory and in 2012, Glade et al. (2012, p. 503) mapped a total number of 1.063 landslides in another inventory. Landslides occur in all of the four lithological units present in Waidhofen an der Ybbs, however, the Flysch zone features by far the highest landslide density (61.8 %) (Petschko, Bell, Glade, & Brenning, 2012, p. 770). Second is the Klippen zone with 6.4 % (Petschko et al., 2012, p. 770). The most common style of movement in the study is sliding. Out of the many landslides Petschko et al. (2010) counted, 522 were classified as distinct slides, 141 as areas with slides, 25 as areas with flows, and 3 as complex slides. While in some regions like the "Bucklige Welt" slides are typically shallow and small, they can develop into extensive slides in Scheibbs, Gresten as well as in Waidhofen an der Ybbs, due to the mechanical properties of the underlying rocks and their tendency to develop into thick layers of weathered, unconsolidated rock (Lotter & Haberle, 2013, p. 14).

An older inventory, provided by Schwenk et al. (1992), examined reported landslides between 1953 and 1990 in terms of landslide type and the factors that likely contributed to the reported landslide events. Although the inventory does not provide an accurate representation of the relative frequency of landslide types (some types are under-reported), it yields a comprehensive picture on landslide processes in Lower Austria.
According to Schwenk et al. (1992, pp. 604–609) rockfalls occur primarily in mountainous areas where rock walls are exposed and subject to weathering processes. They are most common in the Northern Calcareous Alps, which are characterized by a high relief intensity (Schwenk et al., 1992, pp. 604–609). Similarly, rock slides are most common in the mountainous area of Lower Austria where paths of movement (potential slide surfaces) exist within the rock unit, for example between different layers in a rock or in a joint plane or slickenside (Schwenk et al., 1992, p. 617). The same is true for earth or debris flows, which are most common in the Northern Calcareous Alps where loose and non-binding taluses are

abundant (Schwenk et al., 1992, p. 644). Often they succeed a slide event (Schwenk et al., 1992, p. 644). The type of landslide reported by far the most often are earth slides (Schwenk et al., 1992, p. 619). Other than rockfalls, slides occur in areas with a gentler relief. These areas are usually more populated and humans as well as infrastructure are frequently affected by slides (Schwenk et al., 1992, p. 619). Earth slides happen most frequently in the Flysch zone and Klippen zone due to a combination of factors, most notably geology, slope steepness and the presence of thick layers of weathered soils (Schwenk et al., 1992, pp. 619–620). Considering land use, landslides tend to occur more often in pastures than in forests and acreage (Schwenk et al., 1992, p. 627). In forests, the roots help to stabilize the ground. The acreage is mostly located in the valley bottoms, where the slope angle is not big enough for landslides to happen (Schwenk et al., 1992, p. 627). The mean slope angle on slopes exhibiting landslides in the Flysch and Klippen zone is 29° and the commonly occurring type is the rotational slide (Glade et al., 2012, p. 627).

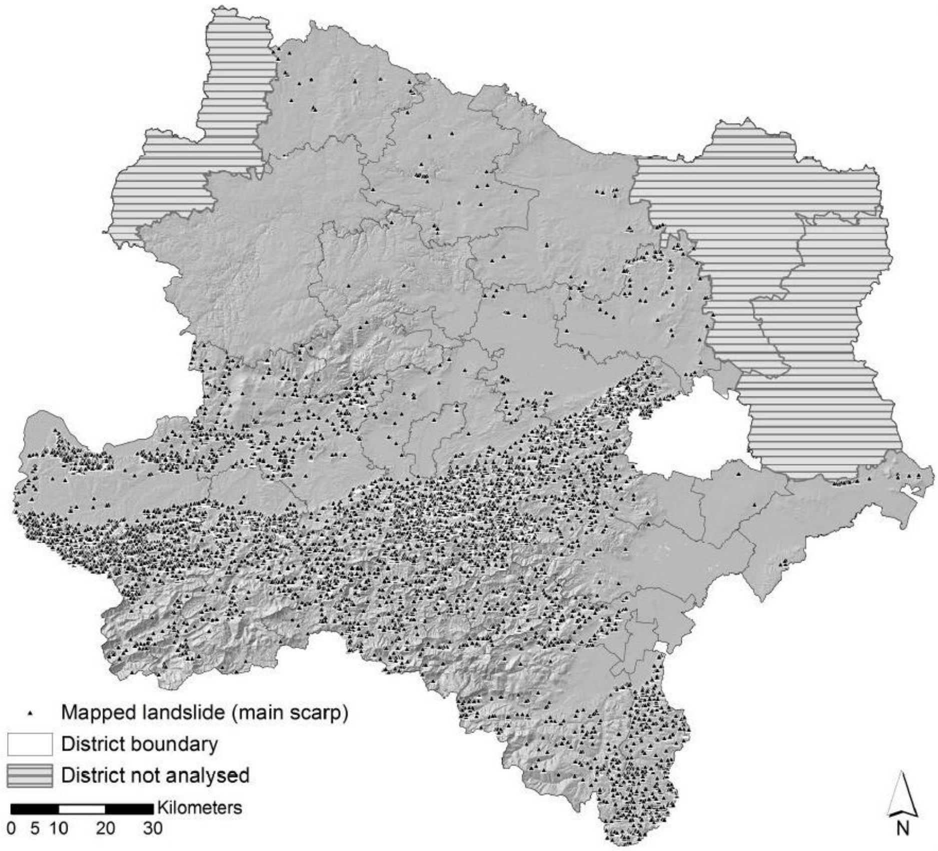

Figure 18. Spatial distribution of landslides across Lower Austria (Glade et al., 2012, p. 503)

Geologic Factors

A decisive cause of landslides in Waidhofen is geology (see section 3.3.3) as indicated by several inventories (see section 3.4). Schwenk (1992) reasoned that geology is responsible for a high susceptibility to landslides even in non-high alpine region with moderately steep slopes. The link between geology and landslide activity is illustrated in Figure 17. The rocks in the Flysch zone are impermeable to water and highly susceptible to sliding. Consequently, the flood hazard is high when heavy rainfalls occur (Schnabel et al., 2002, p. 34) and lithologically induced landslides are common (Wessely et al., 2006, p. 17).

Soils

As mentioned above, thick mantles of weathered rock and soil are common in the study area. In addition to their thickness, these soils often contain clayey, silty layers that are known to be especially fragile towards sliding. Their shear strength is already low compared to other soils and decreases further when they become wet (Schwenk et al., 1992, pp. 620–621). In binding soils, which are common in the study area, the shear strength is the determining property of soil stability (for non-binding soils it is the angle of friction). The lower the shear strength (or the angle of internal friction), the easier it is to disturb the force-balance within the slope. If present, layers of sand or gravel above these layers have a particularly bad effect on slope stability, since they lead water downwards easily and promote a flow of water in line with the slope along the weak layer of silt and/or clay. (Schwenk et al., 1992, p. 622)
A slide tends to occur along the binding soil layers, which is why they are considered pre-existing failure lines. In autochthonic and homogenous soils (soils from only one original rock), the slide plane does not develop until the force balance is disturbed. Usually, it is of circular shape. In some cases, the bedrock, which is impermeable to water, will act as the slide plane. (Schwenk et al., 1992, p. 625)

Climatic Causes

Although the geology and the soils present in the study area make landslides very likely, they are most often triggered by the action of water. Schwenk et al. (1992) observed that most landslides happened shortly after storms, persistent rainfall or during the annual thawing. Water can have such a devastating effect on slope stability because it changes the force balance in the slope.

Prinz (1982, p. 267, as cited in Schwenk et al., 1992, p. 622) describes the mechanism of disturbing the force balance by water as follows: First, the shear strength of the soil is reduced with increasing water saturation and a change in consistency. Second, promoting forces grow because of an increase in weight (due to the water saturation of the soil) and pore-water pressure increases. Additionally, flow pressure might emerge. Third, resisting forces decrease as a result of the uplift. Thus, as the consistency of the material changes and cohesion and internal friction is weakened, shear strength of the layer might be reduced enough to trigger movement.

Factors Relating to Vegetation

It has been observed by Schwenk (1992, p. 627) that landslides most likely occur in pastures and less in forests or acreage. Acreage in Waidhofen an der Ybbs is concentrated in the valley bottoms, where the relief does not allow for landslides. Forested areas might be less prone to landslides because of the stabilizing effect of the roots. While it is true that roots can decrease slope stability due to the destructive force of growing roots, it can be reasonably assumed that, in the study area, roots tend to stabilize slopes more than destabilize them since the soils are thick and the roots might have a beneficial effect in holding the soil in place.

Anthropogenic Factors

Natural external factors such as undercutting of a slope through a river are only rarely the cause of a landslide in Lower Austria. Far more often human intervention causes a landslide in the study area, for example on account of building houses, roads or other infrastructure. On cultivated land, the practice of levelling leads to a decrease in slope stability. The human impact in Waidhofen an der Ybbs on landslide activity is big, however, humans only rarely trigger a landslide. (Schwenk et al., 1992, p. 599)

4 Methodology

Landslides are a complex phenomena and their study requires a multi-disciplinary approach (Perrone et al., 2014, p. 129), usually consisting of multiple methods. By combining methods that complement each other, the drawback of each method may be overcome, and the reliability of the acquired data increased. The following chapter will give an overview of the methodology of the study as well as all the instruments used.

Since information on the subsurface of the Hofermühle-landslide and adjacent slopes is scarce at this point, the focus of this study lies on subsurface investigation techniques. Considering the aim of the study as well as the availability of instruments, a combination of geoelectrics (Electrical Resistivity Tomography) and geotechnical methods (Percussion Drilling and Dynamic Probing Heavy) appeared most promising for the subsurface-exploration of the Hofermühle-landslide. Figure 19 provides an overview of the methodological approach.

Dynamic Probing Heavy (DPH) provides punctual information about the ground resistance to penetration. It may be used for the qualitative determination of layering in the subsurface. Specifically, it is expected to yield information about the depth of very dense or particularly loose layers in the ground, e.g. the bedrock or weakness zones (see section 2.6). Electrical Resistivity Tomography (ERT) yields 2-dimensional information on electrical properties of the subsurface. From a contrast in the electrical properties, subsurface structures such as sliding surfaces and high water content areas may be detected. However, the relation between indirect properties, i.e. electrical properties or mechanical properties, and the properties of interest are not straightforward, potentially causing ambiguity in the interpretation of data obtained through ERT and DPH. Therefore, ERT and DPH is supplemented by Percussion Drilling (PD). PD provides ground truth information on soils specific values and is expected to yield information on the materials involved as well as explain some variation in the distribution of resistivity values or penetration resistance. Thereby, PD may be used to validate results obtained through indirect methods. At the same time, ERT, primarily, and DPH, secondarily, are used to extrapolate data obtained through PD (see Figure 19).

The first step in the investigation of the landslide was a brief field exploration. Next, the measurements were conducted in several field campaigns. In the first field campaign in August one ERT profile running from north to south on the slope adjacent to the slide was conducted. The corresponding GPS-points were collected one week later on a separate day. On another day in August, three penetration tests (DPH) and one drilling (PD) were performed. During one last campaign at the end of November six more ERT profiles, running from north to south and parallel to each other, were recorded and their GPS-points collected. After collecting the different data, laboratory work and data analysis were performed.

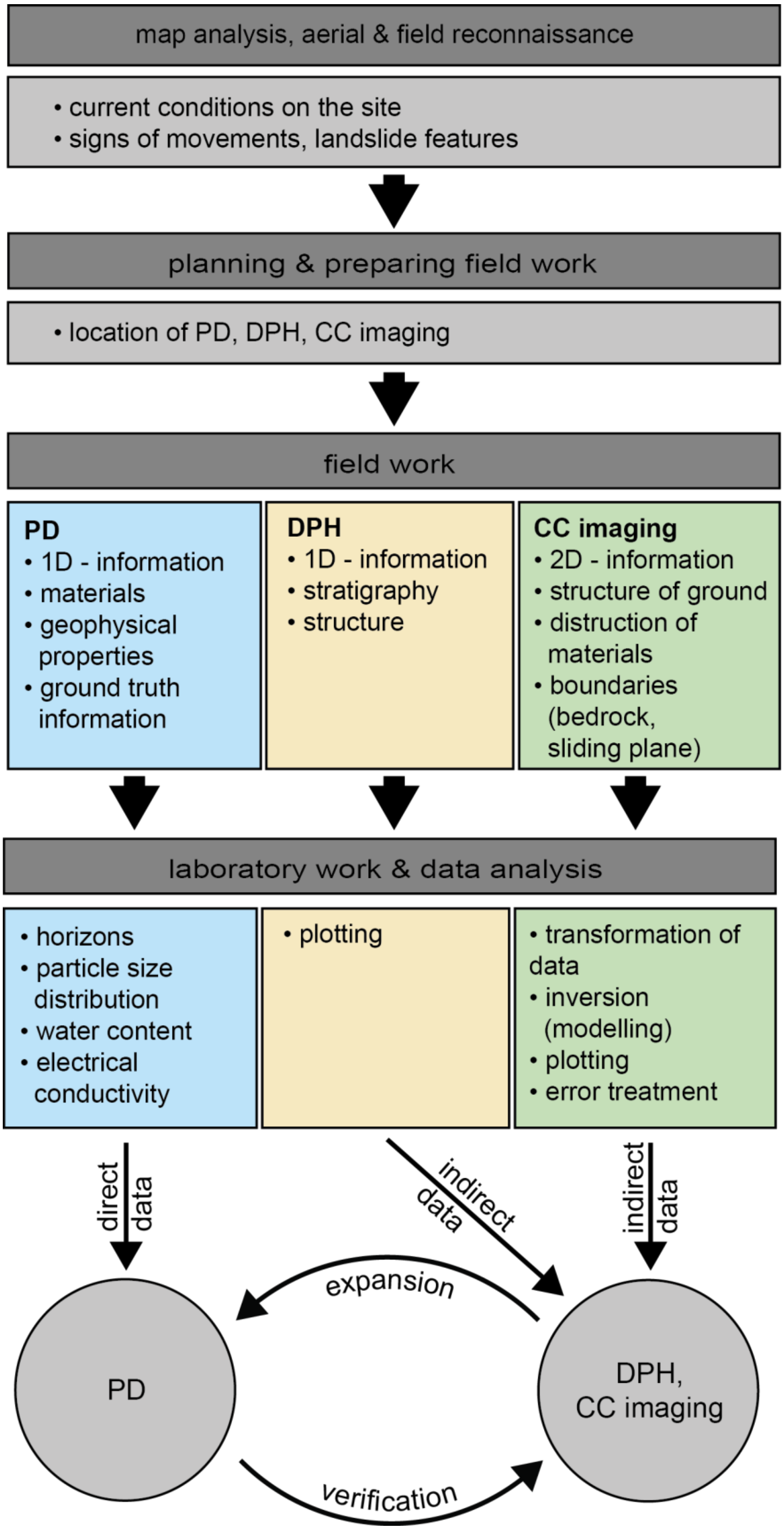

Figure 19. Methodological approach: The image shows the steps of the study in a chronological order.

4.1 Aerial and Field Reconnaissance

The first step in the investigation was a brief aerial and field reconnaissance. The objective of this phase was first to determine the area most relevant for the investigation, that is, the area most endangered to future movement, and, second, to specify the locations for ERT, PD and DPH. Satellite images were used to locate prominent landslide features and characterize the environment in the closer perimeter of the study site (meadows, forests, infrastructure, etc.). The digital elevation model for Lower Austria provided information on the relief in the form of a map. Based on the relief map the extent of the landslide activity on the slope as well as in areas close to the study site was estimated. Finally, the relief map was also used to determine a location that is accessible for the device that will be used for DP and DPH (GTR 780 V by Geotool). During a brief field exploration in June 2017, the study site was examined for more subtle signs of movement, which might have gone unnoticed in the analysis of aerial images and maps.

4.2 Percussion Drilling

Percussion Drilling was conducted on one site on the slope. The instrument used is a GTR 780 V (or GTR 780 Standard) by Geotool. It features a hydraulic rig as well as an auto reverse valve for the rod extraction unit. The operating weight is 63.5 kg and the dropping height can be varied.

Cylindrical steel tubes equipped with plastic inliners (plastic pipes) were used as sample tubes. The sample tubes and pipes were both 1 m long. The diameter of the plastic inliners was 50 mm. Through percussive action, the sample tubes were pushed into the ground and soil samples were collected. Table 3 lists the device settings.

PD was confined by the slope angle to a relatively flat area near the crown of the landslide. To ensure comparability of the acquired data, the drilling was conducted near the ERT profile 1 and 2 and DPH 2. The location is given in Table 3 and indicated in a map at the end of this chapter (Figure 21). Due to time constraints, only 4 m of disturbed samples (1-meter-long cores) could be extracted from the ground.

Table 3. Device settings for GTR 780 V by Geotool

Location of drilling		Device settings GTR 780 V (or GTR 780 Standard)	
Latitude:	47.95030756	Operating mass:	63.5 kg
Longitude:	14.71473719	Dropping height:	750 mm
Accuracy:	± 5.0 m	Diameter:	50 mm

As indicated in section 2.8, the clay and water content as well as the electrical conductivity of the soil solution are the properties most influential to the conductivity of a soil. In a laboratory analysis, soil samples from the drill cores were thus analysed in terms of horizons, particle size distribution, water content and electrical resistivity of the soil solution. To analyse the drill core, the plastic inliners were cut open on two sides. The soil itself was then cut through with a knife, so that each 1 m long segment was halved.

4.2.1 Visual Characterisation

The first step in the analysis was determining the horizons according to colour and texture differences. Some parts of the cores were excluded from further analysis, since they appeared to have fallen down the bore-hole during the drilling.

4.2.2 Particle Size Analysis

The particle size distribution was examined for eight soil samples. The analysis was conducted by combining sieving and sedimentation analyses in accordance with ÖNORM L 1061-1 and ÖNORM L 1061-2. The particle size analysis consisted of several steps. First, two soil samples per segment were taken from the core. Using a knife, each probe was reduced to small pieces and dried at around 43 °C. Once dried, remaining clumps of soil were broken up in a mortar and individual pieces of gravel were removed. Next, portions of the dried samples were scaled and mixed in a 100 ml beaker with sodium diphosphate ($Na_4P_2O_7$), a deflocculating agent that helps disaggregating soil and suspending colloidal clay particles. After resting overnight, the beaker was placed beneath an ultrasonic mixer for four minutes until the sample showed no signs of flocculating.

The coarse grain fraction (gravel and sand) was then separated from the fine grain fraction (silt and clay). All disaggregated samples were then filtered through a sieve with a mesh size of 63 µm using de-ionized water. A funnel was placed onto the measuring cylinder and the sieve was placed on top of the funnel. The runoff, containing the silt and clay fraction, was collected in a 1000 ml measuring cylinder for further analysis while the coarse grain fraction was transferred from the 63 µm sieve to a small bowl using a washing bottle and dried at 43°C. After drying, they were manually filtered through a series of sieves of different mesh sizes (2 mm, 630 µm, 200 µm und 63 µm). They were then scaled and the weight ratio of each fraction (gravel, coarse sand, medium sand and fine sand) was calculated.

For the analysis of the fine fraction (silt and clay) the Köhn pipette method (ÖNORM L 106-2), which takes advantage of Stokes law, was applied. Thereby, particles are separated from each other according to their sedimentation velocity, for which an equivalent diameter of spherical particles of equal density and sedimentation velocity can be deduced. The cylinder containing the runoff was first filled up with de-ionized water up to the 1000- ml marking. The soil suspension was then homogenized. At fixed intervals, a specific amount of the soil suspension was taken using a pipette. The weight fraction of a specific particle size was estimated by comparing the weight difference of two consecutive samples. The samples were transmitted to a bowl, dried at 105 °C and weighed within an accuracy of 1/10 mg.

The obtained data was plotted in two sets of diagrams. For an overview, the results were plotted in broad categories (gravel, sand, silt and clay) against the depth (see section 5.2.3, Figure 26). For a more detailed analysis of the fine fractions, the fractions sand silt and clay were each split into three categories and plotted in a frequency chart (see section 5.2.3, Figure 27 to Figure 30).

4.2.3 Water Content

The natural water content was analyzed according to ÖNORM L 1062. In total, eleven soil samples were taken from the drill core. They were then placed on a petri dish, scaled and dried overnight at around 105 °C. When dried, each sample was scaled once more. The water content was determined by measuring the difference between the mass before and after drying. The acquired data was then plotted against depth (see Figure 26).

4.2.4 Fluid Conductivity

Eight soil samples were analysed in terms of the fluid conductivity. The extract was produced according to ÖNORM L 1092. The samples (two from each segment of the drill core), were reduced to small pieces in a mortar, placed on a petri dish and dried at 43 °C for around two days. After the samples dried, 10.00 g of soil were filled into glasses and mixed with 100 ml distilled water. The solution rested overnight. The samples were then shaken well and set aside so that solid particles could settle on the bottom of the glass. From the solution of water and dissolved charge carriers (ions), a small amount was decanted into another glass. The conductivity of the solution was then measured with a conductivity meter. The temperature of the fluid was recorded too. Results are plotted in a diagram of electrical conductivity against depth (see Figure 26).

4.3 Dynamic Probing Heavy

Three penetrations tests were conducted during the field campaign. The use of the instrument was restricted by the slope angle to an area close to the crown of the landslide. The positions of the three sites are given in

Table 5 and Figure 21. DPH was conducted with the same device as PD. Instead of sample tubes, a rod with a cylindrical cone was used instead. The GTR 780 V (or GTR 780 Standard) is designed for dynamic probing according to DIN EN ISO 22476-2 and DIN EN ISO 22476-3 and can be applied for lightweight, medium heavy and super heavy dynamic probing tests by adjusting the operating mass and the dropping height. In this study, the operating mass was 63.5 kg and the dropping height was set to 750 mm. The cone angle was 90° and its diameter was 43.7 mm. The device settings used in this study are presented in Table 4. In order to reduce skin friction, the rods were rotated 1.5 times every 1 m penetration, as suggested by Mayne and Quental Coutinho (2012, p. 400).

The bracing to keep the rod in a fixed position while operating the device was missing, causing looseness in the rod. Thus, the DIN 4049 norm could not be fully implemented. Nonetheless it appears safe to assume that the data quality is good enough for a qualitative assessment, especially because profiles will not be compared to other locations or techniques.

Table 4. Device settings for Dynamic Probing Heavy GTR 780 V (or GTR 780 Standard) (Geotool)

Operating Mass:	63.5 kg	Cone Angle:	90°
Dropping Height:	750 mm	Diameter:	43.7 mm

Table 5. Location of DPH profiles

Profile 1 (6 m)		Profile 2 (6 m)		Profile 3 (13 m)	
Latitude:	47.94994422	Latitude:	47.95033233	Latitude:	47.95028585
Longitude:	14.71491874	Longitude:	14.7147058	Longitude:	14.71474563
Accuracy:	± 4.0 m	Accuracy:	± 4.0 m	Accuracy:	± 4.0 m

4.4 Electrical Resistivity Tomography

The method used for the survey is the Electrical Resistivity Tomography (ERT). It provides a 2D image of the electrical conductive properties, as in surface imaging.

While the device can be used for measuring both electrical conductive and capacitive properties (as in Complex Conductivity imaging), and several profiles for the assessment of the induced polarization effect were recorded, only the resistivity data is presented in this study.

The measurement of electrical properties was conducted by with a multi-electrode set-up. In such set-ups, more electrodes than needed for a single measurement (four) are used so that multiple measurements can be taken in a single reading. Multiple electrodes are plugged into the ground at equal distances in a straight line. Each electrode is connected to a multi-core cable with multiple electrode take-outs, a switching unit and, usually also a computer. The electrodes can be used as either transmitter or receiver (current and potential electrodes) and their function is switched automatically (or manually, as desired) in a predefined sequence by the switching unit (and computer). Figure 20 provides an illustration of the measurement principle. Efficiency is increased when multiple channel resistivity meters are used. These allow the simultaneous measurement of adjacent dipoles (pairs of potential electrodes).

The variation in the combination of transmitter and receiver electrodes provides a pseudo section for the apparent electrical property that is investigated (e.g. resistivity or chargeability).

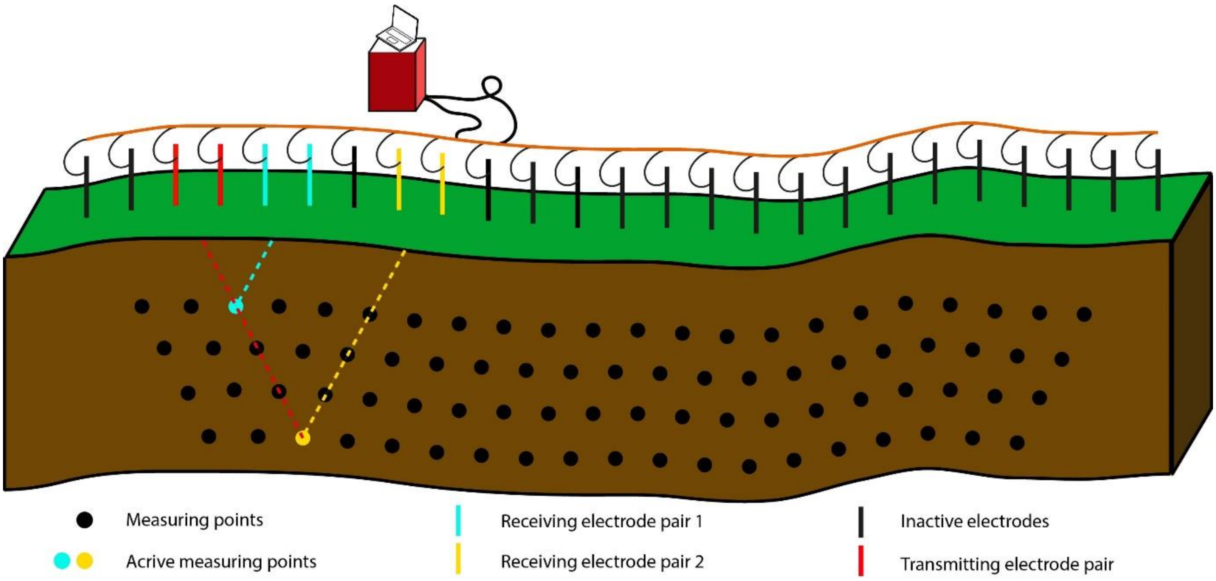

Figure 20. Measurement principle for multi-electrode electrical surveys for a profile in the diploe-dipole configuration

The depth of the investigation largely depends on the distance of the outermost electrodes. Longer profiles than can be achieved with a given set of electrodes (or a given cable length) are created by means of the roll-along technique, where further segments are added to the first one by simply moving the cable with the electrodes along a transect. However, the geometry of the setting prevents that the new segment is simply attached at the end of the first one. To achieve an image with a continuous depth, some of the electrodes of the first and the second section must overlap.

4.4.1 Instrument

The resistivity-meter used is a SYSCAL Pro all in one-unit (consisting of transmitter, receiver and booster). It is designed for high productivity surveys of the investigation of near-surface structures in the ground. Both resistivity and chargeability data can be collected by measuring the primary voltage and the decay voltage. The resolution of the primary voltage is 1 µV. The unit features multi-core cables to which electrodes can be attached at a fixed spacing (e.g. every 1 or 5 meters) and plugged into the ground.

4.4.2 Taking the Readings

The ERT profiles were taken in two field campaigns. In the first field campaign in August 2017, one ERT profile running directly along the crown of the landslide was recorded (see Figure 21). The profile was collected with a roll-along of three sections, each counting 72 electrodes with 1 m intervals. The electrode overlapped by a count of 18 and 17 electrodes, resulting in a total number of 181. The profile was 180 meters long. The resolution of the data was 25 cm. It extended from the thin vegetation band on the upper part of the slope (north) to a couple of meters ahead of the forest (south). With this setting, two objectives were fulfilled. First, the area most relevant to the survey, as pinpointed in the map analysis as well as aerial and field reconnaissance (see section 5.1) was covered. This area is located on the orographic left of the Hofermühl-creek, on the upper part of the slope (see Figure 23). Second, the profile extended over the area accessible for the Geotool crawler, ensuring sufficient data coverage and comparability with the results obtained from PD and DPH.

In a second field campaign in November 2017, six more ERT profiles running north to south were recorded. This time, the electrode spacing was increased to 5 m to obtain a better resolution in a greater depth. The profiles were laid-out in parallel lines at 5 m intervals from west to east (see Figure 22). The resolution of the data was 1 m.

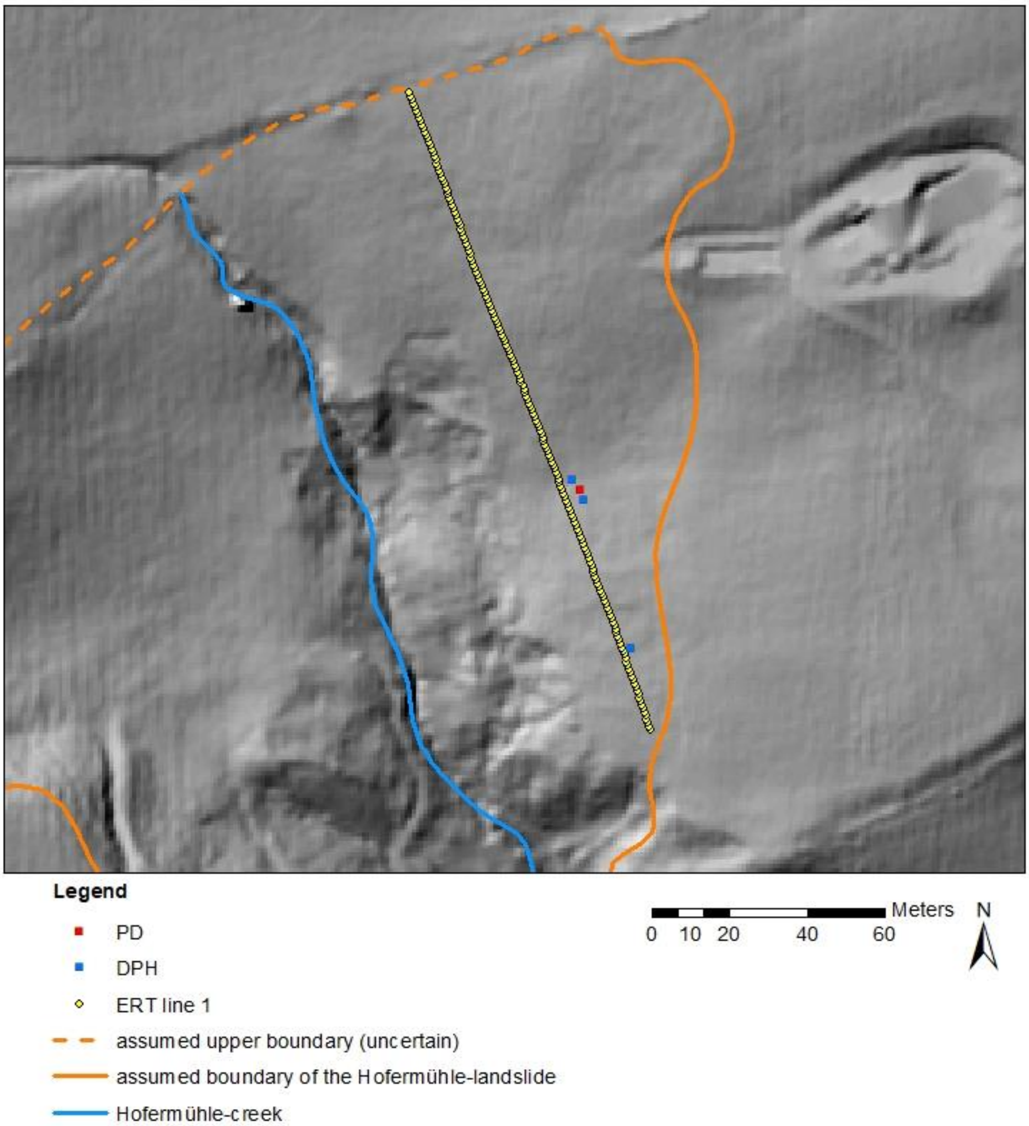

Figure 21. Location of ERT line 1 (yellow), PD (red) and DPH (blue); base layer: Land Niederösterreich

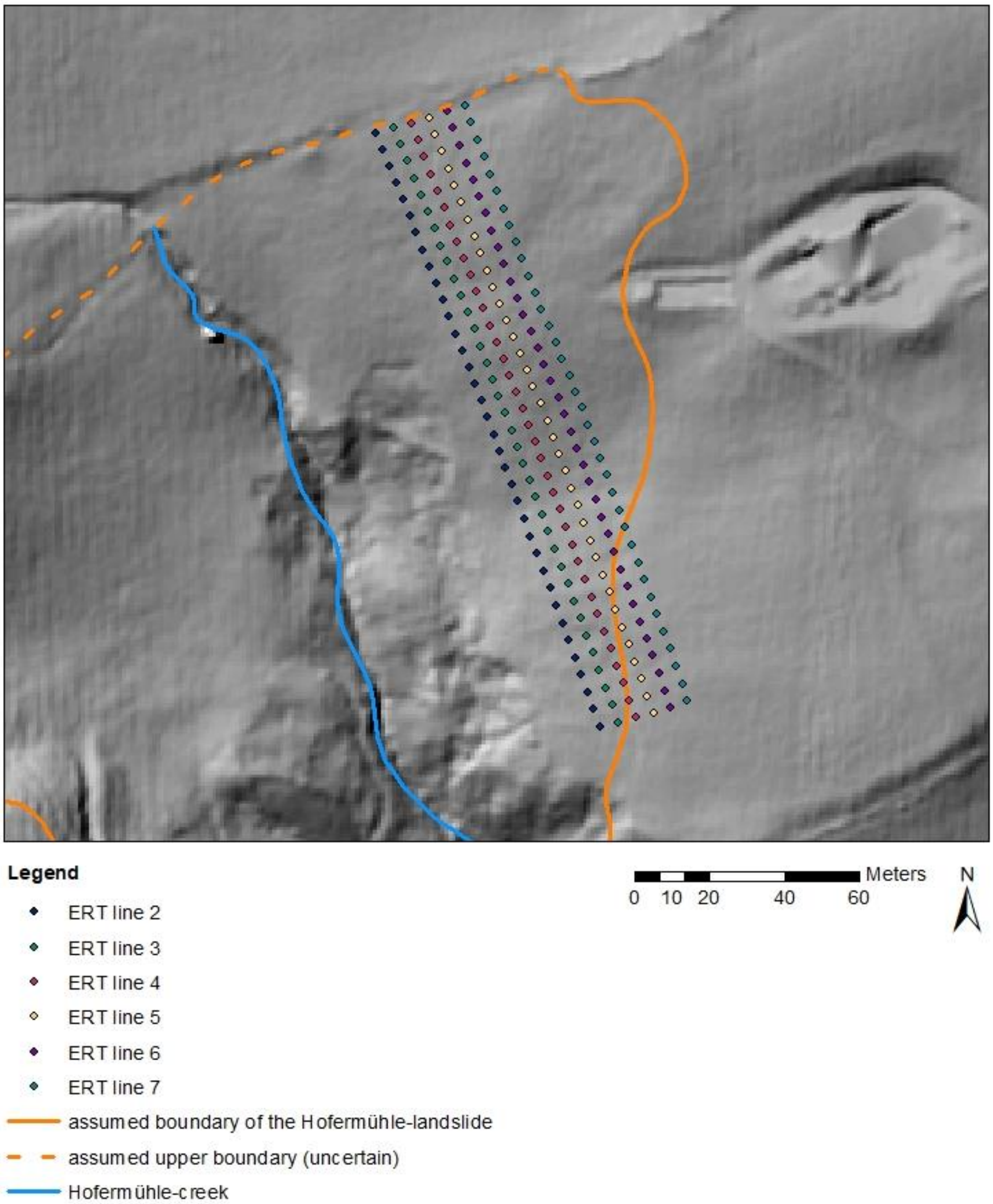

Figure 22. Location of ERT lines 2 to 7; base layer: Land Niederösterreich

4.4.3 Inversion

In the next step, the inversion of the obtained data was conducted to obtain a model for the distribution of subsurface electrical properties. Following Kemna (2000, pp. 58–60), the model represents a unique solution for a problem characterized by inherent non-uniqueness, such as the (complex) resistivity problem. Non-uniqueness describes the possibility, that numerous models may match the acquired data. Therefore, the models search must be regularized by additional constraints (Kemna, 2000, p. 58). Mathematically this is formulated as an optimization problem, in which an objective function is systematically minimized. The inversion of the data was conducted using the software “CRtomo”, which is based on the inversion approach of Andreas Kemna (2000). The Kemna’s inversion approach is based on a well established, regularized inversion process, the Tikhonov approach, and refined to a complex form to allow for complex data and parameters, as obtained in ERT, in the inversion algorithm. (Kemna, 2000, pp. 58–60)

The global objective function to be minimized is (Kemna, 2000, p. 64):

$$\Psi(\mathbf{m}) = \left(\mathbf{d} - \mathbf{f}(\mathbf{m})\right)^{\mathrm{H}} \mathbf{W}_{\mathrm{d}}^{\mathrm{H}} \mathbf{W}_{\mathrm{d}} \left(\mathbf{d} - \mathbf{f}(\mathrm{m})\right) + \lambda \mathbf{m}^{\mathrm{H}} \mathbf{W}_{\mathrm{m}}^{\mathrm{T}} \mathbf{W}_{\mathrm{m}} \mathbf{m} \tag{26}$$

$m \ldots$ *model vector*

$d \ldots$ *data vector*

$\mathbf{W}_{\mathrm{d}} \ldots$ *diagonal weighting matrix*

$\mathbf{W}_{\mathrm{m}} \ldots$ *real model weighting matrix*

$H \ldots$ *complex conjugate transpose (Hermitian)*

$f \ldots$ *operator of the forward problem*

$\lambda \ldots$ *regularization parameter (real and positive number)*

The minimization of the objective function (eq. (26)) is performed in an iterative process by a combination of the complex-valued conjugative-gradient method and the Gauss-Newton method. This process successively improves models. Starting from a model m_o a quadratic approximation of Ψ at the current model m_q is minimized at each inverse iteration step q. In each inverse iteration step q, a complex linear system of equations is created, serving as the basis for the next model update Δm_q.The iteration process is repeated until the desired data misfit target value is achieved. (Kemna, 2000, p. 64)

Defining Errors

An important step in the inversion is the characterization of the error in the measurements. The error consists of an absolute and a relative component. The absolute error refers to the error present in each measurement (associated with the resolution of the device). It is the parameter defining the error in low resistance measurements (< 1 ohm). The relative error represents a percentage value and is mainly affecting high resistance values (R > 1 ohm). Clear data sets typically show a relative error of 1 %, noisy 10 %.

Defining precisely the error enhances the inversion, and, in further consequence, the interpretation of electrical images, in three ways (Flores Orozco, Gallistl, Bücker, & Williams, 2017). First, it allows the assessment of the reliability of the acquired data. Second, it is necessary for the identification and removal of outliers associated with systematic errors. Third, it enables the adjustment "of error models describing the characteristics of inherent random errors to be incorporated within the inversion" (Flores Orozco, Gallistl, et al., 2017).

This last point is particularly important, given that the error accepted in the inversion determines how closely the inversion will reproduce the data. It has been demonstrated that an underestimation of the data error (overfitting) is linked to the presence of artefacts in the final electrical images due to the incorporation of some of the residual variation (e.g. noise), while an overestimation of the data error (underfitting) commonly leads to a loss of resolution and a lack of contrast in the electrical images. (Flores Orozco, Gallistl, et al., 2017)

Errors for the ERT profiles were estimated with a method established by Flores Orozco et al. (2017). A detailed description of the method can be found in (Flores Orozco, Gallistl, et al., 2017).

The analysis of the pseudo sections is typically a good starting point for the estimation of the data quality. Random errors can be described approximately by the mean and standard derivation, which can be determined by a comparison of quadrupoles that were used twice in a single survey, meaning that two measurements of electrical properties are available for a single point in the subsurface. In the first survey, there were overlapping electrodes between each section of the roll-along. Therefore, some points in the subsurface were measured twice.

In the second survey there were no overlapping electrodes in any profile, however, the first profile was measured twice in two different directions (normal and reciprocal), yielding two values for a large number of points in the subsurface.
Ideally, the two measurements should give the same result for the electrical property in that specific location but in practice the values will most certainly differ. Comparing the difference by calculating the two values for several quadrupoles allows assessing the precision of the measurement as well as the type of error. Small differences indicate a precise measurement; a normal distribution of the differences hints at a random error. Derivations from the normal distribution may indicate a systematic error.

Creating a Finite Element Grid

The solution of the inversion problem also involves the solution of the forward problem (Kemna, 2000, p. 45). In the solution of the forward problem, the finite element method is adopted (Kemna, 2000, pp. 49–51). Therefore, a finite element mesh needs to be designed for the inversion. The finite element mesh is related to the geometry of the survey, i.e. it varies with the number of electrodes as well as the electrode spacing. For an accurate finite element mesh, the GPS positions of the electrodes must be known. Hence, a finite element mesh was created for each profile in the survey.

Modifying Smoothness

The model search can be confined by modifying the smoothness in the inversion to account for anisotropy in the ground (for example fractures or layering), which may cause the electrical properties to depend on the direction of the measurement. Anisotropy is important to consider in the inversion to achieve an accurate image of the subsurface. If ignored, deduced true ground electrical properties may not be correct.

In CRtomo, the model search can, bust does not have to be, confined to a horizontal or vertical layered ground (anisotropic smoothing). Since the structure of the ground at this point is unknown, no smoothness constraint for any particular layering was adopted in the inversion.

5 Results

5.1 Aerial and Field Reconnaissance

Aerial and field reconnaissance was conducted to obtain an overview of the study site and identify the areas of interest for the study. Today, several signs of past and present movement are observable at the site. Figure 23 provides a map of the current conditions on the site. A large part of the landslide body is already overgrown with vegetation; however, the plants (mostly spruce (Picea Abies)) are smaller in height than older and unaffected trees around the slide, indicating the disruption by the slide (Figure 24). Some trees growing on the landslide body are tilted, others have curved tree trunks, indicating unstable ground. The crown (Figure 24 B) of the landslide remains clearly visible. Blocks of vegetated soil appear to be breaking off the crown and indicate current movement (Figure 24 B).

Throughout the slope, there are cracks in the vegetation cover and in the soil, most notably around the crown (Figure 24 A). On the upper side of the slope, on the orographic left of the Hofermühle-creek, hollows and cracks are clearly identifiable (Figure 24 C). Both appear to have increased at the cm-scale between August and November, suggesting movement. Movement was not tracked; however, further landslide processes appear likely in this area of the slope.

In two areas on the slope water logging is visible at the surface. These areas are located on the relatively flat parts of the slope and are marked in the map below (see Figure 23). One of these areas is vegetated with common rush (Juncus effuses), a plant that is typical for wetlands but can also grow in areas with moist soil. These observations support the conclusion that water infiltrates into the slope somewhere and accumulates in these areas, maybe supported by impermeable layers in the ground. According to the landowner, new drainages have been installed on the east side of the river, however, the exact position of both the old and new drainages is unknown.

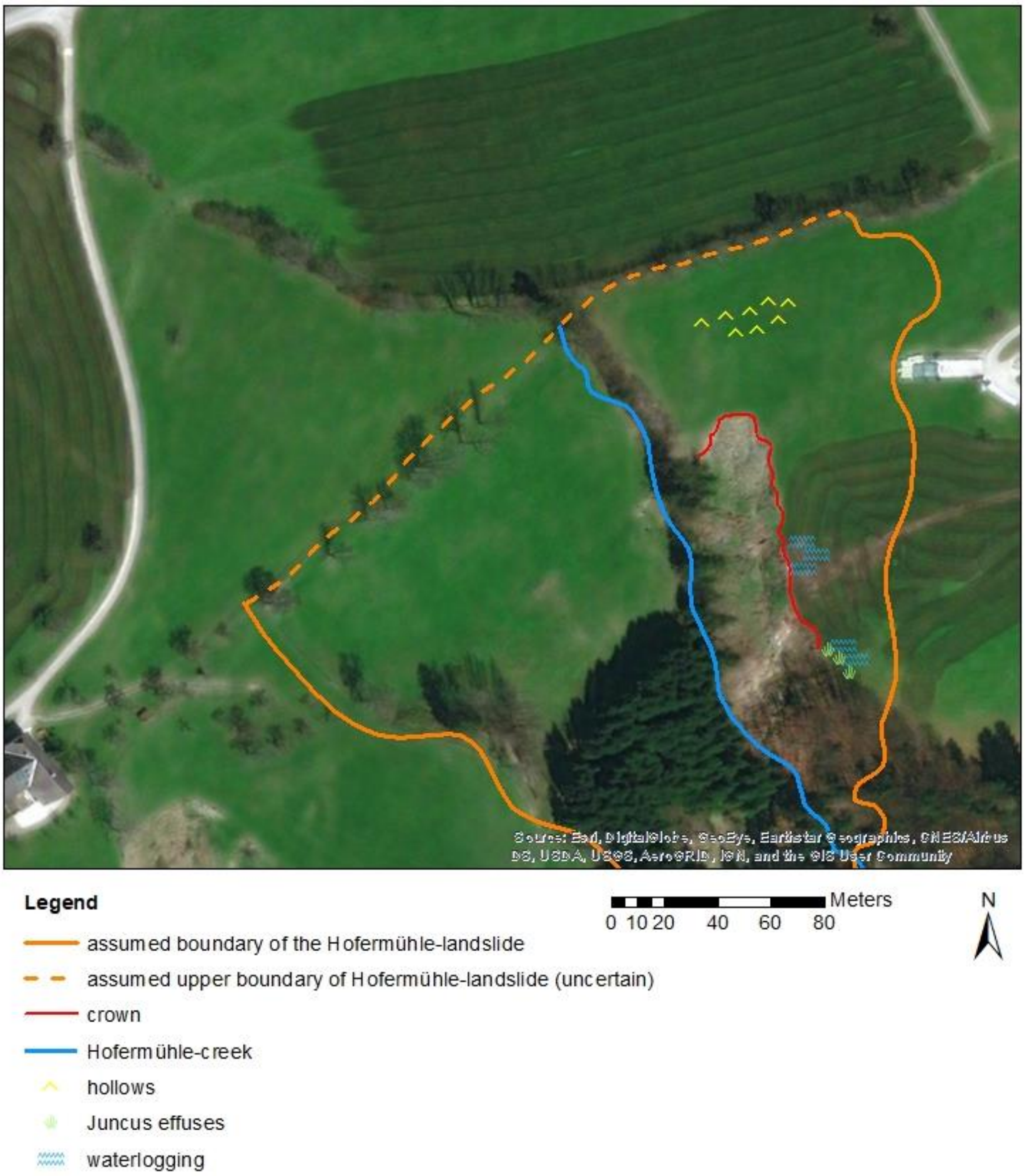

Figure 23. Site conditions; map source: Esri, Digital Globe, GeoEye, Earthstar Geographics, CNES/Airbus DS, USDA, USGS, AstroGRID, IGN, and the GIS User Community

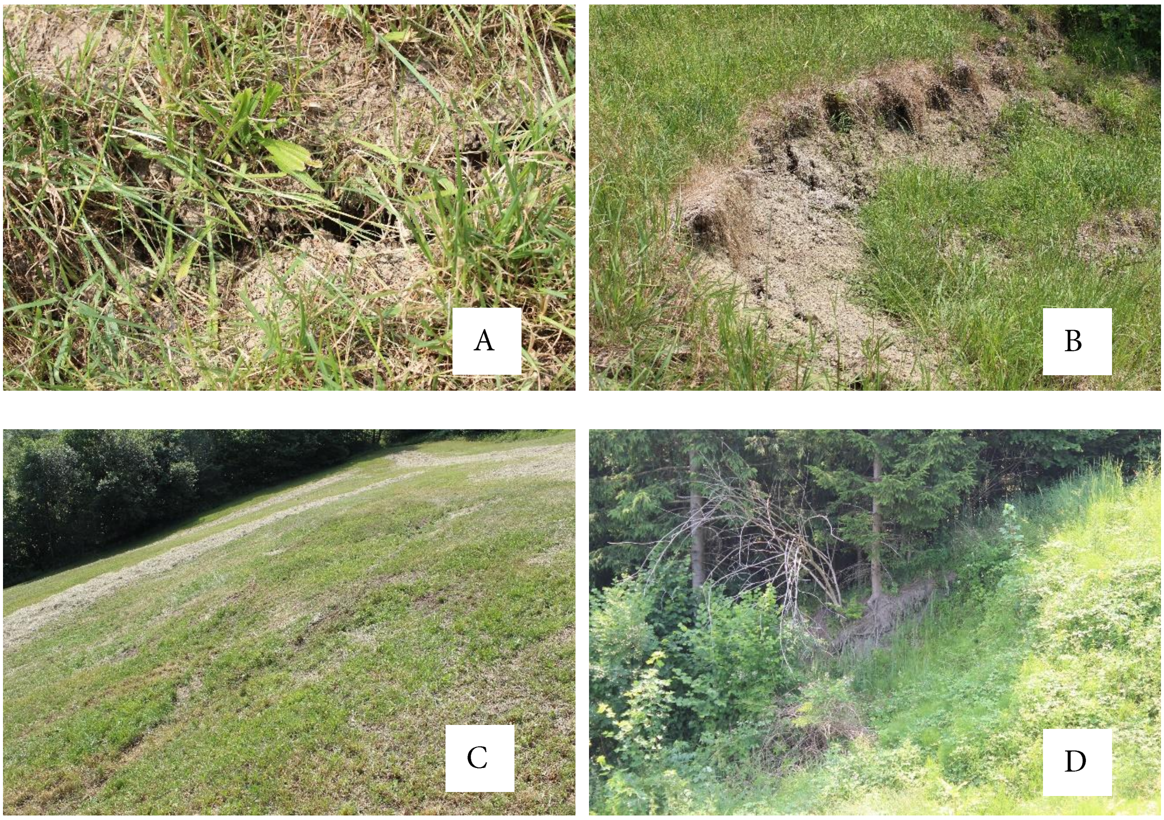

Figure 24. Indicators of past and present movement at the Hofermühle in Konradsheim, Austria. June 2017

5.2 Percussion Drilling

PD provided ground truth information on soil specific values for a single location (see section 4.2). The following section presents the findings from the laboratory analysis of the drill cores. Starting with the visual characterization, the section will then present results relating to particle size distribution, water content and electrical conductivity of the soil solution. Finally, an interpretation of the results is offered. The relation between data acquired through PD and other methods applied in this study will be discussed in chapter 8.

5.2.1 Visual Characterization

In the visual characterisation, the drill core was characterized primarily in terms of colour and other visual signs. Moisture and consistency was also considered. The drill core was subdivided into homogenous sections, each of which would be sampled later. Figure 25 shows photographs of each segment of the drill core, starting with the uppermost section.

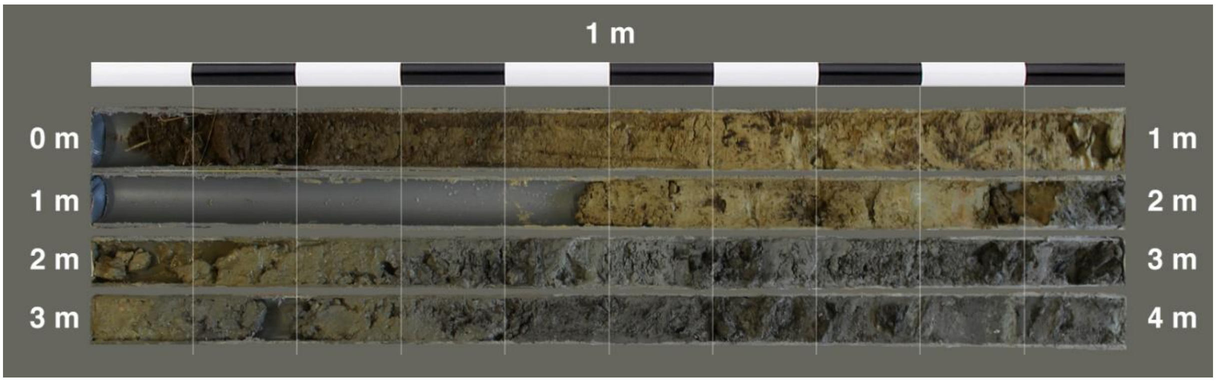

Figure 25. Sections of the drill core as obtained through PD. On the left and right, the relating depth is given and the scale bar on top of the photographs indicates 10 cm increments. The second drill core (1 m – 2 m) features significant core loss, most likely due to the soft nature of the ground.

Percussion drilling revealed thick regolith and deep soils, the bedrock certainly lies below 4 m. However, the exact extent of the regolith at this location could not be evaluated as the drilling was stopped at 4 m due to time constraints. The materials brought to surface with PD are generally fine, moist and feature a pasty consistency. Some sections of the core were lost during the drilling, most likely due to the soft nature of the ground (Figure 25). Consequently, depth information in the following section may not be accurate. Three sections can be distinguished clearly by their distinct colour. The first 40 cm to 50 cm are characterized by a dark brown colour. Following materials feature a lighter brown before the colour changes to grey at a depth of around 190 cm. While the transition between dark and light brown is gradual, it is sharp from light brown to grey and marked by the presence of a large rock. The upper 30 cm to 40 cm of core 3 (2 – 3 meters) and 4 (3 – 4 meters) are mixed, brown and grey and exceptionally wet. Given their distinct colour and consistency, that differs considerably from surrounding material (above and below), it appears safe to assume that these portions fell down the borehole during the drilling, thus showing up at a wrong location in the drill core.

The dark brown colour in the first 50 cm signals the presence of organic materials (i.e. humus). Roots are clearly visible, especially in the first 20 cm. The materials in this section are rather loose.

The light brown colour that is characteristic of the materials between approximately 50 cm and 190 cm indicates chemical weathering. In humid and temperate climates, the brown colour is the result of hematite hydrating to goethite as well as the oxidation of iron (Ahnert, 2009, pp. 70–71). As both water and air are needed for these processes, it can be concluded that this section was exposed to frequently changing conditions, i.e. cycles of wetting and drying. Further evidence for oxidation processes are the many mottles that are present in the drill core to a depth as low as 165 cm; however, they are most pronounced between 60 cm and 90 cm. The mottles are either dark brown to black (from manganese) or brown to reddish brown (from iron) and have the shape of dots or streaks. Most of them are smaller than 1,5 cm. Chemical weathering, as described above, typically goes hand in hand with the formation of clay minerals (loamification) (Scheffer et al., 2010, p. 295). This process cannot be determined through a visual interpretation but may only be determined in the laboratory analysis. At this point it can only be recorded that the materials appear fine, except for some gravel or aggregates and individual large rocks (as for example at 190 cm of depth).

Between around 180 cm and 190 cm, is a section of particularly compacted, pasty material of reddish brown, reddish yellow and grey colour. This section marks the rather sharp transition of the colour of the materials from brown to grey. Such fine and compacted materials may indicate an impermeable layer, given that they extend over larger parts of the slope.

The remaining material in the cores (from 190 cm to 400 cm of depth) is grey and does not show any prominent colour or textural changes, except for lenses of material that feature a lighter grey and appear to contain more coarse particles between 370 cm and 400 cm of depth. Single rocks could be recognized at a depth of 280 to 300 cm. These are brittle and break apart easily. At around 380 cm to 400 cm the material is already highly compacted, as is predictable for larger depths. The grey section of the drill core is most likely influenced by water in the slope, as can be concluded from the water table in the borehole as well as the grey colour that is typical for materials devoid of oxygen.

5.2.2 Interpretation

The transition between the soil and the underlying regolith is not sharp (as would be the case if the bedrock was close to the surface). The first 2 m (until around 190 cm) have clearly been altered by soil forming processes (such as weathering). This section of the material may be classified as soil and may be divided into an A-horizon (uppermost 50 cm), featuring a high humus content and the typical dark brown colour, and a B-horizon (from around 50 cm to 190 cm), characterized by illuviation. The underlying earthy materials show only slight changes, they appear to have kept their original colour and are only partially weathered. They furthermore appear devoid of any marks of biological activity (such as roots or animals). As such, this material may be classified as C-horizon and part of the regolith. As indicated, the ground exhibits characteristics of brown earth, corresponding with the eBOD classification (BFW, 2007) for the given slope. However, some features of the soil type pseudogley could also be found, such as the mottles in the upper part of the drill core as well as the one highly compacted section between 180 cm and 190 cm, which may restrict water flow in the subsurface. In any case, there is strong evidence for changing soil-water conditions caused by cycles of wetting and drying.

5.2.3 Particle Size Analysis

Particle size analysis was conducted for eight soil samples from the drill core, two for each section. The soil samples are named PS 1 to PS 8, with PS 1 being the sample that was taken closest to the surface and PS 8 taken from the end of the grill core. Results are presented in graphic form only; the numerical values are in Appendix B. Additional Results. The samples were divided into fine soil (< 2 mm), consisting of clay, silt, sand and coarse soil (> 2 mm) (gravel). Figure 26 gives an overview of the particle size distribution according to these categories. Figure 27 to Figure 30 show the particle size distribution for only the fine soil section (< 2 mm). Therefore, the categories silt and sand were once more split up into the categories “coarse”, “medium” and “fine”.

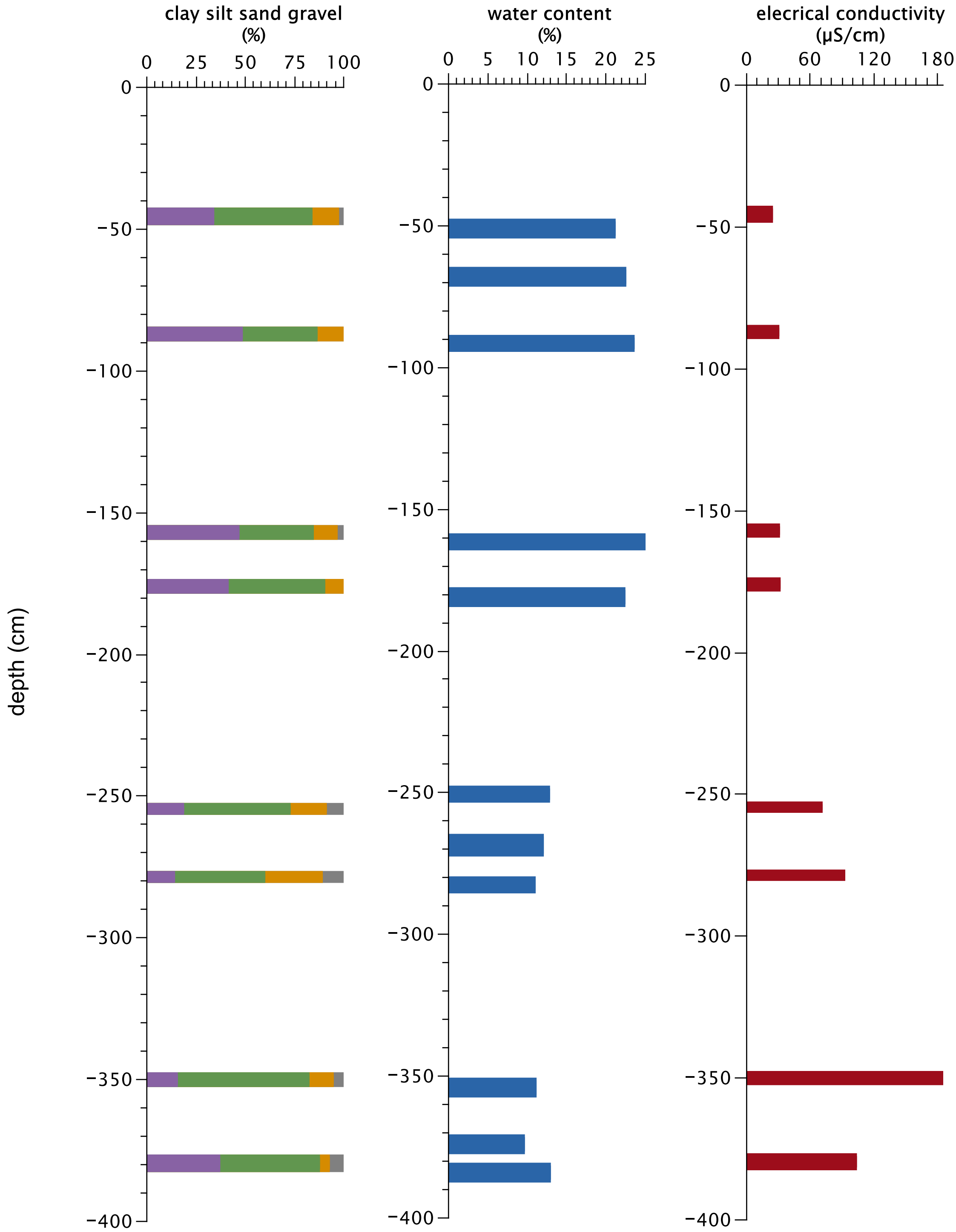

Figure 26. Particle size distribution, water content and electrical conductivity of selected soil samples from the drill core

The following section describes the data as shown in Figure 26, hence the gravel fraction is considered when percentages are given. The fine soil fraction prevailed over the coarse soil fraction in all soil samples, their ratio varying between 88:12 and 100:0. The relative distribution of grain sizes varies significantly. Clay varies between 13 % and 48 %, silt varies between 37 % and 67 %, sand between 5 % and 30 % and gravel varies between 0 % and 12 %. Differences in the particle size distribution appear to coincide with the colour change from light brown to grey. The samples taken from the 2 m (PS 1 to PS 4) show a similar particle size distribution that differs significantly from the particle size distribution in PS 5 to PS 8. While differences in the particle size distribution in PS 1 to PS 4 are marginal, there is slightly more variance in the particle size distribution between PS 5 and PS 8, as can be seen in Figure 26.

The clay content in PS 1 to PS 4 is particularly high, ranging from 33 % - 48 %. In comparison, PS 5 to PS 7 have a clay content of only 13 % to 19 %. PS 8 featuring a clay content of around 36 % is more comparable to PS 1 to PS 4. Similarly, PS 5 to PS 8 feature a slightly higher to considerably higher silt fraction than PS 1 to PS 4 (50 % - 67 % for PS 5 – PS 7 vs. 37 % - 50 % for PS 1 – PS 4). The sum of clay and silt is higher than 80 % in all samples, except for PS 5 and PS 6 (72 % and 59 %, respectively). PS 5 and PS 6, on the other hand, feature much more sand than the rest of the samples (18 % and 29 %, respectively. The gravel fraction is also significantly higher in PS 5 to PS 8 compared to PS 1 to PS 4 (5 % - 12 % for PS 5 – PS 7 vs. 0 % - 4 % for PS 1 – PS 4).

Figure 27 to Figure 30 show the particle size distributions for the fine soil fraction for selected samples from the drill core. The remaining graphs are included in Appendix B. Additional Results, to promote readability. The bars in the diagrams show the mass fraction of each fraction, while the red line represents the cumulative mass fraction.

PS 3 and PS 4 show a similar particle size distribution. PS 5 and PS 6 have a similar particle size distribution. The particles are more evenly distributed to the categories, than PS 1 to PS 4. While their silt fraction is comparable to PS 1 to PS 4, they contain less clay and more sand, specifically coarse sand. PS 8 does not match the general pattern, as mentioned above, and is more like PS 1 to PS 4, although featuring a slightly bigger silt fraction.

The particle size distribution of PS 3 is exemplary for PS 1 to PS 4. PS 1 was taken from the transition zone between the A-horizon and the B-horizon, while PS 2 to PS 4 come from the B-horizon. The particle size distribution in the fine soil fraction varies slightly, however the relative distribution is the same in samples PS 1 to PS 4. The samples in this section of the core (first 2 m) are mostly made up of fine grains. Clay and silt make up the largest portion of the samples, both accounting for well over 85 % of the particles in the fine soil fraction, as can be seen in Figure 27. Sand only makes up more than 10 % of the total mass of the fine soil fraction.

Figure 28 provides the particle size distribution of the fine soil fraction for PS 6, which is also representative of PS 5. PS 5 and PS 6 do not contain as much clay as the remaining soil samples. The clay fraction makes up 20 % and 15 %. The silt fraction makes up the largest part of the samples, most notably the medium silt fraction. However, it is the high sand content that makes PS 5 and PS 6 stand out from the rest of the samples. In PS 5, sand adds up to 20 %, and in PS 6 sand sums up to 33 %. Within the sand fraction, the coarse fraction constitutes the majority.

Figure 29 provides the particles size distribution for PS 7. The diagram shows that PS 7 has a considerably higher amount of silt than the other samples, measuring 71 %. The silt fraction of the sample is largely made up of coarse silt. Again, silt and clay account for most of the particles in the fine soil fraction (87 %).

Figure 30 shows the particle size distribution of PS 8. The sample was taken at around 380 cm of depth where soil characteristics vary strongly. If PS 8 had been taken at a slightly different location, the sample would most likely show another particle size distribution. Thus, PS 8 might be representative only for a small section of the core. The diagram clearly indicates the dominance of clay and silt for PS 8. Together they amount to almost 95 % of the particles in the fine soil section, which is the highest value in all samples. Consequently, there is only very little sand in the sample.

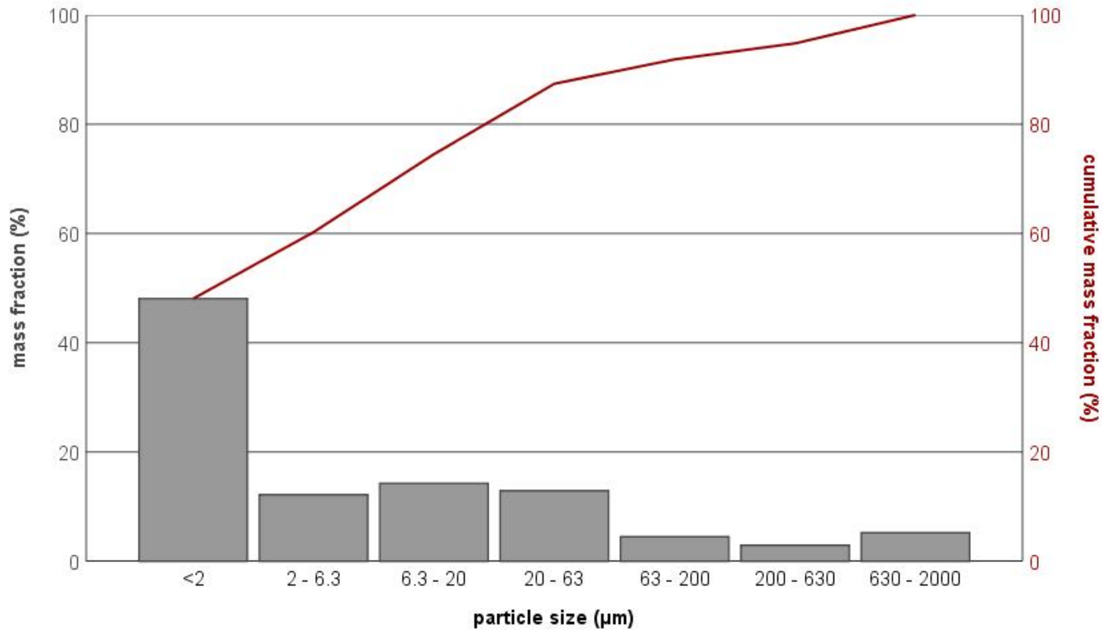

Figure 27. Particle size distribution for the fine soil section of PS 3

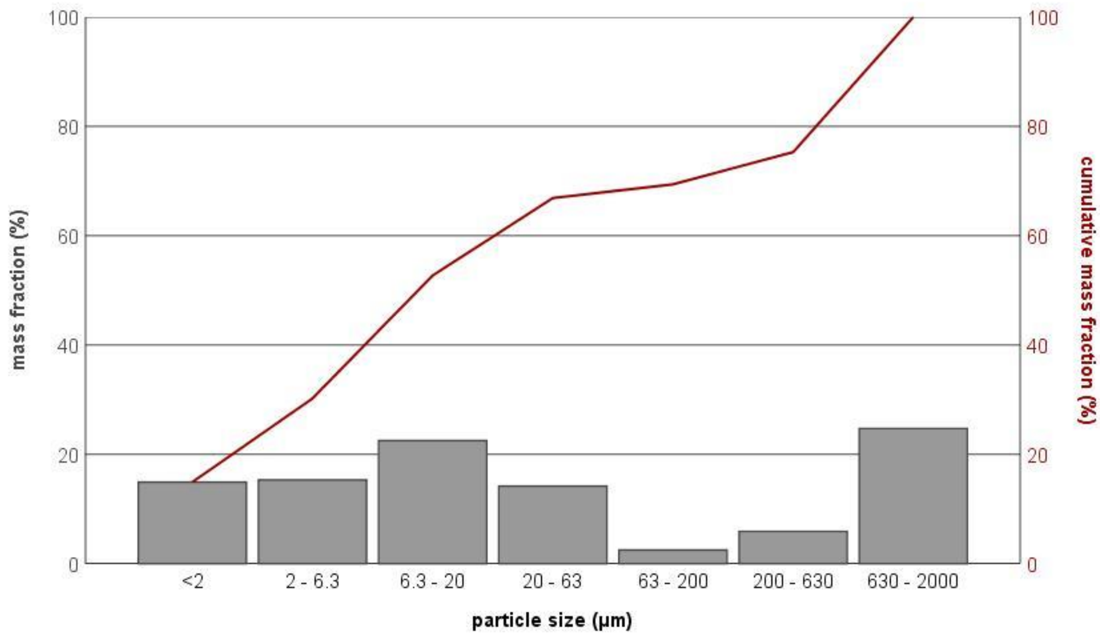

Figure 28. Particle size distribution for the fine soil section of PS 6

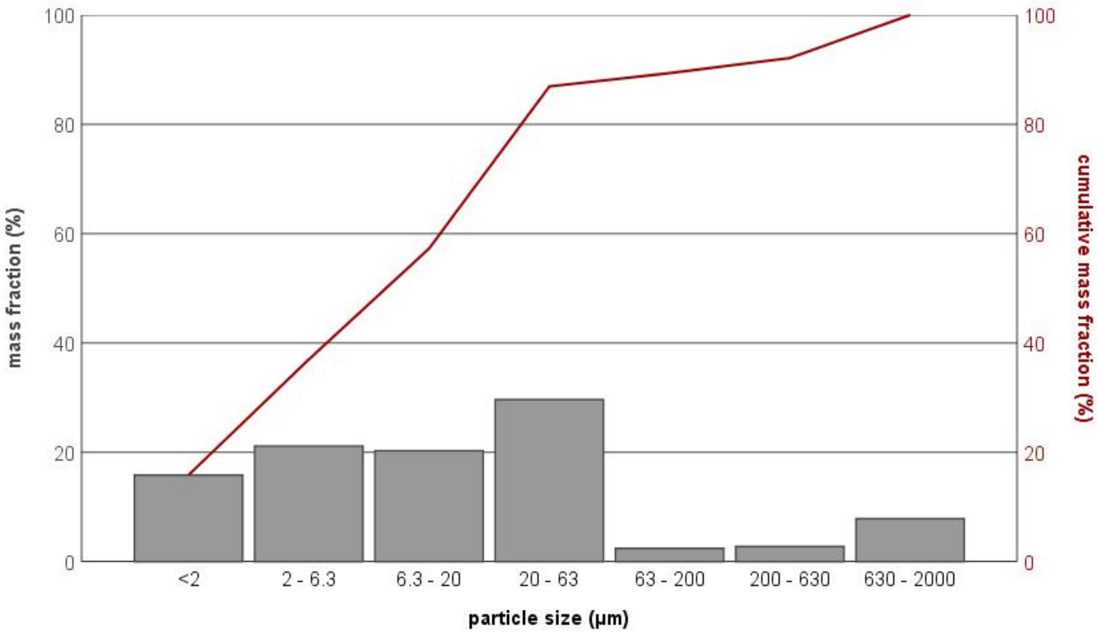

Figure 29. Particle size distribution for the fine soil section of PS 7

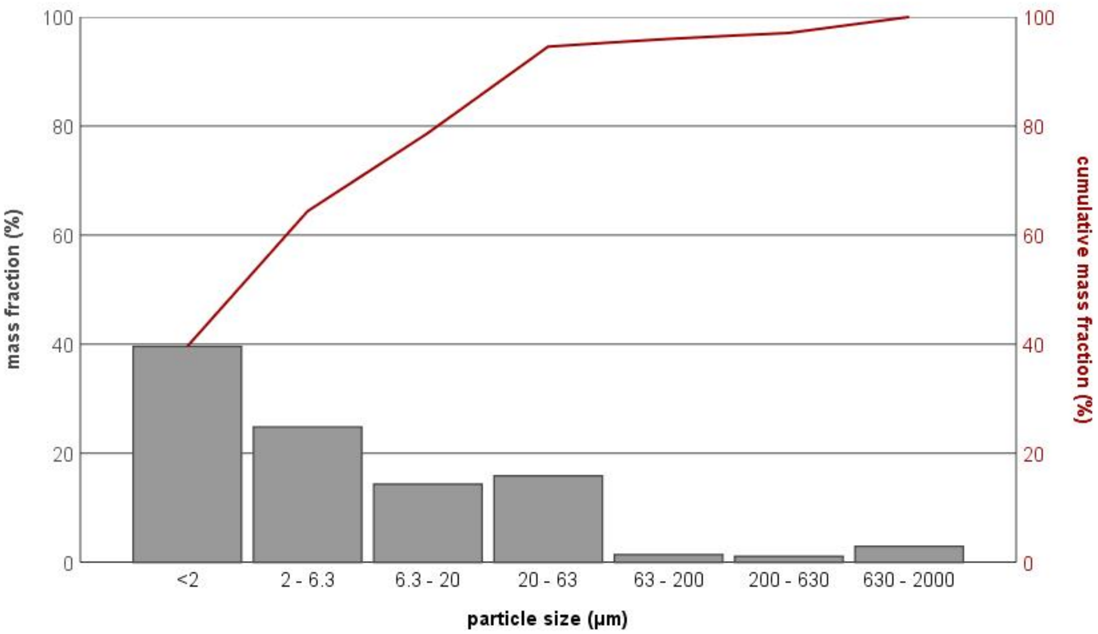

Figure 30. Particle size distribution for the fine soil section for PS 8

5.2.4 Water Content

The natural water content was analyzed for eleven soil samples. The results are depicted in Figure 26. Appendix B. Additional Results contains the measurement data. In the eleven samples, the water content varied between 9 % and 25 %. While the water contents in one single core are quite uniform, soils in larger depths are slightly drier. The upper two cores (0 m–2 m) are significantly moister than the lower cores (2 m-4 m). At this point it is important to note that the water content extracted using the standard method is not necessarily accurate for clayey soils, as they may retain some water even when dried at 105 °C for 24 hours. To remove all the water from such soils, much greater heat would be necessary.

The differences between the upper two meters of the drill core and the lower two meters might thus be slightly bigger than the measurements suggest. The change in water content coincides with the change in colour within the core (as was the case for the particle size distribution). The higher water content in the upper section of the drill core might be explained by the higher clay content and its greater capacity of holding water.

5.2.5 Fluid Conductivity

The fluid conductivity was evaluated for eight soil samples. Results are shown in Figure 26. The measurement data is included in Appendix B. Additional Results. The conductivity meter used here measures only the contribution of electrolytic conductance. Generally, the electrolytic conductivity is low, but significant variation occurs in the drill core, ranging from 23 $\mu S \cdot cm^{-1}$ to 185 $\mu S \cdot cm^{-1}$. The variation is minimal within the upper two meters and within the lower two meters, but there is a sharp increase in conductivity between core 2 and core 3. While the electrical conductivity in samples from the upper two meters remains below 31 $\mu S \cdot cm^{-1}$, it reaches values of up to 185 $\mu S \cdot cm^{-1}$ in the third core.

5.2.6 Interpretation

Percussion Drilling confirmed thick soils and regolith for the study site. Soil and regolith are more than four meters thick in the location examined. One major risk factor, namely the presence of fine-grained materials, could be determined for the investigated slope.

PD also delivered strong evidence of distinct layers in the ground. As has been shown, all parameters investigated in the laboratory analysis vary within the first and the second half of the drill core. In comparison, the top two meters of the drill core are noticeably moister, less conductive and feature a higher clay content than the lower two meters. The investigated parameters seem to correspond with the horizons identified in the visual characterization and so provide further evidence to distinguish between the two halves of the drill core. The comparatively high clay content of the first two meters is a strong indicator of weathering processes. Both a high clay content and the brown colour of the soil are typical for weathered B-horizons where loamification (responsible for high clay contents) and brunification (responsible for the distinct brown colour) go hand in hand. The increase in conductivity with depth appears counterintuitive for cultivated land, as fertilization typically leads to an increased availability of charge carriers in the upper decimeters of the soil. Even though the land is cultivated and fertilized, the conductivity is noticeably lower near the surface. One possible explanation for the variance of electrical conductivity within the drill core is the transportation of charge carriers from the upper to lower sections in the ground, so that more charge carriers are available in the lower part of the drill core to conduct the electrical current.

5.3 Dynamic Probing Heavy

Dynamic Probing Heavy was conducted on three points on the lower (accessible) part of the slope. The probes are named DPH 1 to DPH 3. Figure 31 provides the results in graphic form for all three locations. The diagrams in *Figure 31* show the blow count number (N_{10} values) for each 10 cm increment. They are scaled equally to facilitate comparison. It should be noted that the quantitative use of the results is controversial due to the effect of skin friction, most notable in cohesive soils (Khodaparast et al., 2015). However, in this study the three tests were conducted in a spatially confined area so that ground conditions, and the effect of skin friction on the measurement can be assumed to be constant. If skin friction is assumed to be relatively constant, then variations in N_{10} values are most likely not affected by skin friction. Hence, the collected data can be considered appropriate for a qualitative assessment of a soil profile as well as for a relative comparison of the profiles.

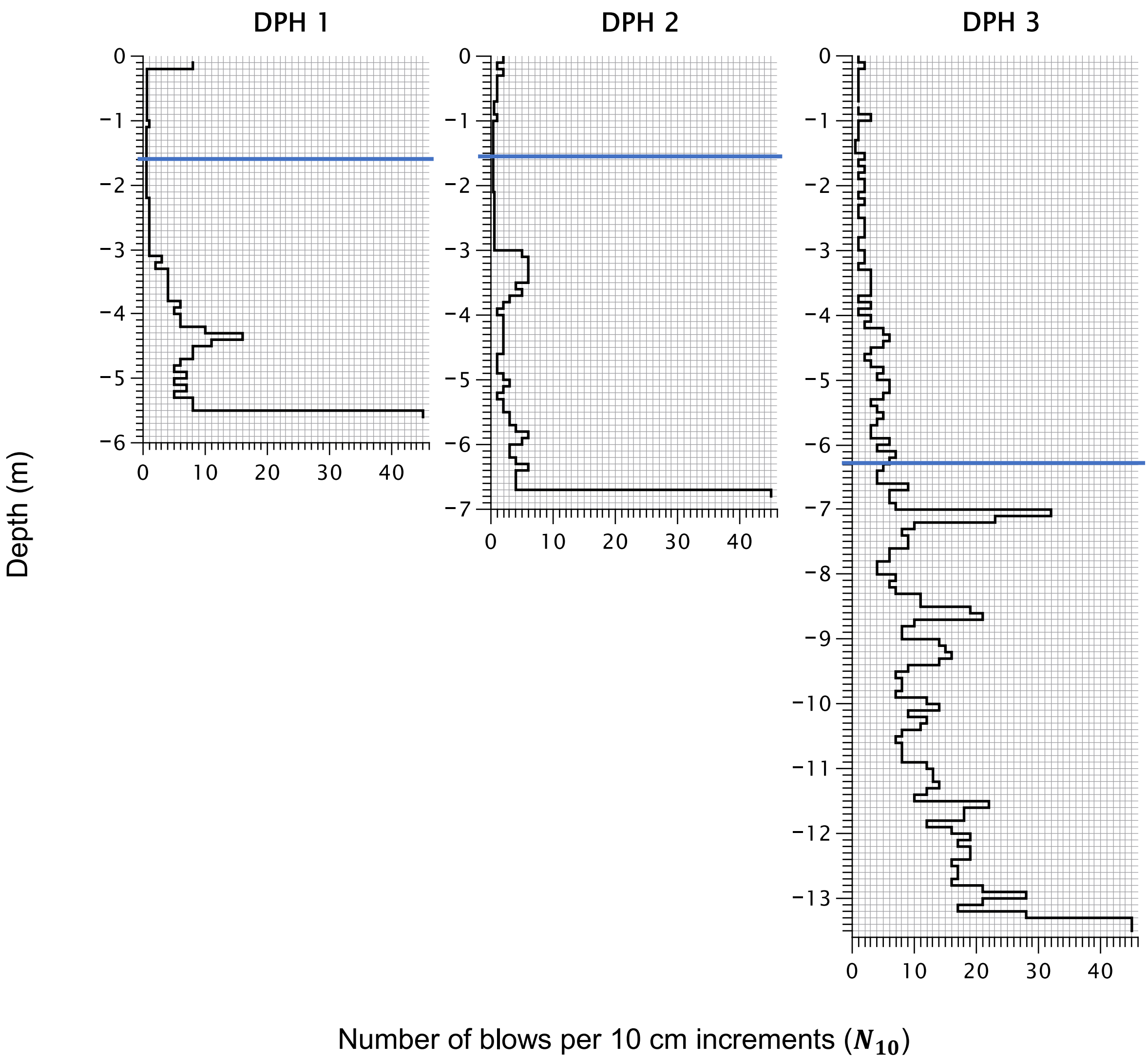

Figure 31. Blow count number for each 10 cm increment for each DPH profile. The blue bars mark the depth at which rods became wet.

Refusal was met at varying depths; in 5,.0 m for DPH 1, 6.70 m for DPH 2 and 13.50 m for DPH 3. DPH 1 and 2 are characterized by very low blow count numbers (<1 – 2) between 0 and 3 m, indicating very soft ground. One exception is the first increment of profile one, showing a higher value. Such anomalies do not necessarily indicate a harder layer but might also be caused by rocks in the ground. DPH 3 shows slightly higher values for this section of the profile yet blow count values below 4 still indicate soft ground. In DPH 1 blow count numbers peak at 16 at 4.40 m, then drop again until the set threshold value of 45 blows is reached at 5.50 m. The higher blow count numbers between 4.30 and 4.50 m hint at a more resistive layer. Blow count numbers in DPH 2 and DPH 3 do not surpass a value of 8 in this section (0 to 5.50 m), indicating very soft to stiff soil. While in DPH 2 refusal is met at 6.70 m, only a sharp increase in blow count numbers is recorded for DPH 3. From this depth onwards, blow count numbers increase steadily, but with noticeable variation (between 4 to 28 blow counts) until the threshold value of 45 blows is reached. The depth at which ground materials are wet varies considerably, as indicated by wet rods (see Figure 31).

5.3.1 Interpretation

The depth at which refusal was met varies considerably between the three profiles. From this variation, the conclusion might be drawn that the bedrock varies in depth between the profiles, hence across short distances. Another explanation for the variance in refusal depth is the existence of a more resistive layer between 5 and 7 m of depth. The peak in blow count numbers in a depth of 7 m in DPH 3 hints at a resistive layer (a blow count number of 28 indicates hard soil), which is located at a similar depth as the depth of refusal in DPH 1 and DPH 2. Hence, it may be hypothesised that refusal in DPH 1 and DPH 2 was met not because of bedrock but because of a more resistive layer, which could be more easily penetrated in DPH 3. DPH furthermore indicates that water conditions within the slope vary strongly. Compared to DPH profile 2 in which rods became wet at a depth of 110 cm, considerable wetness occurred only at a depth 630 cm in DPH profile 3, even though the two profiles are near each other and the difference in altitude is small.

5.4 Electrical Resistivity Tomography

To assess spatial variations of electrical properties in the ground, seven parallel ERT profiles were collected by means of time-domain IP measurements. The following section presents the images of the distribution of the electrical resistivity only. For improved readability, only selected images are shown in this section; the remaining images are included in Appendix B. Additional Results. In each image, the electrical resistivity is provided for points in a coordinate system consisting of a y-axis, for lateral variations, and a z-axis, for variations in height. The values for electrical resistivity are indicated on a colour scale. Low values of electrical resistivity are assigned dark blue hues, higher values are represented in dark red. For each profile the corresponding image of the sensitivity of the measurement is provided, which is crucial for the quality assessment and interpretation of the data. Sensitivity values are equally plotted in a coordinate system and values are represented in a colour scale as well, in which blue stands for low sensitivities and red for high sensitivity. Measurements that were collected in a low sensitivity area are not shown in the images of the electrical resistivity, causing a jagged line at the bottom of the profiles. Profile 1, and profiles 2 to 7 are presented in two separate sections, since they were collected with different electrode spacings.

5.4.1 Inversion Results for Profile 1

Profile 1 was collected by means of a roll-along, creating three separate images with overlapping sections. The three images were combined to obtain one image of the whole transect, as shown in Figure 32. The resolution of the image is high due to the electrode spacing of only 1 m, allowing the depiction of small-scale variability in the electrical resistivity. The sensitivity of the measurement is especially high near the surface (see Figure 33) but decreases rapidly with increasing depth. It becomes particularly low from around 10 to 15 meters of depth and onwards (Figure 33). Therefore, data with low sensitivity has not been included in the image. Moreover, the electrode spacing of only 1 m guarantees an accurate representation of the topography of the slope, as the position of each electrode was recorded. Considering the topography in the inversion makes the subsurface model more realistic.

The electrical resistivity of profile 1 is generally low and exhibits only little variation. Values for electrical resistivity range from around 15 Ωm to 45 Ωm. The first five meters of the subsurface feature a higher variability in the electrical resistivity. In general, resistivity seems to increase slightly with depth, as can be inferred from the transition from blue to green, yellow and even orange shades at the bottom of the profile. The area in the middle section of the profile is characterized by slightly higher values that seem to extend to the surface. In the lower left part, the image shows a circular shape from around 70 meters to the start of the profile. The circular shape of low resistivity coincides with a flatter topography, as can be seen in Figure 32.

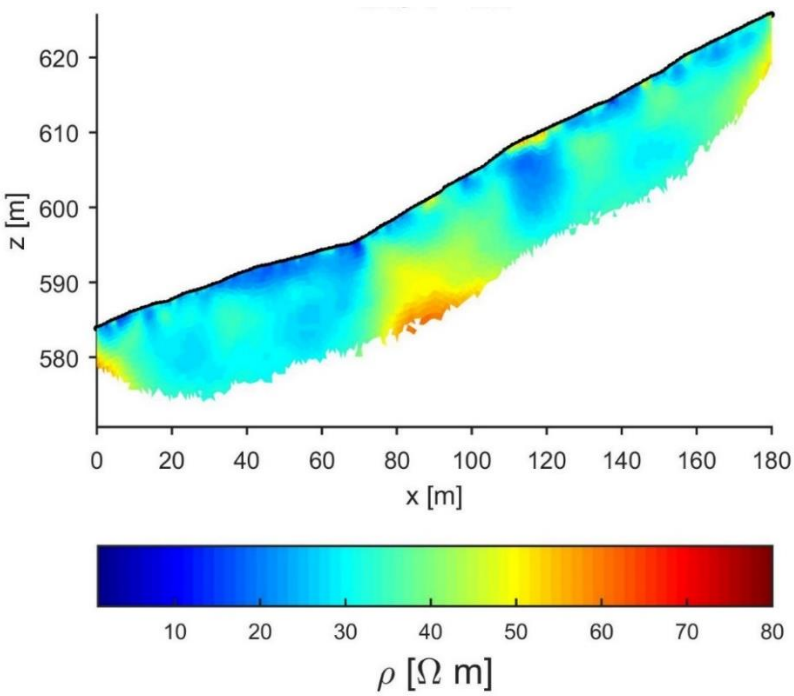

Figure 32. Distribution of electrical resistivity of ERT profile 1 (1-m electrode spacing)

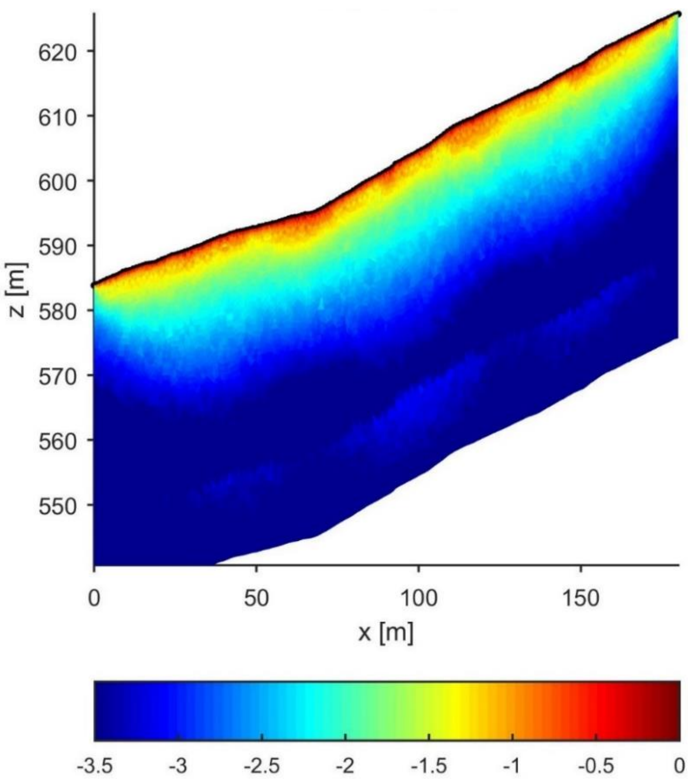

Figure 33. Sensitivity of measurement in ERT profile 1 (1-m electrode spacing)

5.4.2 Inversion Results for Profiles 2 to 7

Profiles 2 to 7 ran along parallel transects from north to south in 5 m intervals (Figure 22). The electrical resistivity and sensitivity are provided in Figure 34 to Figure 39. To compare profile 1 and profile 2, they ran along the same transect. The electrode spacing was increased to 5 m to achieve higher sensitivity in larger depths, and, ultimately, collect data on the distribution of electrical properties for greater depths. Increasing the electrode spacing leads to an overall loss of resolution in the images of profiles 2 to 7, compared to profile 1. As a result, areas with distinct resistivity values as shown in profile 1 (Figure 32) are combined to larger areas of equal resistivity in the images of profiles 2 to 7. Furthermore, the larger electrode spacing decreases the accuracy of the topography as GPS data was collected in 5 m intervals. For a comparison, the resistivity and sensitivity of profile 2, which was recorded along the same transect as profile 2 are provided in Figure 34 and Figure 35.

As all images depict a similar pattern, only profile 2 (Figure 34), profile 3 (Figure 36) and 5 (Figure 38) are shown here as an example, while the other images are attached in Appendix

B. Additional Results. The contrast of the pattern and the spatial extent of the structures composing the pattern vary slightly between the images. The contrast in profile 2 is low, the pattern becomes more pronounced from profile 2 to 6, before it decreases again slightly in profile 7.

In all images, four areas can be distinguished. Right below the surface is a layer that is characterized by a high spatial variability in the electrical resistivity. The resistivity changes quickly from one spot to the next within this layer, as can be deduced from the quickly changing colours in the images. The layer is approximately 5 to 7 m thick. The spatial variation underneath this layer is considerably lower. Three large "bubbles", that are areas with equal resistivity, can be identified. On the right and left of each image are two blocks of low resistivity, as indicated by blue shades, one extending from around 0 to 50 m, the other extending from around 100 to 180 m. The area on the right of the images (on the upper half of the slope) is generally bigger and slightly more conductive than the area on the left side of the image. Resistivity varies from around 15 Ωm to 30 Ωm in these blocks. Both "bubbles" appear to narrow with increasing depth but borders cannot be established for these structures since insufficient data is available for this depth. The two conductive blocks are intersected by an area of higher resistivity, as indicated by yellow and orange shades. Values for electrical resistivity in this area vary between around 40 Ωm and 65 Ωm. In profile 2, the area does not contrast as clearly with the blocks on the sides. The more resistive area broadens with depth and appears to extend to the surface.

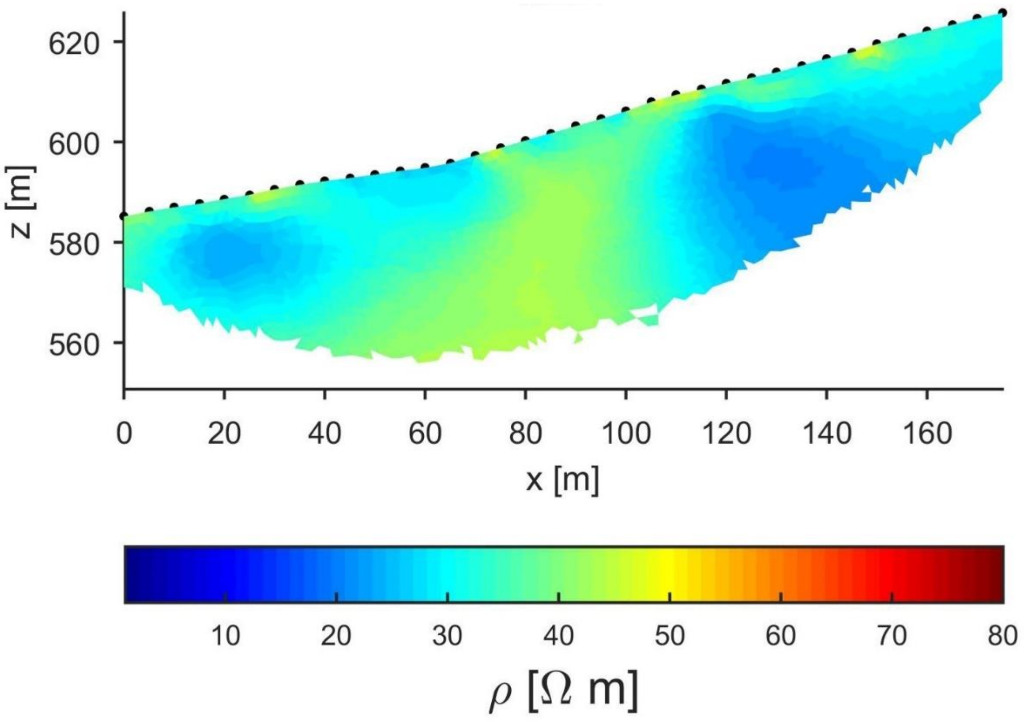

Figure 34. Profile 2 (5-m electrode spacing, same transect as profile 1). In comparison to ERT profile 1 (1-m electrode spacing), the image shows less details but therefore provides data for larger depths.

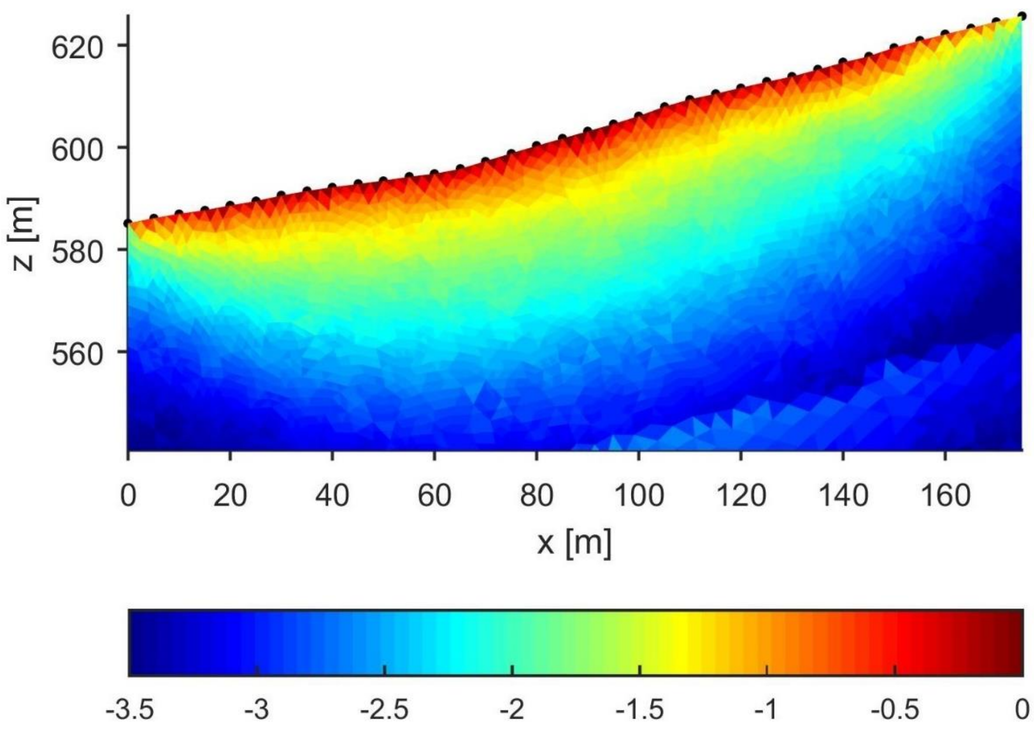

Figure 35. Sensitivity for profile 2 (5-m electrode spacing). In comparison to profile 1, the sensitivity in larger depths is greater.

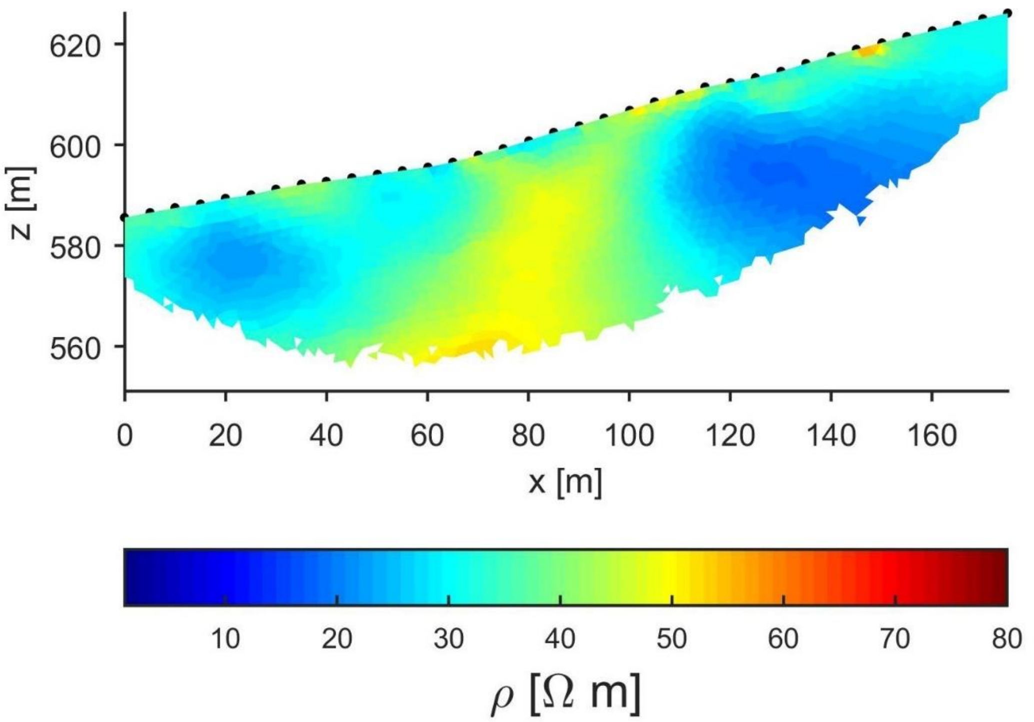

Figure 36. Distribution of electrical resistivity for ERT profile 3 (5-m electrode spacing)

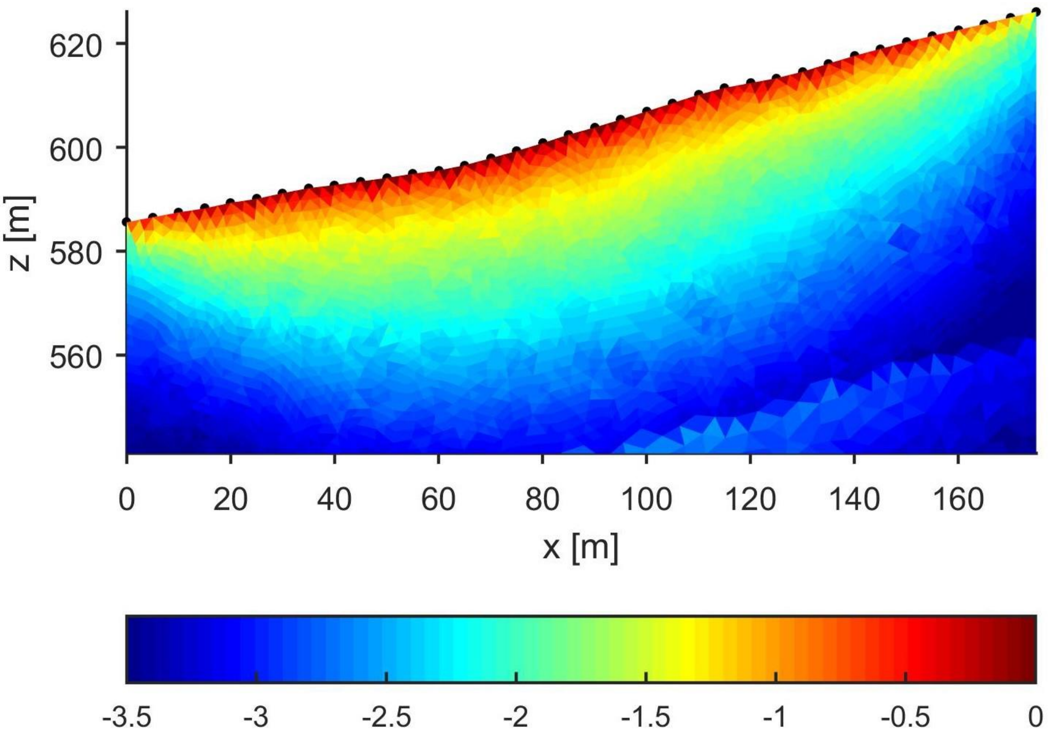

Figure 37. Sensitivity of measurement in ERT profile 3 (5-m electrode spacing)

In profile 4 to 7, one area of high resistivity stands out, as indicated by dark red colours. Profile 5 (Figure 38) is shown as an example. In each profile it is located between around 90 to 120 m. In profile 4 this anomaly is only superficial, but it extends to greater depths in profiles 5 and 6, creating the impression of a connection to the resistive area that intersects the two bubbles of lower resistivity. While the connection of these areas in the images suggest that there is material in the ground that extends the whole way from the bottom to the top, the connection could just as well, if not more likely, be a result of the smoothing in the inversion (see section 2.8) which prevents sharp transitions between areas of varying resistivity. It follows that if two areas of similar resistance lie close to each other, they will be depicted as one area in the image.

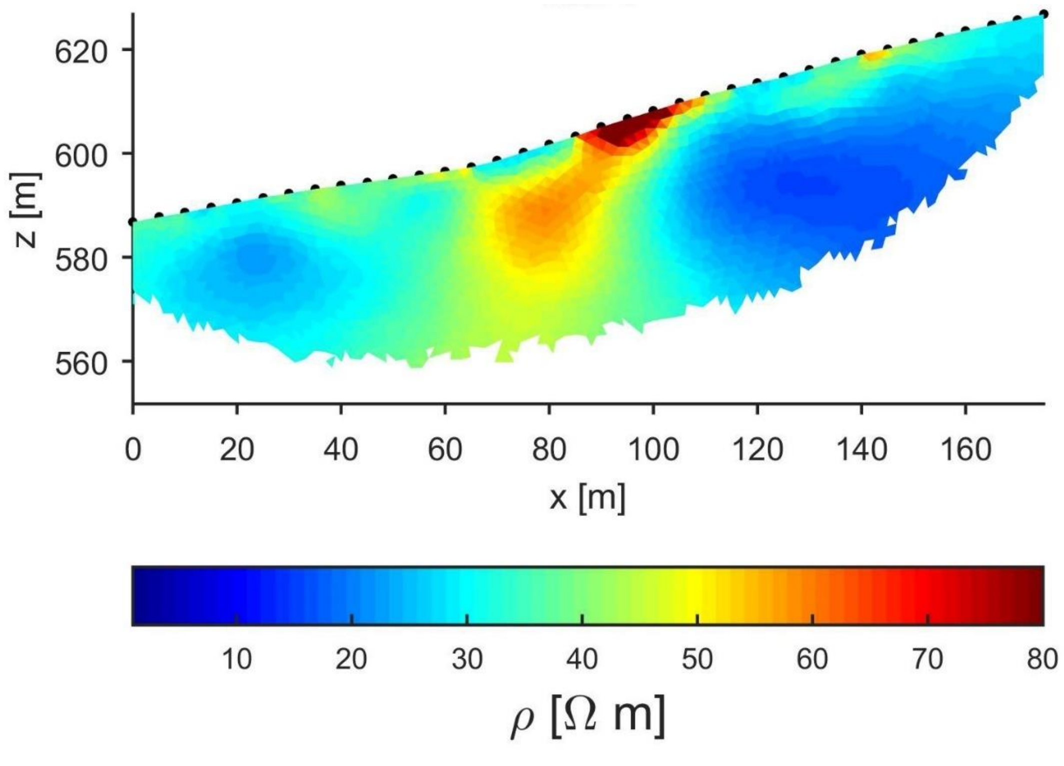

Figure 38. Resistivity distribution of ERT profile 5 (5-m electrode spacing)

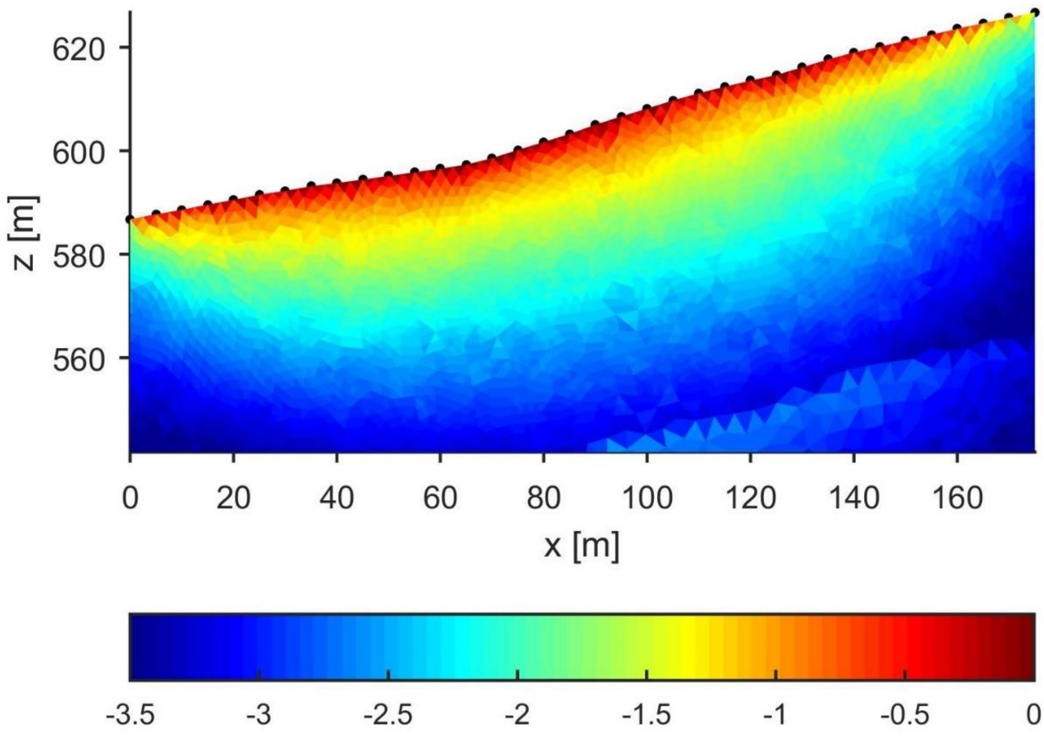

Figure 39. Sensitivity of the measurement for ERT profile 5 (5-m electrode spacing)

5.4.3 Error Analysis for the Inversion

Error analysis has been conducted by employing Flores Orozco et al.'s method (2017) and was considered in the inversion to improve the accuracy for the representation of the subsurface's electrical properties. As will be demonstrated in the following section, errors in the measurement are small and only few outliers are present in the data. Accordingly, the error accepted in the inversion was set equally small so that the model would closely reproduce the data.

The pseudo-sections already suggest clean data sets. As an example, the pseudo-section of profile 2 is provided here (Figure 40); the remaining images are included in Appendix B. Additional Results. The pseudo-section shows the values of the apparent resistivity, as obtained through the measurement, against a pseudo-depth and -distance. The apparent resistivity is indicated in logarithmic form by a colour scale, in which blue values represent low resistivities and red values represent high resistivities. Outliers are recognizable in the pseudo-sections as single points (each point representing one measurement) that stand out from surrounding points, i.e. the value departs significantly from those of surrounding measurements. The pseudo-sections contain either none or only a few such values.

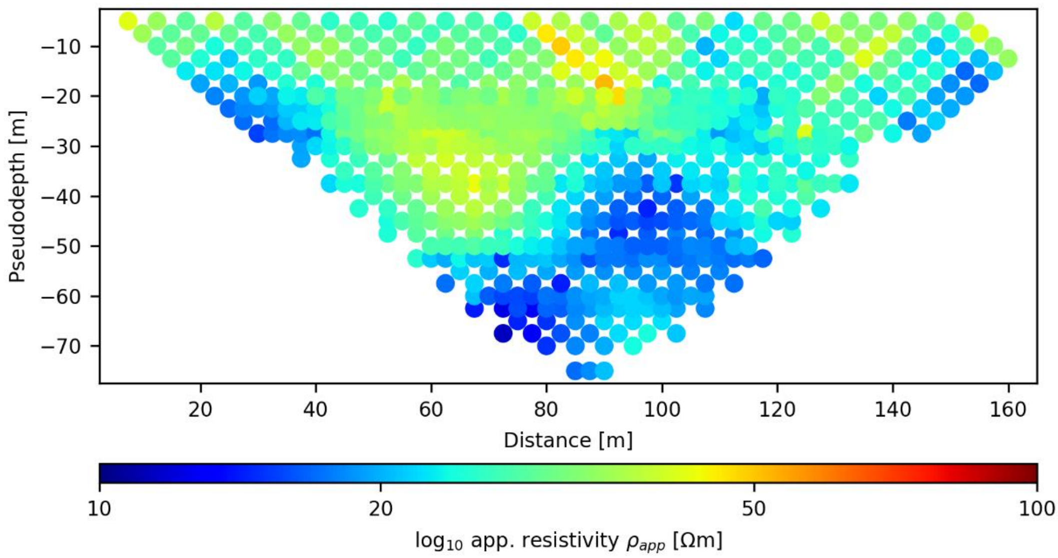

Figure 40. The raw data of ERT profile 2 plotted in a pseudo-section

The random error can be well described by the mean and standard error. Mean and standard error can be identified by comparing pairs of electrodes that were used twice in one profile (see section 5.4.3). This analysis also indicates how precise the measurements were. Figure 41 to Figure 43 show the histograms of the difference in the resistivity values obtained by the pairs of electrodes. The blue bars represent the frequency of a difference of a specific magnitude; the red line represents the best-fitting normal distribution for the specific data set. The errors are very small, the mean varying in the order of four to five decimal places. As can be seen in Figure 41 to Figure 43 by comparing the blue bars to the expected normal distribution, the distribution of the errors clearly departs from the normal distribution, as would be expected for random errors. Most of the errors are centered around zero, with only a few exceptions.

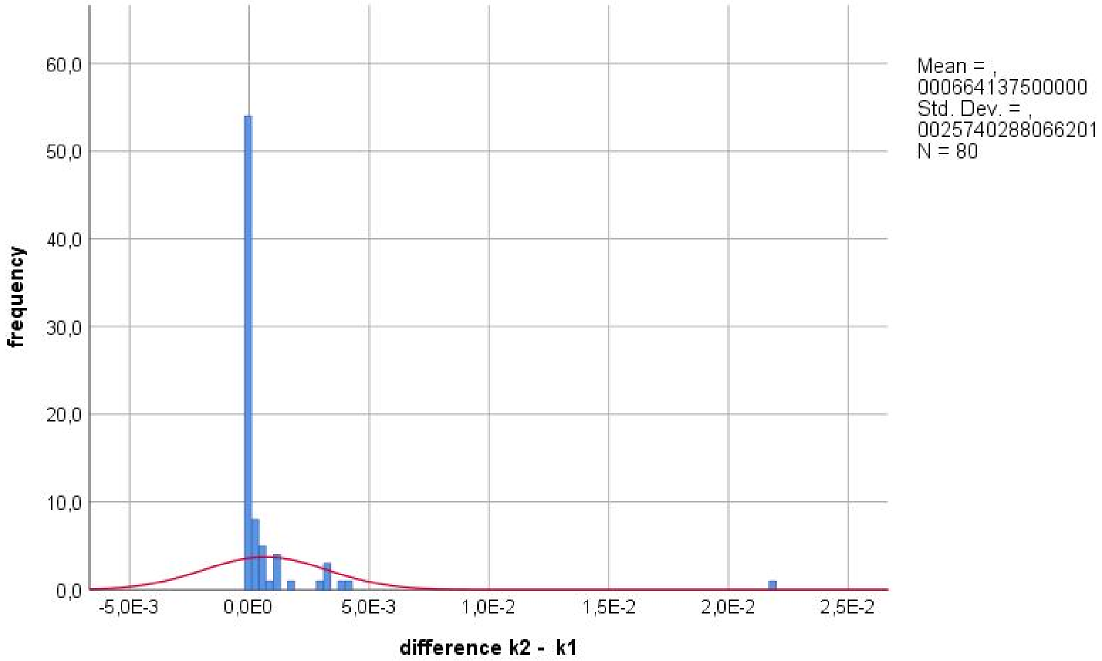

Figure 41. Histogram for error estimation for ERT profile 1. Difference in electrical resistivity between k1 (first segment of the roll-along) and k2 (second segment of the roll-along)

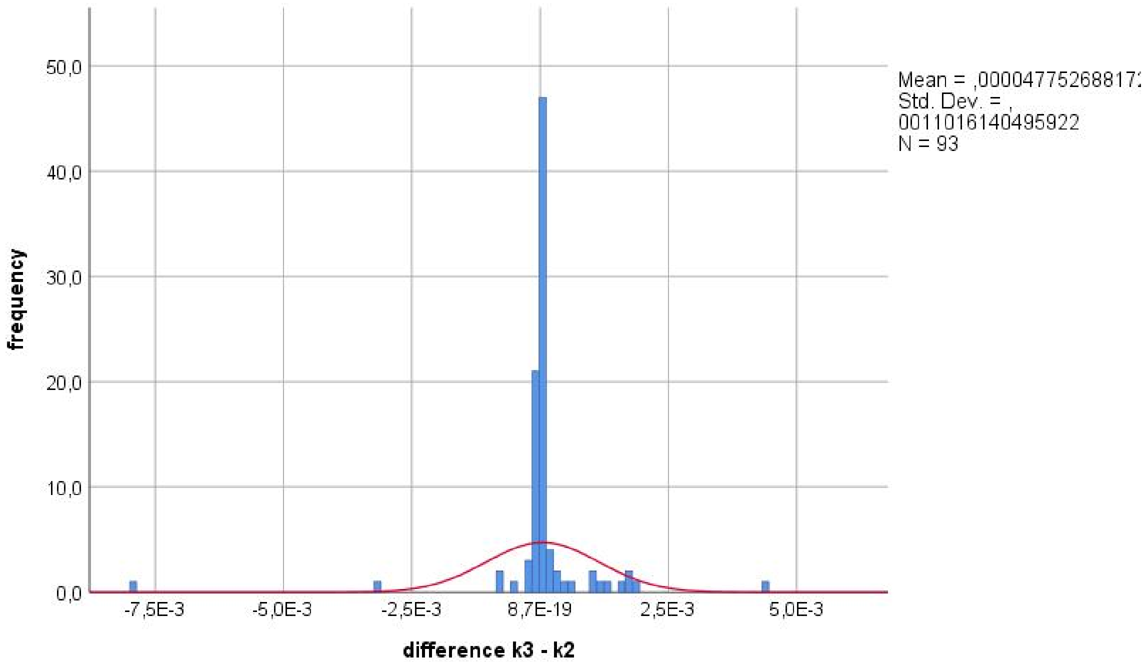

Figure 42. Histogram for error estimation for ERT profile 1. Difference in electrical resistivity between k2 (second segment of the roll-along) and k3 third segment of the roll-along)

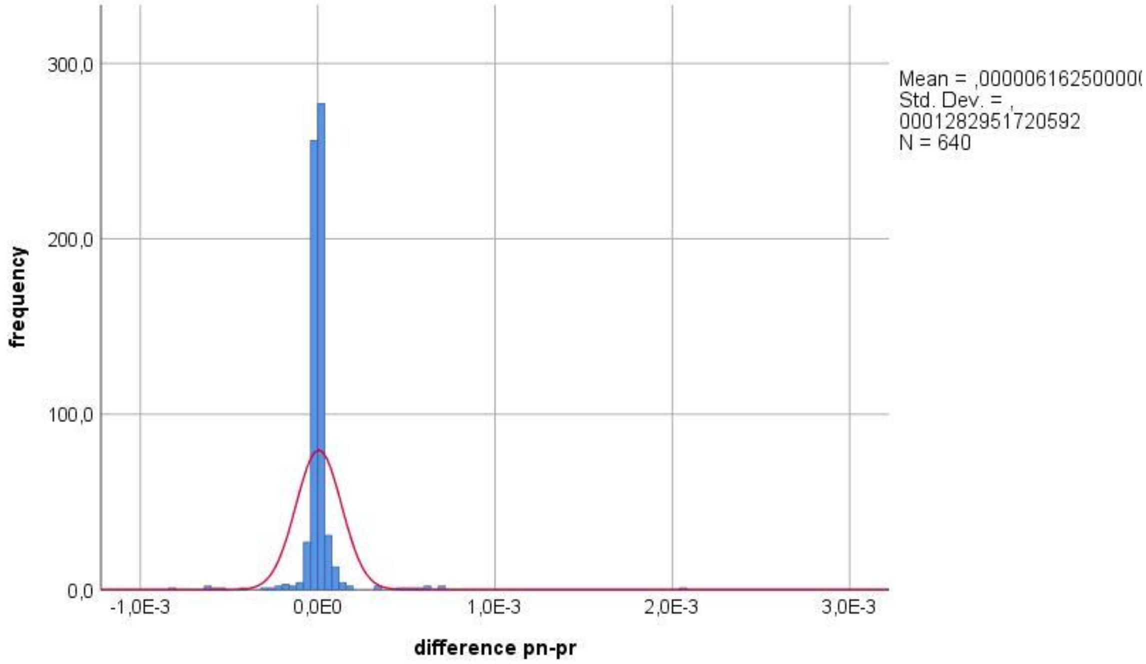

Figure 43. Histogram for error estimation for ERT profile 2. Difference of values obtained in pairs of electrodes used twice in the measurement

The departure from the normal distribution is clearly visible in a normal Q-Q-plot of the values. Figure 44 provides the Q-Q-plot for errors obtained through the comparison of normal and reciprocal pairs in profile 2. In this plot, the quantiles of the error distribution is plotted against the best fitting normal distribution for these values. That way, the two probability distributions are compared. If both distributions are equal, the points would fall along a line, and normality can be assumed for the distribution of the errors. Figure 44 and Figure 45 show that the points fall along a line in the middle of the graph but curve off in the extremities. This indicates that the data set includes more extreme values and more values in the middle of the graph than would be expected if they truly came from a normal distribution. However, considering the absolute value of the errors, even the extreme values are small compared to the associated resistivity value. Compared to the contribution of the relative error to the overall error, even the extreme values would not influence the inversion. Clear data sets are typically assigned a relative error of 1 %, which would correspond to an absolute value in the order of 1 or 2 decimal places for the resistivity data sets. In contrast, most of the values considered outliers are of the order of 3 decimal places, with only very few in the order of a relative error of 1 %.

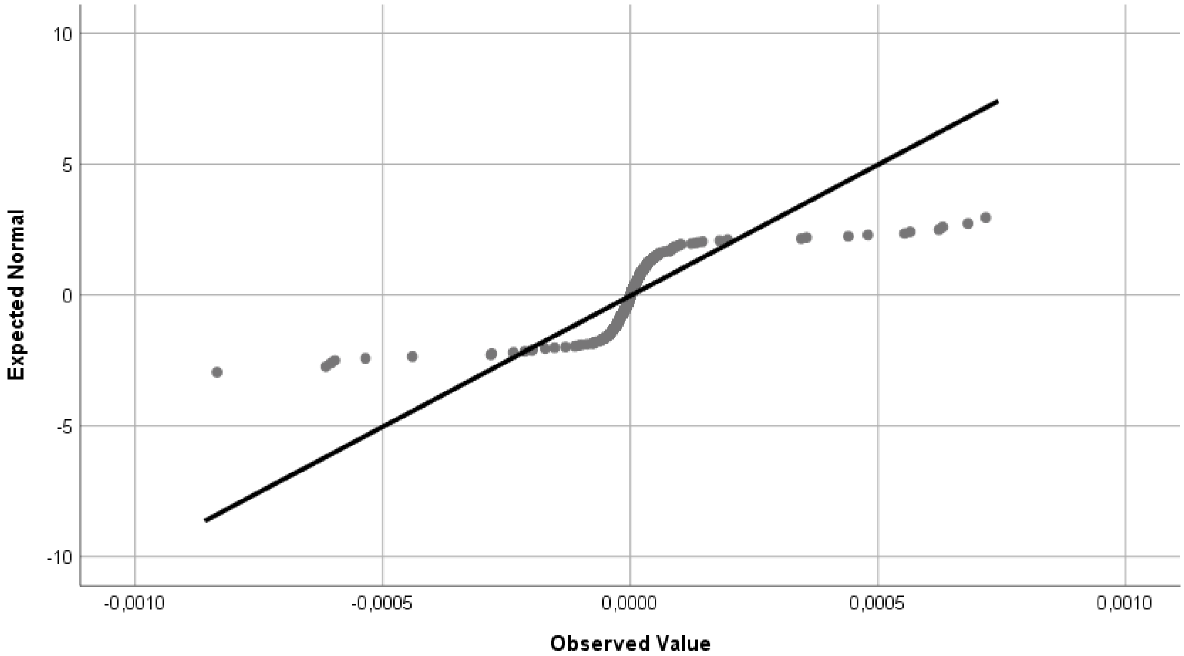

Figure 44. Normal Q-Q plot for normal and reciprocal pairs of ERT profile 2. The distribution of the differences in the measurement values between two pairs of electrodes (grey dots) clearly departs from the expected normal distribution (black line).

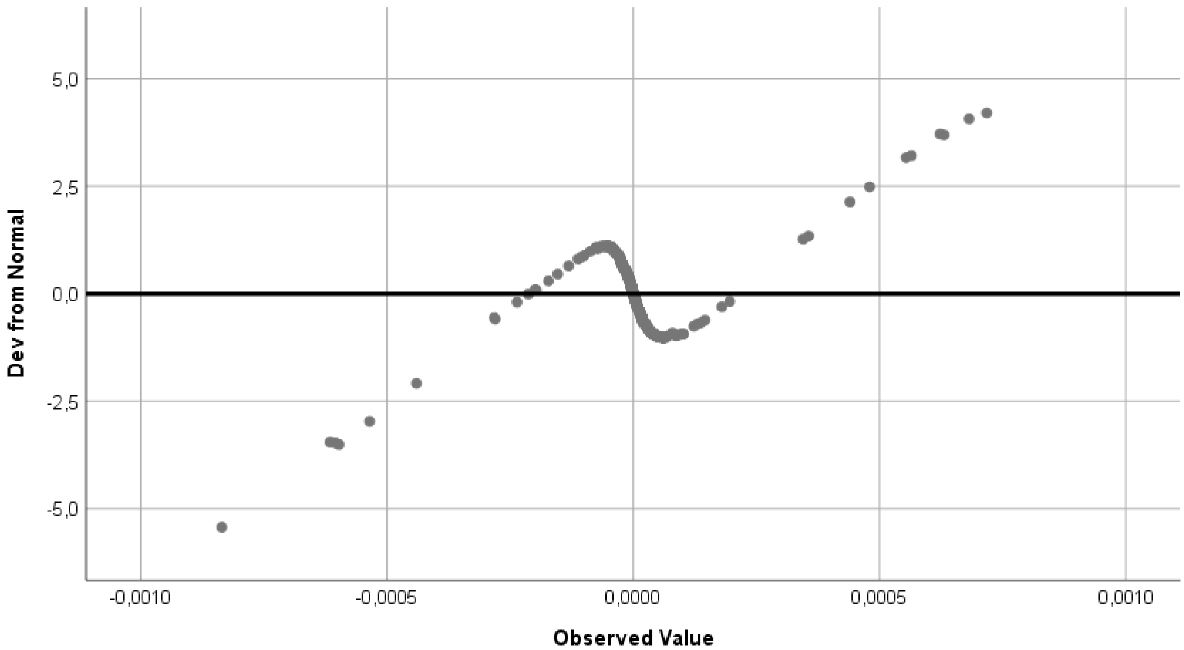

Figure 45. Detrended normal Q-Q Plot for normal and reciprocal pairs of ERT profile 2. The plot for the detrended normal shows how much the individual values depart from the normal distribution.

5.4.4 Interpretation

The error analysis clearly demonstrates that the errors in the measurement are very small. Hence, one can reasonably assume that the data quality is high. However, it is important to note that the data quality alone does not determine the quality of the electrical images. The accuracy of the inversion plays an important role as well. The quality of the inversion will be estimated based on ground truth information obtained through PD in chapter 6. The values for electrical conductivity, as measured with ERT, is high in the study site, with variance between approximately 10 Ωm and 80 Ωm. Such exceptionally high conductivity can most certainly be linked to the presence of fine-grained materials, specifically clay (see section 2.8), which is a defining risk factor in the study area (see section 3.4). Variance in electrical properties may indicate variance in materials or material properties. Given that flysch itself, the predominant parent material, is already heterogeneous, spatial variance in electrical properties may be expected as the electrical images reflect some of these characteristics.

6 Discussion

In the following chapter, the results will be discussed with regard to the research questions. It will be evaluated what each method contributes to characterizing the subsurface of the Hofermühle-landslide. A connection to previous chapters, specifically chapter 3 will be established. First, each method will be evaluated individually. The benefits and limitations of each method regarding the characterization of the subsurface of the Hofermühle-landslide will be addressed. Then, it will be analysed how the individual methods correspond to each other and whether the combined application of the chosen methods leads to an information advantage compared to the application of individual methods. Lastly, potential models for the characterization of the subsurface of the Hofermühle-landslide will be presented.

6.1 Individual analysis of each method

In the following section, the results obtained through each individual method applied in the study will be discussed and evaluated in terms of their informational value for the determination of subsurface structures in the Hofermühle-landslide. Limitations of each method will be considered. Thereby, the first research question will be addressed:

What information about subsurface structures can be obtained through each Percussion Drilling, Dynamic Probing Heavy and Electrical Resistivity Tomography?

6.1.1 Percussion Drilling

Percussion drilling was the only direct method applied in the study and provided ground truth information about subsurface properties for a single location on the slope. The visual and laboratory analysis of the drill core revealed thick soils and regolith, consisting of moist and fine-grained materials and low fluid conductivity. Structural elements identified through PD are related to vertical variance of subsurface properties.

PD confirmed the presence of thick layers of regolith and soil for the investigated slope, which are typical of the study area (see section 3.3.4), as the bedrock certainly lies below 4 m (in this location). In terms of a landslide-hazard this is particularly problematic as it can be assumed that there is a large amount of material on the slope that could be displaced during a landslide event.

As PD shows, the materials present on the slope are predominantly composed of silt and clay. The investigated slope thus appears typical of the study area, where cohesive and slightly cohesive soils containing loamy or fine-sandy layers are common (see section 3.3.4). Regarding the landslide hazard, such fine grained materials are particularly problematic since they naturally have low shear strength (see section 3.4). It can be assumed that the force balance on the slope is easily disturbed.
Clayey and silty materials, as shown in section 3, are characterized by a high capacity to hold water and are largely impermeable to it. As indicated in section 3.4, slides in the study area tend to occur along the binding and impermeable soil layers. Regarding the properties of materials present in the slope, the formation of a sliding plane along such layers is possible on this site, specifically in the connection with precipitation. Although the whole drill core is made up of such fine-grained materials, one section stands out in this regard. As stated in section 5.2.3 the material between 180 cm and 190 cm of depth seemed particularly compacted and may thus be a part of such a layer. Nevertheless, the formation of a circular sliding plane in a landslide event (see section 3.4) appears equally possible, considering that former slides were rotational slides.

All parameters examined (colour, particle size, water content and electrical conductivity of the soil solution) varied substantially between the first 2 m and the second 2 m of the core, indicating a structural change at around two meters (for the given location). The vertical variance thus indicates a layered earth, with layers characterized by varying degrees of weathering. The variance in soil properties determined the horizons for the drill core. As argued in section 5.2, the soil may be classified as cambrisol, yet it also features characteristics of pseudogley. Regarding what is known from literature (see 3.3.4), both soil types are common in the study area. It is also known that soil properties vary spatially, and that different soil types may alternate quickly at a given site, meaning that a soil type identified on the basis of one drilling is most certainly only representative for small areas.

One major drawback of PD is that it only gives point information, limiting the application of the method for the investigation of lateral variance in soil specific properties. As only one single drilling was conducted in this study, the informational value of the measurement regarding the whole slope is even more limited. Furthermore, parameters like the water content of subsurface materials are highly dynamic and vary both spatially and temporally, depending on weather patterns and subsurface flow. Hence, the measurement is merely representative for one point in time for a single location.

Since lateral variations in subsurface properties were not assessed at all in PD, it remains unclear whether the layering found in the drill core is typical for the slope, or whether the layering varies across the slope. However, it can be reasonably assumed that general information obtained through PD (such as the dominance of fine grained and soft materials) are representative of large parts of the slope.

6.1.2 Dynamic Probing Heavy

Dynamic Probing Heavy provided indirect data about the penetration resistance of the ground. Blow count numbers are low near the surface and increase below 3 m of depth in all profiles. The refusal depth in the three profiles varied between 5,50 m and 13,50 m.

DPH mainly allows the assessment of vertical variance. However, since data from three locations is available, assumptions about lateral variation of subsurface properties and related subsurface structures may be drawn accordingly. The low blow count numbers in each DPH profile for the first 3 m indicate very soft to soft ground, which is often related to an increased risk of slides. From the similar pattern in the three profiles it can be reasonably assumed that a continuous layer of soft (and strongly weathered) materials of approximately 3 m thickness stretches over larger areas on the slope. Beneath 3 m, blow count numbers are generally higher, certainly related to higher material compaction in larger depths. Yet, they are also more variable between the three profiles below 3 m. Although the variance is not drastic, it suggests that the structure of the ground may be more heterogeneous between a depth of 3 to 6 m.

One limitation of DPH is that the penetration resistance is related to various parameters. This can make a straightforward interpretation of blow count numbers in terms of subsurface structures difficult, as variation in blow count numbers can have several reasons (e.g. compaction, water content, etc.). As in the case of PD, some parameters that determine penetration resistance (e.g. water content) are dynamic and vary spatially and temporally and may lead to variance in penetration resistance that is not related to subsurface structures. For this reason, the results were only analysed qualitatively.
Another limitation of DPH is that the information obtained is point information, resulting in the same drawbacks as already discussed for PD. Contrary to PD, three tests were conducted so that spatial variance in layering could be assessed to a certain degree by comparing the profiles. However, the three tests were conducted near each other and focused on the lower (accessible) part of the slope, limiting the informational value for the entire slope. Specifically, no information is available for the upper part of the slope which is, as morphology suggests, endangered by further movement.
Last, DPH provides only indirect data, causing ambiguity in their interpretation. As has been discussed in section 5.3, the strong variation in refusal depth might be explained either through variance in the depth of the bedrock, or by the existence of a hard layer which was not penetrated in DPH 1 and 2. As both explanations are equally plausible given the current data available, no final judgement regarding the extent of the regolith is possible at this point.

6.1.3 Electrical Resistivity Tomography

ERT yielded indirect, 2-dimensional information on the distribution of electrical properties in the subsurface for a depth of max. 25 m. Subsurface materials are generally characterized by a low electrical conductivity, as shown in the electrical images. The magnitude of variance in electrical resistivity in the images is small, yet even subtle differences might be indicative of subsurface structures.

ERT revealed that the upper meters of the ground are spatially variable in their electrical properties, however the magnitude of variance is relatively small. Between approximately 5 and 25 meters of depth, the spatial variation of the electrical resistivity is lower, however the magnitude of variance appears slightly higher in all ERT profiles, as has been discussed in section 5.4, suggesting that materials or material properties are more uniform.

Certainly, they are less altered by weathering and are more similar to the parent material than in the uppermost meters. As pointed out in section 3.3.4, the soils in the study area are heterogeneous and spatial variance is high, meaning that different soil types or soils featuring different characteristics may alternate quickly at a certain location. Many soils in the study area are made up of loamy or fine-sandy layers, sands, coarse sands or scattered layers of rock debris (Schwenk et al., 1992, p. 622), as has been stated in section 3.3.4. The variance in the soils most likely corresponds with the heterogeneity of the parent material, flysch, which is itself composed of varying layers of marls, clays and sandstones (see section 3.3.3). Furthermore, weathering and geomorphological processes, such as creep, may have increased spatial variance even more through the continuous transformation and translocation of materials on the slope. Surely, both varying materials and soil properties contribute to the resistivity contrast in this section. Variance in electrical properties might reflect the heterogeneity of the parent material and the soils present in the slope.

The exceptionally high conductivity of the subsurface, as determined in ERT, clearly hint at the dominance of fine grained and weathered materials. Thus, it can be assumed that materials on the slope are composed of rocks or weathered rock that are predominantly made up of fine grains, such as clay and silt, as would be expected for the study area (see section 3.3.3). Given the range of values for the electrical resistivity, some materials could be excluded for the specific slope, such as rocks with a high resistivity (e.g. granite).

From the comparison of the electrical images (specifically the images of ERT profile 2 to 7) it can be concluded that subsurface structures remain constant over large parts of the slope, since all images show a similar pattern in the distribution of electrical properties. Likewise, the image of ERT profile 1 corresponds to the images of ERT profile 2 to 7 in localizing particularly fine-grained materials for the uppermost 10 to 15 m. However, there are some limitations to comparing the images obtained in different field campaigns. First, the images were collected with different electrode spacings, resulting in a difference of resolution in the electrical images. Second, different environmental conditions might have caused some variance in the images. A qualitative comparison still appears valid.

All in all, it can be deduced from ERT images that the ground on the entire slope is composed of more heterogeneous, most likely strongly weathered material overlying spatially less variable, supposedly less weathered material. Because ERT only provides indirect data, the interpretation of electrical images without any external information is challenging and vague. Materials involved cannot be determined with certainty, meaning that there will always remain some degree of ambiguity in the interpretation of results, as in DPH. This is also true for this study.

Even though ERT imaging was successfully implemented to identify one major risk factor regarding the landslide hazard on the slope, namely the dominance of fine-grained materials, definite structures of the subsurface cannot be deduced from the images of electrical resistivity alone. In this context, the high clay content of subsurface materials turned out to be a major limiting factor for the deduction of subsurface structures (e.g. the distribution of materials) from images of the electrical resistivity. Because of the high conductivity of materials near the surface, most of the current only passed through the uppermost meters of the subsurface, instead of permeating larger depths, as would have been possible in theory for the given electrode spacing. This leads to a loss of sensitivity for greater depths, meaning that there is less data available for them. Because of that, it cannot be determined from the ERT images how much further the highly conductive areas, as indicated by blue bubbles in profile 2 to 7 (See Figure 32 to Figure 38), extend.

6.1.4 Preliminary Conclusion

Materials associated with a high risk of landslides were suggested by each individual method. PD confirmed the presence of clays and silts for the investigated slope. DPH and ERT suggest that these materials are present on large areas on the slope. Yet, subsurface structures relating to the distribution of materials on the slope could not be determined exactly by the individual methods. Although each method yielded valuable details about the subsurface of the

Hofermühle-landslide, it is impossible to generalize the information for the whole slope or to exactly relate variance in parameters assessed to subsurface structures (as for indirect data). Moreover, some methods (PD and DPH) have not been applied to their full potential and a more thorough application of the two would increase data availability and potentially make the collected data representative for larger areas of the slope.

6.2 Combined Analysis of the Individual Methods

The previous section clearly demonstrated the limitations in the application of individual methods for the investigation of slope-subsurface structures. In theory (see chapter 2.5 and chapter 4), combining different methods allows to overcome certain limitations of individual methods, and achieve a more realistic interpretation of the subsurface. In this section, the methods will be compared pair-wise and the following research question will be addressed:

What information about subsurface structures can be obtained through the combination of Percussion Drilling, Dynamic Probing Heavy and Electrical Resistivity Tomography?

Sub-questions:

To what extent can direct data from PD be used to validate indirect data as obtained through DPH and ERT?

To what extent can DPH and ERT be used to extrapolate data obtained through PD?

In addition, the limitations of comparing data in different forms will be evaluated. For an overview, Figure 46 shows a section of the ERT profile 1, together with the location and depth of PD (red bar) and DPH (pink bars).

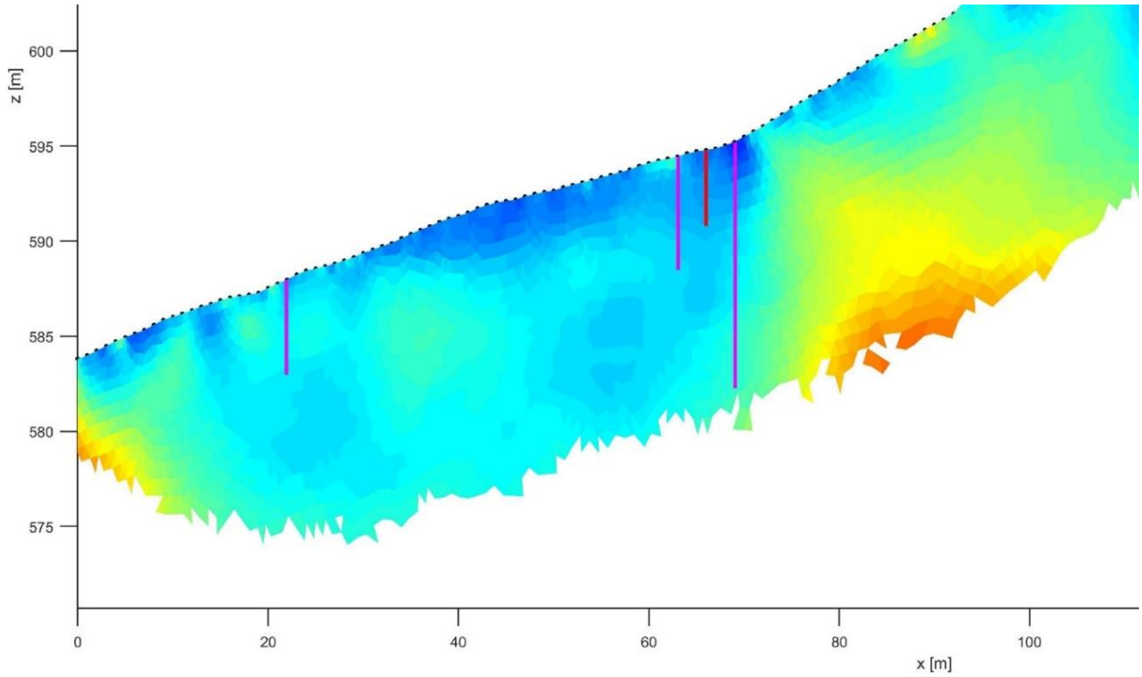

Figure 46. Location of DPH (pink) and PD (red) in relation to the ERT profile 1. The image does not show the full ERT profile.

6.2.1 Comparing Radically Different Data Sets

To overcome limitations of individual methods and achieve a more realistic interpretation, as discussed in the previous section, different methods were combined for the exploration of the subsurface of the Hofermühle-landslide. Thereby, each method provided data on different properties and in a radically different form.

Comparing fundamentally different data is challenging in many ways. One challenge is that the individual methods provide data on different parameters, meaning that a causal relationship does not necessarily exist between the individual datasets. However, different parameters might be diagnostic of the same subsurface structures. Through a critical comparison, links between datasets from individual methods may be established. Yet, the connections between parameters are merely assumptions, and by no means proven relationships.

The individual methods not only provide data on completely different parameters, but also in a radically different form. While PD and DPH give point information on subsurface properties, ERT yields 2-dimensional information. Another example of varying formats is

DPH and PD, even though both yielded point data. DPH provided continuous values for penetration resistance (for 10 cm increments), PD only provided sporadic data, as can be seen in Figure 26. A direct comparison is therefore not possible. A single high blow count number cannot be adequately linked to parameters evaluated in PD. A systematic laboratory analysis for 10 cm increments would have enabled a more detailed comparison yet this approach would drastically increase the time necessary for laboratory analysis.

The comparison between PD, DPH and ERT is even more difficult, as PD, DPH and ERT are measures with radically different scales. The resolution of PD and DPH is much higher than the resolution of the ERT images, no matter the electrode spacing. The resolution of PD and DPH data is on the cm-scale, while the data on electrical values have a resolution of 25 cm for 1 m electrode spacings and 100 cm for 5 m electrode spacings. Electrical properties as obtained by ERT can hardly be linked to structures (i.e. layers) identified in PD and DPH. As an illustration, the case of a horizontally layered ground is considered. In this example, the ground is assumed to consist of layers of varying thickness and varying (electrical) properties. Figure 47 provides an illustration of the example. The column in the middle of the image represents a layered ground. Each layer is characterised by distinct geophysical and electrical properties. The colours in the image indicate the electrical properties of the layers. On the left and right side of the layered ground, single pixels of electrical images are depicted. The pixels on the left side represent the relative size of one pixel in an ERT profile with 1 m electrode spacings and the pixel on the right side shows the relative size of a pixel in an ERT profile with 5 m electrode spacings. When comparing the size (thickness) of one layer in the ground to the size of one pixel in the electrical image, it becomes clear that the resistivity values in the electrical images may not accurately represent the resistivity distribution in the subsurface. The upper pixel on the right side of the layered ground is much bigger than the layers in the ground and so the resistivity value in the electrical image may be caused by all the layers. Consequently, the individual layers may not be depicted in the electrical image. The same is true for the lower pixel on the left side (red). The thin layer (yellow) that has a lower electrical resistivity than the surrounding ground may not be visible in the pixel. Likewise, it is possible that one layer in the ground dominates the electrical value of a pixel, again leading to a misrepresentation of the actual subsurface structures. Only when the pixels in the electrical images are of equal size or smaller than the structures in the ground, the measurement values will accurately represent the distribution of electrical properties in the ground.

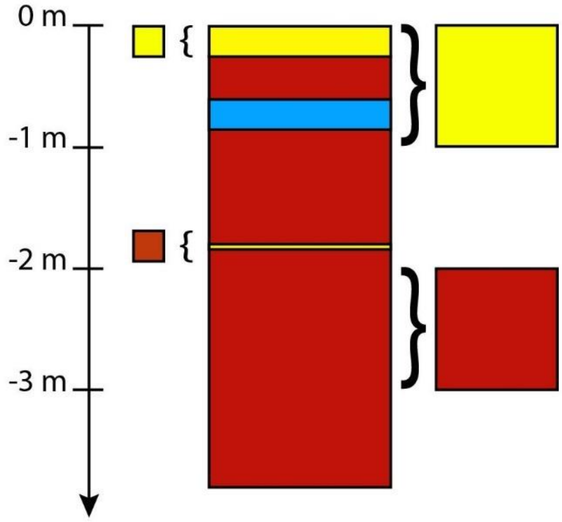

Figure 47. Illustration of difficulty when comparing measures of differing scales. The column in the middle represents a ground consisting of six layers, all having distinct electrical properties. The squares on the left side of the column show the relative size of a pixel in the electrical images for a 1 m electrode spacing. The squares on the right side of the column depict the relative size of a pixel for a 5 m electrode spacing. Depending on the size of the pixel compared to the size of a layer, the pixel may or may not accurately represent the distribution of the electrical resistivity in the ground.

In practice, it is not possible to achieve an exact match between the distribution of subsurface electrical properties and the corresponding electrical image as the variation of the electrode spacing is limited. Differences in the resolution make a straightforward comparison of obtained data difficult, if not impossible. But while a comparison of measures with such radically different scales is surely not preferable, it is feasible, if the focus lies on general patterns instead of details.

6.2.2 Analysis of PD and DPH

PD and two DPH tests were conducted near one another. Hence, both methods investigate similar subsurface conditions which is prerequisite for any comparison between the two methods. As already outlined, PD and DPH both provide point information, yet on different parameters and in different forms (continuous and sporadic). Further difficulties to consider in this comparison are differences in the compaction of materials. Even though the methods are similar, it can be assumed that the different shape of the drill bit compared to the rods has an influence on the compaction of the materials in the subsurface, meaning that values in the DPH profile for a specific depth do not necessarily correlate with values from PD for a specific depth. Thus, results obtained through PD and DPH may only be compared qualitatively.

The comparison of the two methods indicates a correlation between the particle size distribution and penetration resistance. As can be seen in Figure 31, blow count numbers increase significantly at a depth of 3 m, most notably in DPH 1 and DPH 2. As found in the laboratory analysis of the drill core, the uppermost 2 m of the drill core contain significantly more clay and less sand than the lower 2 m of the drill core. Fine-grained materials are usually related to low blow count numbers. Hence, PD confirms the interpretation of data obtained through DPH.

Presumably, higher blow count numbers also correspond with slightly increased values for compaction, specifically in DPH 1 and DPH 2. Even though the compaction was not measured in the analysis of the drill core, but only assessed qualitatively, it can be said for certain that materials in greater depth, specifically between 3 and 4 m of depth, were increasingly compacted, as they appeared much harder and more difficult to break apart. It is important to notice at this point that the correlation between DPH 2 and PD is probably stronger, as the two were conducted very close to one another, while DPH 1 was conducted further down the slope.

Nevertheless, the assessment of vertical correlation between PD and DPH was limited, first because only one drilling is available and, second, because data from PD is only available within the first 4 m of the ground surface. PD data for greater depths would have been particularly useful to see if refusal in DPH 2 was met because of bedrock, or because there was a harder layer in the regolith (see section 5.3.1).

One important way in which the combination of PD and DPH led to a better understanding of subsurface structures is through extrapolation. As only a single drilling was conducted, no information about lateral variance in soil physical properties could be acquired with PD. Therefore, DPH may be used to extrapolate information, which was obtained through PD, to other areas on the slope. While extrapolation bears the risk of producing inaccurate results, it may increase the informational value of PD, specifically if it does not go too far beyond the known data. Despite some minor variance, all DPH profiles are characterized by very low blow count numbers within the first 3 m of the ground surface. DPH hints at the existence of a relatively continuous, soft layer over slightly more heterogeneous materials. It may be concluded that similar ground conditions prevail over larger areas on the slope and that results obtained through PD, specifically on the uppermost 3 m of the ground, may be representative for larger parts of the slope.

6.2.3 Analysis of ERT and PD

As outlined before, a direct comparison of data obtained through ERT and data obtained through PD is particularly challenging because of varying scales. It should be noted, that the image of ERT profile 1 features a better resolution than ERT profile 2 and is thus better suited for a comparison of the different methods. Consequently, only a qualitative comparison of soil physical parameters evaluated through PD on the one hand, and electrical parameters obtained through ERT on the other hand, is feasible. The comparison of results obtained through PD and ERT enhances the deduction of subsurface structures in two ways. First, results from PD may be used to validate ERT and achieve a more realistic interpretation of the variance in electrical resistivity in the ground. Second, ERT may be used for extrapolating data obtained through PD. To ensure comparability, PD was conducted near ERT profile 1 and 2 (see Figure 21).

Ground truth information on soil specific values as obtained through PD and is necessary to validate the interpretation of ERT. As electrical resistivity is only indirectly related to geophysical properties, and the relation between geophysical properties and electrical properties is not yet entirely understood (see 2.8), ambiguity in the interpretation of electrical images is a common problem in the application of geoelectrical measurements. PD, being the only way of directly determining the materials and their properties involved, it is used in this study to narrow down the range of materials that cause the variation in electrical resistivity.

As discussed earlier in this section, ERT suggest the dominance of fine grained materials, specifically clay, for large parts of the slope, as can be deduced from exceptionally high conductivity (see previous section). PD provides proof for this assumption in two ways (even if only for one location). First, the particle size analysis is clear evidence for the dominance of fine-grained materials, as silt (49 %) and clay (31 %) account for 80 % of the total mass of the particles on average for one location on the slope. Second, the comparison of the fluid conductivity of several samples, as assessed in the laboratory analysis, and the electrical resistivity (or conductivity) determined through ERT, provides further evidence for the prevalence of fine-grained materials in the subsurface. The electrical conductivity of the soil solution, as measured in the laboratory analysis, is mostly due to electrolytic conduction, as the soil was dissolved in water. When comparing values for electrical conductivity of the soil solution with values for electrical conductivity for the drilling location, one can see that the values depart from one another. Electrical conductivity as indicated in the ERT is much higher than the electrical conductivity determined in the laboratory. While the conductivity as measured in ERT lies between around $1.25 \cdot 10^6\ \frac{\mu S}{cm}$ and $10 \cdot 10^6\ \frac{\mu S}{cm}$, it only reaches values between approximately 20 $\frac{\mu S}{cm}$ and 200 $\frac{\mu S}{cm}$ in the laboratory. This shows that electrolytic conduction contributes little to the overall conductivity of subsurface materials, and that interfacial conductivity prevails over electrolytic conductivity. This finding is evidence for a high clay content in the subsurface. But while ERT measurements are a strong indicator of a high clay content, they are no proof, as is PD. Even if only for one location on the slope, the relationship between a high clay content and increased conductivity is demonstrated by the combined application of PD and ERT. Because surface conductivity is much higher than electrolytic conductivity, it may mask the correlation between saturation and the electrical resistivity so that variation of saturation (hydrological conditions) may not be delineated from ERT images. Rather, the ERT images are more indicative of the clay content, than the water content.

While the results obtained through PD and ERT are in close agreement with each other regarding the identification of fine-grained materials on the slope, PD could unfortunately not be used to evaluate the causes of spatial variance in the electrical properties across the slope. This is because PD only covers a small fraction of the ERT (Figure 46), where there is only little variation in electrical properties. Also, no data from PD is available for larger depths, so that these depths cannot be considered in the comparison of PD and ERT. Lateral and horizontal variation in electrical images cannot be explained through PD. Having ground truth information for areas in which electrical properties vary significantly would have allowed to draw more certain conclusions about the causes for variance in the electrical images, as the reason for variance might be directly observable in PD (as for example a change of materials).

Another way in which PD and ERT complement each other is by extrapolation. Provided that the specific values for electrical resistivity indicate identical materials, one can extrapolate the information from PD to other areas on the slope. It can be assumed that areas showing similar electrical properties also feature similar geophysical characteristics. If so, then the two other areas may have a similar composition as the location in which PD was conducted. The two areas are indicated in Figure 48. Yet, this assumption might not necessarily be true, as specific values of electrical resistivity can stem from a range of materials and material properties.

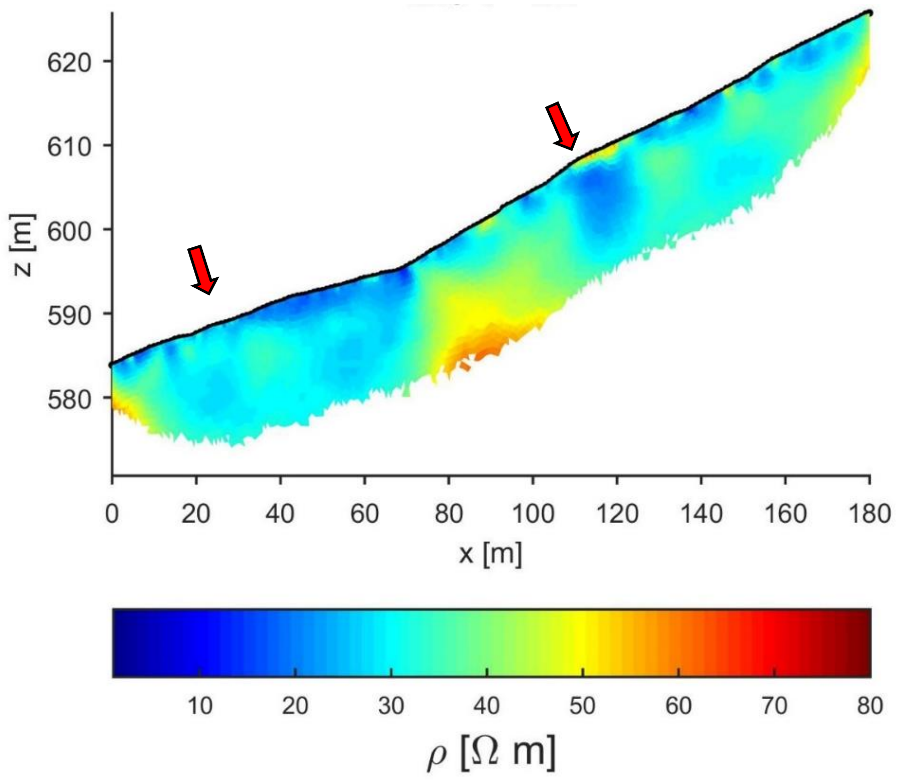

Figure 48. Potential extrapolation of PD to other areas on the slope exhibiting similar electrical characteristics, the arrows indicate areas that feature similar electrical properties like the area in which PD was conducted.

6.2.4 Analysis DPH and ERT

The radically different resolution of the two measurements forbids a direct comparison of the datasets obtained through DPH and ERT, as explained earlier. Specifically, single peaks or minimums in blow count numbers cannot be directly linked to electrical properties as shown in the ERT. This is particularly evident when comparing the refusal depth in DPH to electrical images. Through DPH the depth of hard layers can be determined well, even though in this specific case some uncertainty remains whether the bedrock or a hard layer caused refusal in DPH 1 and 2. As can be seen in all electrical images, the transitions between areas of varying resistivity are rather smooth and no sharp boundaries, such as suggested by DPH, can be identified in the electrical images, which might be related to varying scales. Moreover, the smoothing in the inversion was set to not confine the model search to a specific layering, thus information on layers might have been lost in the final images.

Apart from that, a certain connection between the resistivity to penetration and electrical resistivity is not established. However, soft materials, which are more easily penetrated in DPH, are often associated with a high content of fine grained materials. Such materials are a defining risk factor for landslides in the study area. Hence, a correlation between penetration resistance and electrical resistivity in the ERT may be established for the investigated slope.

Unfortunately, both DPH 1 and 2 are located in areas where electrical properties do not vary drastically and cannot be used to assess the correlation of vertical variance in both blow count numbers and electrical values. DPH 3 however covers a larger range of electrical values. As can be seen in Figure 46, values for electrical resistivity increase steadily with depth, as indicated by the transition from blue to light blue and green/yellow shades. Likewise, blow count numbers (N_{10} values) increase steadily with depth in DPH 3, as shown in Figure 31. While a causal relationship may not be assumed at this point, it can be hypothesized that the variation on both blow count numbers and electrical values indicate a structural change, i.e. in the form of a materials change or, more likely, changing geophysical parameters, such as the compaction of materials and the particle size distribution.

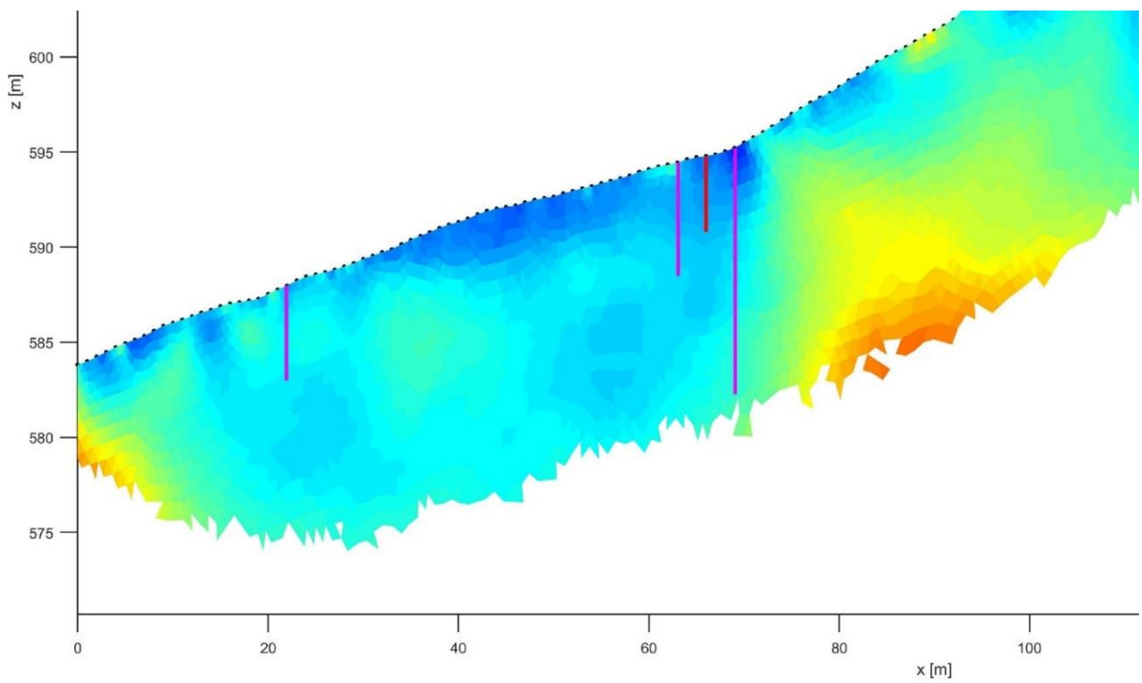

Figure 49. Location of DPH (pink) and PD (red) in relation to the ERT profile 1. Note that the image does not show the full ERT profile.

For the analysis of the correlation in lateral variance between blow count numbers and electrical resistivity a similar problem as discussed in the previous paragraph arises. As can be seen in Figure 49, all DPH profiles are located within an area of similar resistivity, meaning that a feasible analysis of correlating spatial variance between the two datasets is limited. Since neither blow count numbers nor electrical resistivity vary significantly in the upper 5 m, the correlation between the two cannot be assessed. However, both methods coincide in identifying fine-grained materials in the uppermost section of the subsurface. This may indicate that the uppermost section of the ground in the lower area of the slope features largely similar characteristics.

6.2.5 Analysis Aerial Information and ERT

Lastly, satellite images offer noteworthy opportunities for the interpretation of electrical images. As has been argued in section 5.4, the highly resistive areas near the surface may indicate materials from external sources, as the resistivity values strongly depart from surrounding values. Indeed, the highly resistive areas, as indicated through dark red to orange shades in the electrical images, align spatially with a former gravel path, which is not visible anymore except on an old aerial photograph (Figure 50). The old aerial photograph shows two gravel paths, the southern one clearly visible, the northern one barely visible. Interestingly, the northern gravel path, which is only barely visible on the photograph, correlates with a drastic increase in resistivity values in the electrical images, while the southern gravel path does apparently not cause such an anomaly in the image. One reason might be that the northern gravel path is older and has already subsided deeper into the ground than the southern gravel path. Gravel near the surface might not alter the path of the current in the subsurface powerfully enough to cause a resistivity contrast in the electrical images, but gravel that has already subsided several decimeters to meters might do.

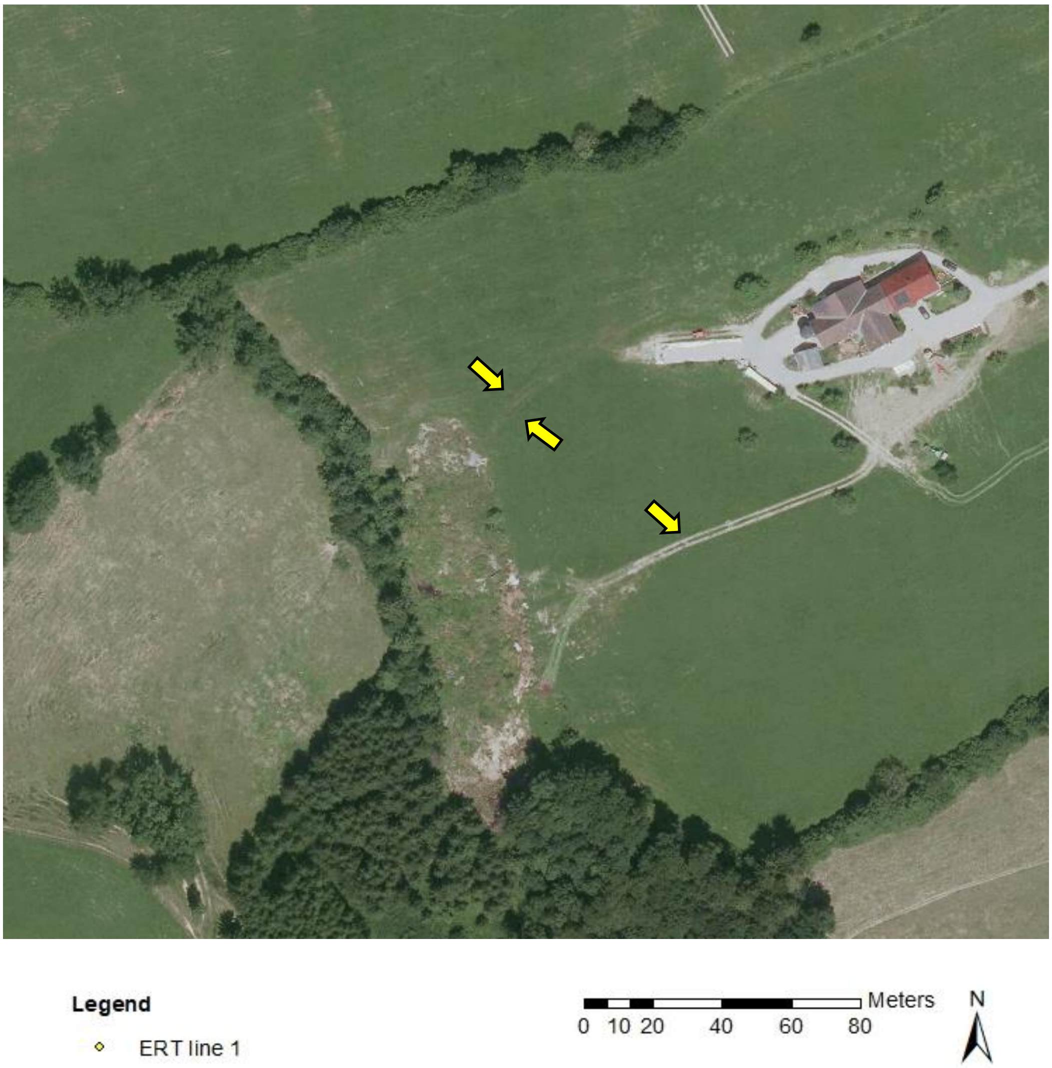

Figure 50. old aerial photograph of the slope shows former gravel paths as indicated through arrows; source: Land Niederösterreich

6.2.6 Preliminary Conclusion

The combination of different methods significantly improved the understanding of subsurface structures of the Hofermühle-landslide. Regarding the identification of fine-grained materials on the slope, the results obtained from different methods are largely consistent. Specifically, PD turned out to be indispensable for the validation of results attained with indirect methods for the subsurface exploration. The data interpretation of indirect methods could not have been proven without ground truth information obtained through PD. Given the data from the different methods, one can reasonably assume that fine-grained and clayey materials prevail over large parts of the slope. The results confirm that risk factors relating to the geologic setting (thick layers of fine grained materials) play an important role in slope dynamics at the Hofermühle-landslide (see section 3.4).

Despite the benefits that arise from the combination of methods, several questions regarding subsurface structures, i.e. the distribution of materials, remain unanswered. Particularly explaining the spatial variance in the DPH profiles and ERT images is not possible at this point since ground truth information for validation of indirect data is available for only one location on the slope. To determine exactly the cause of variance in electrical properties, PD data for areas with varying electrical properties would be necessary.

6.3 Models for the Subsurface of the Hofermühle-landslide

Not claiming to deliver a complete account, this section will provide two interpretations of the subsurface of the Hofermühle-landslide based on the information obtained through all methods. Thereby, the following research question will be addressed:

What subsurface model can be established from data obtained through PD, DPH and ERT?

An interpretation of data is necessary because indirect methods do not provide a one-to-one representation of the ground. Any model for the interpretation of the electrical resistivity distribution is based on the fundamental assumption that equal resistivity values in the electrical images indicate similar subsurface conditions, which of course, must not be true. While it is unlikely that subsurface structures vary so drastically as to render ERT images useless for an interpretation of the subsurface, identical resistivity values, strictly speaking, only imply similar electrical properties.
Sharp boundaries as well as lateral or horizontal structures may not be accurately represented in the electrical images due to smoothing in the inversion. Even though the electrical images, specifically the ones with electrode spacing of 5 m, suggest round, bubble-like structures, these structures are not necessarily representative of subsurface structures. Because the model search was not restricted by an anisotropic smoothness constraint (e.g. for vertical or

horizontal layers), it is possible that layers present in the subsurface are not represented adequately in the final images and appear the form of bubble-like structures instead. Knowing that many locations in the study area feature a layered ground, some kind of layering may also be expected for the Hofermühle-landslide.

Given what is known from each individual method, two models may be derived for the subsurface of the Hofermühle-landslide. Clearly, each model is an assumption as well as it is a generalization. The models are merely a representation of collected data in an integrated form. Since ERT offered the most extensive data on spatial variance (as it is the only method producing 2-dimensional information), the interpretation will start with the ERT images and then consider data from other methods to achieve a consistent interpretation of the subsurface.

6.3.1 Model 1: Vertical Layers

The first model assumes that the distribution of electrical resistivity is caused by tilted to almost vertical layers in the ground. Hence, the bubbles in the images may be interpreted as layers that have a relatively vertical orientation. It is easy to see how a vertically layered ground may cause horizontal variance in electrical properties, as seen in the electrical images. If alternating distinct layers in the ground are characterized by varying electrical properties, the resistivity contrast may mimic the distribution of the respective layers. Considering that the smoothing in the inversion prevents sharp boundaries and that the resolution of the images limits how accurately specific layers in the ground are represented, one may not expect to see exactly the boundaries between layers. The potential boundaries between vertical layers are shown in Figure 51 as dotted, tilted lines.

For a more detailed interpretation, external data sources as well as data from the other methods applied may be included. Considering what is known from geologic surveys in the study area, the vertical layers as proposed in this model may be interpreted as alternating layers in the bedrock or weathered rock. As has been stated in section 3.3.3, the rocks present on the slope have a dip of 35°W – NW (Sausgruber, 2013, p. 2). The ERT were laid out in almost the same direction. Running from SE to NW, the cross section of the profiles would theoretically show tilted layers from the side, if present. The direction of the dip suggested in this model based on the electrical images thus coincides with the dip of the rocks on the slope, as known from the study of Sausgruber (2013, p. 2). Hence, the images may reflect the alternating layers of the bedrock. As established by Sausgruber (2013, p. 2, 2016), the rocks present on the slope are weathered sandstones, marls and clays. Considering the geologic underpinning, the blue areas in the electrical images may indicate sections of the bedrock or weathered rock that consist of more fine-grained materials (for example from clays and marls), while the yellow section in the middle could represent sections of the bedrock or weathered rock that contain coarser particles (e.g. from sandstones).

Another vertical structure that may explain the lateral variation in electrical resistivity values is a disturbance zone located in the middle of the ERT profiles. An electrical current may not easily pass a disturbance in the rock (or weathered rock), leading to higher resistivity values in electrical images, as indicated by yellow to orange shades in the images.

DPH and PD suggest that soft to very soft materials composed of mostly fine-grained materials cover large sections of the slope. Although not visible in the electrical images, introducing one horizontal layer to the model represents these findings. Unfortunately, the depth of the regolith could not be determined with certainty in DPH and ambiguity remains in the interpretation of refusal depths in DPH (see section 5.3.1). Thus, two scenarios are conceivable. First, it is possible that the refusal depths of the DPH profiles truly indicate the depth of the bedrock. This would fit the current model. If a line representing the boundary between regolith and bedrock is drawn in accordance with the refusal depth in DPH, as shown in Figure 51, one can see that this line separates the uppermost, spatially variable section of the ground (as can be expected for regolith) from the more homogenous area underneath (as can be expected for the bedrock). One contradiction to this interpretation is that, if the bedrock is assumed at a depth of around 5 to 15 m, this would mean that parts of the bedrock feature a higher conductivity than the loose materials above, while most of the time the opposite is the case. This first scenario is illustrated in Figure 51 by line I.

Assuming on the other hand that the bedrock lies deeper than DPH refusal depths suggest at first view, the three bubbles in the electrical images may be interpreted as slightly weathered rock that still strongly reflects the properties of the parent material. This second version is illustrated in Figure 51 by line II.

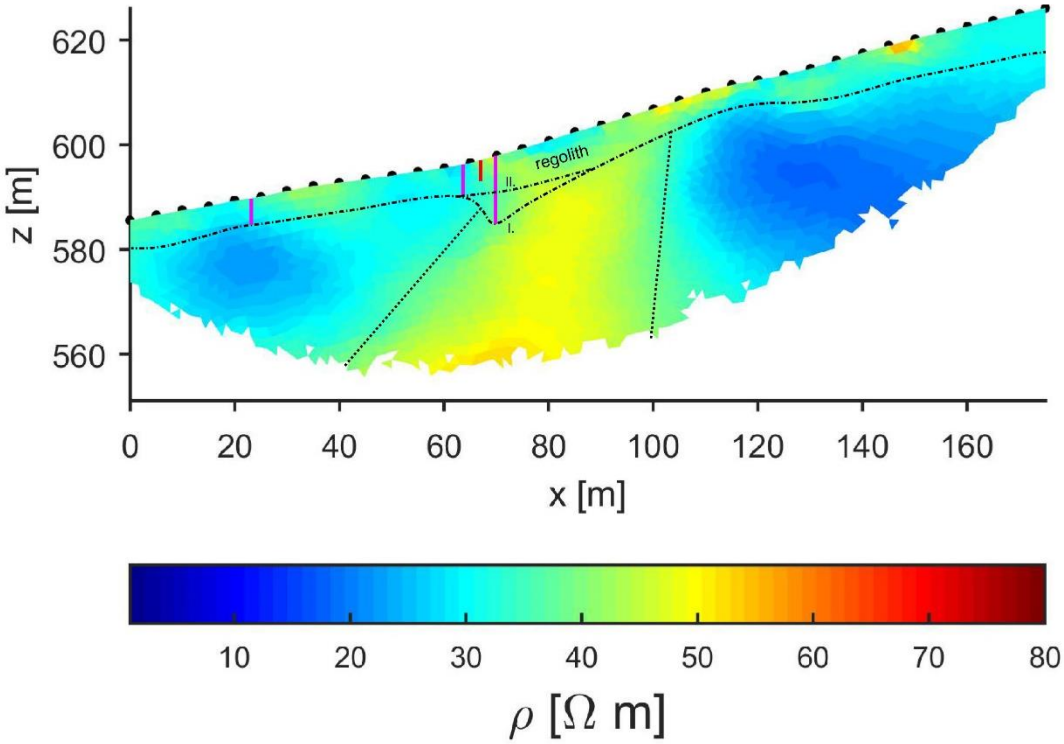

Figure 51. Subsurface model for vertical layers

6.3.2 Model 2: Horizontal Layers

Another interpretation, probably less obvious at first glance, is that the pattern in the electrical images is produced by a horizontally layered ground (Figure 52). However, the image of ERT profile 1 provides ample support for this interpretation. Assuming that layers were lost in the inversion due to smoothing, they cannot be adequately depicted in the ERT profiles 2 to 7. To explain why a horizontally layered earth produces a vertically layered image, one must further assume that the horizontal layers, if present, are of varying thickness and that areas which are separated in reality are represented as connected in the images. The layering may thus be assumed in the following way:

As in model 1, one may assume a layer of varying depth and spatially varying electrical properties. Underneath a thick layer of very conductive materials may follow, as indicated by dark blue shades. This is then followed by another, more resistive layer, indicated by yellow to orange shades at the bottom of each electrical image (as well as at each side of the image of ERT profile 1). Such layers are not visible in the electrical images. The second layer does not appear continuously in the electrical images of ERT profiles 2 to 7; rather it is intersected by a more resistive area in the middle of each image. However, the image of ERT profile 1 suggests that there exists a connected layer. Looking at ERT profiles 2 to 7, it can be assumed that there are two areas of similar resistivity in the uppermost layer and the lowermost layer that have been connected in the inversion. The electrical images of ERT profiles 2 to 7 show that there are areas featuring a higher electrical resistivity right below the surface. In the electrical images of ERT profiles 4 to 7, these areas even extend to greater depths. If the lowermost layer features a bump located in the middle of each ERT profile, it is easy to see how these areas might have been connected in the inversion due to smoothing.

So far, the potential layers have been characterized only in respect to their electrical properties, which are not the properties of primary interest. The following section will therefore interpret the data in terms of materials involved, and their distribution.
Data from both geologic surveys and the tests in this study suggest soft materials made up of fine-grained materials for the uppermost meters of the ground. PD furthermore indicates the presence of strongly weathered materials in the first 2 m of the ground and weathered rock underneath. Consequently, the uppermost layer featuring small scale variability in the electrical properties may be interpreted as regolith and soil, indicated by the dashed line in Figure 52. The area underneath, indicated by dark blue shades, could represent a layer of very fine-grained materials. As of yet, it cannot be determined whether this layer is already part of the bedrock or weathered rock. Given the high conductivity, which is untypical for solid rocks, it is more likely that this area is still part of the regolith, most certainly featuring a very high clay content and highly compacted materials. Subsequently, the third layer may represent the bedrock, as it features a significantly higher resistivity.

In conclusion, the variance in electrical properties shown in the electrical images may be more indicative of the degree of weathering than of variance in the materials, assuming that a lower resistivity in the images hint at more strongly weathered materials. Considering that the parent material, flysch, itself consists of layers (as it is a sediment), one may hypothesize that the horizontal layers might represent the layers of the flysch, however, it is known that the rock layers do not lie horizontally on the slope but with a significant dip. Therefore, the layering of the rock cannot explain horizontal variance in the ERT images.

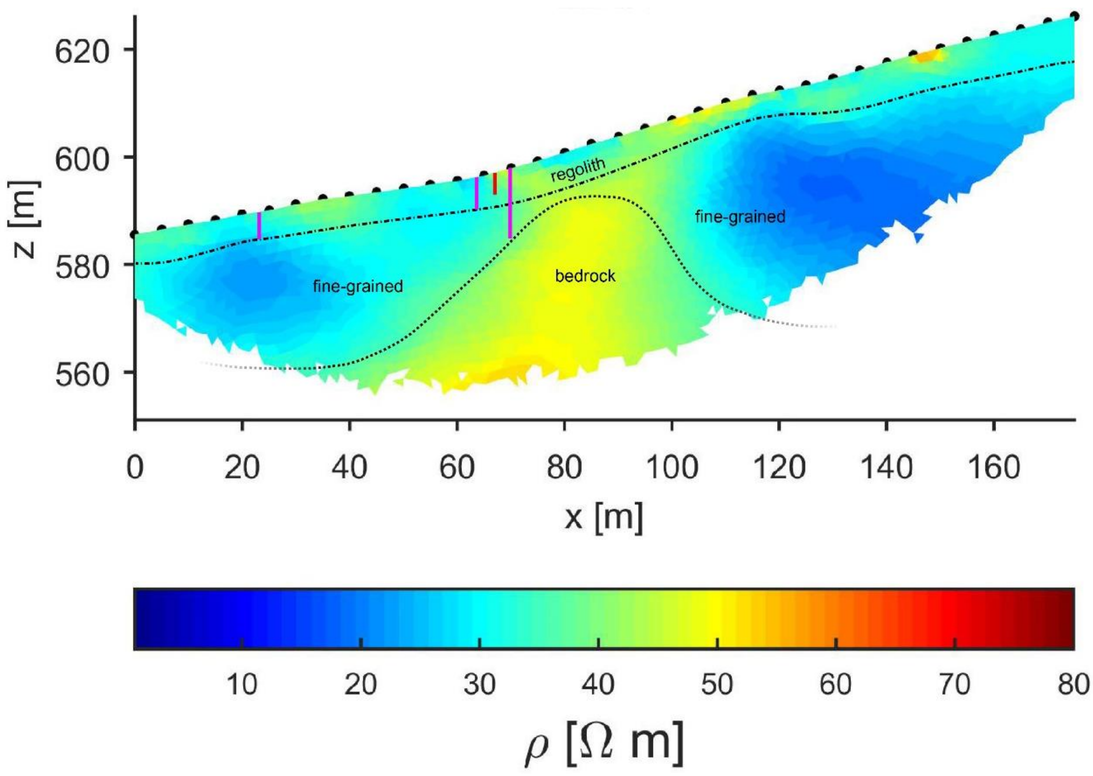

Figure 52. interpretation of the data based on the assumption of horizontal layers

6.3.3 Preliminary Conclusion

Both models agree on the interpretation of the first few meters of the subsurface but differ significantly in the interpretation of greater depths. As of yet, it cannot be determined which model is best representative of the subsurface, since too little direct data for the validation of the resistivity distribution is available. It is unlikely that any of the models presented accurately depicts subsurface structures, but they provide a viable frame for the interpretation of the acquired data. Since the causes of landslide processes at the site will most likely be rooted within the first few meters of the ground (on which both models agree) an accurate interpretation of depths greater than approximately 20 meters may not significantly improve our understanding of landslide processes anyways.

6.4 Evaluation of Hypothesis

Based on the findings presented above, the hypothesis formulated at the beginning of the thesis will be evaluated.

From the variation of the parameters electrical resistivity, penetration resistance, particle size, water content, subsurface structures, specifically, materials involved, their extend and thickness, boundaries and discontinuities such as potential failure surfaces, water saturated areas and the bedrock can be delineated.

The evidence above suggests that the hypothesis can only be partially confirmed. Limitations in the suitability of the chosen methods for the delineation of subsurface structures is partly because too little data is available yet and partly due to the difficulty of delineating subsurface structures from indirect data.

Materials involved were identified by PD. The results show that fine-grained materials (silt and clay) make up over 80% of the materials on the investigated slope. PD and DPH data from several locations indicate that a thick layer of soil (2 m) has developed. The regolith reaches a thickness of several meters (up to 13 m were measured). Based on the fundamental assumption that similar resistivity values in the resistivity images and similar values in the DPH profiles indicate identical subsurface conditions, one may conclude that clayey and silty materials extend across large areas of the slope. Further drillings would be necessary to verify this assumption. The lack of further drillings at different locations on the slope as well as ambiguity in the interpretation of indirect data do not allow to describe in detail the spatial variation of materials and their properties across the slope. Furthermore, PD data is only available for an area in which the electrical resistivity does not vary, meaning that the full potential of resistivity images for the extrapolation of PD data could not be exploited.

Likewise, delineating boundaries and discontinuities within the slope based on the data currently available is limited. The laboratory analysis of samples from the drill core revealed a systematic variation in all parameters assessed (i.e. colour, particle size, water content, fluid conductivity) between 1 – 2 m and 3 – 4 m, from which horizons and the boundary between soil and the remaining regolith was deduced. At the boundary between soil and the remaining regolith, a layer of highly compacted materials was identified. If such highly compacted materials extend over larger portions of the slope, it may be theorized that water accumulates on top, potentially forming a pre-existing failure line. The determination of the depth of the bedrock was limited by ambiguity in the interpretation of indirect data obtained. Based on the evidence collected, it may be assumed that it varies between approximately 5 m and 15 m.

Field observations (water logging at several locations, accumulation of water in the boreholes) as well as the laboratory analysis of the drill core suggest that water conditions may play an important role in slope dynamics at the Hofermühle-landslide. Both horizontal and lateral variations of water conditions were observed (in the field and the laboratory analysis). PD results indicate a high water content and a variation between the horizons identified in the analysis. A single drilling however does not permit the assessment of lateral variations. While in many cases, ERT was successfully applied to assess variation in saturation, the evidence suggests that ERT is not suitable to investigate variation at the Hofermühle landslide (and clay-rich landslides in general). Laboratory analysis compared to resistivity images show that the surface conduction mechanism prevails over electrolytic conduction and thus masks the correlation between saturation and the electrical resistivity, so that variation in saturation is barely visible or distinguishable from clay-rich areas in the resistivity images. Similar difficulties related to ambiguity in the interpretation of resistivity measurements occurred at other landslides nearby (Gallistl, Flores-Orozco, Ottowitz, Gautier, & Malet, 2017).

7 Conclusion

This thesis examined the subsurface of the Hofermühle-landslide using a combination of ERT, PD and DPH. The landslide is in the Flysch zone of Lower Austria, a geologic unit that is particularly susceptible to sliding. Geomorphological features of the slope suggest that further landslide-processes are likely. It is one of six research locations of the project NoeSLIDE, that aims to provide long-term data series to better correlate landslide events and their triggering factors as well test and improve methods for landslide exploration and monitoring. Since no detailed information about the subsurface of the Hofermühle-landslide was available, the thesis focused on the subsurface investigation and characterization of the adjacent slope to the landslide, providing a basis for further research and monitoring. In the course of this thesis, six parallel ERT profiles were recorded to measure the electrical resistivity of the ground. Three DPH tests were conducted to investigate the grounds resistance to penetration and Percussion Drilling was deployed at one location on the slope, providing ground truth information on particle size distribution, fluid conductivity and water content. Based on variation in the data obtained, the subsurface was described in terms of materials involved and their distribution.

The results confirm the presence of fine-grained, silty and clayey materials on the slope. PD and DPH show that a thick layer of soil (approx. 2 m) and weathered rock (approximately 5 m – 15 m) exists on the slope. The ERT results suggest that they span across large areas of the slope. It is common in such materials that impermeable layers develop, acting as potential sliding planes. Evidence for such pre-existing failure lines within the slope were found in the drill core at a depth of around 2 m. The laboratory analysis of samples from the drill core revealed a systematic variation in of the parameters colour, particle size, water content, fluid conductivity between 1 – 2 m and 3 – 4 m. Horizons and the boundary between soil and the remaining regolith were deduced from these parameters. Field observations and the laboratory analysis suggest that water conditions vary both vertically and laterally across the slope. As rainfall is a common trigger of landslides, it can be assumed that water conditions in the slope play an important role in slope dynamics. However, the spatial variance of the water content could not be assessed based on PD data and resistivity images. Although ERT has been applied for investigating and monitoring of hydrological conditions (e.g. water tables, or individuating high water content areas) in landslides (Perrone et al., 2014, p. 133), the evidence suggests that the electrical resistivity alone is unsuitable to assess the spatial variation of water conditions in clay-rich landslides, as the surface conduction mechanism masks the correlation between saturation and the electrical resistivity. This makes it impossible to distinguish areas of high clay content from areas of high water content. The variation in the resistivity images may therefore be more indicative of varying material properties, particularly the clay content.

While the study confirmed one known risk factor for the investigated slope and provided an overview of the subsurface, a detailed and accurate characterization of the subsurface of the Hofermühle-landslide is not possible at this point. The combined application of different methods significantly improved the understanding of the subsurface but several questions regarding subsurface structures, i.e. the exact distribution of materials, the presence of water-saturated zones or the location of sliding planes, remain unanswered. Limitations of the survey relate to a low sampling density (especially for PD and DPH), difficulties in comparing data sets with different scales and formats as well as the high clay content of the materials in the subsurface. Particularly the lack of direct data is problematic because it is necessary for validating the interpretation of data collected by DPH and ERT. Explaining the spatial variance in the DPH profiles and ERT images based on direct data is currently not possible. Consequently, ambiguity in the interpretation of the resistivity images as to whether the resistivity distribution is caused by vertical or horizontal layers, remains.

Evidence suggests that landslide hazard on the slope is significant. Not only is further movement likely, but also the amount of material on the slope that may be activated in the future is considerable, posing a risk to the building at the foot of the slope. This thesis highlights the need for mitigation strategies and monitoring at the site to prevent damage to the building. Ultimately, further analyses are required to link subsurface conditions to dynamic changes of slope stability and make reliable predictions in terms of the landslide hazard.

8 Perspectives

Visible changes at the surface both at the crown of the old landslide as well as at the increase of the hollows on top of the slope during the course of this study indicate that parts of the Hofermühle-landslide and adjacent slope are currently active. Information on the geologic setting of the slope suggest that the magnitude of future events may be considerable, as a large amount of material may be displaced. This raises issues around an accurate description of the landslide hazard on the one hand, and potential monitoring and hazard risk mitigation strategies on the other hand. For an accurate description of the landslide hazard at the site, information on the geological and hydrological setting (as required for risk assessment (Perrone et al., 2014, p. 129) needs to be increased. Specifically, greater clarity regarding the size of the endangered area, the potential volume of displaced material and the probability for slides within a given time frame seems necessary (Fell et al., 2008, p. 86).

Currently active zones seem to exist along the crown of the former landside as well as the hollows at the top of the slope. An important step towards a more accurate estimation of the volume of future slides is to determine exactly the areas of greatest risk for sliding processes (now and in the future). Therefore, both the lateral and the horizontal extent must be considered. Mapping of visible surface features (i.e. cracks, hollows) seem to be a good starting point in this context. More extensive information regarding the affected area may come from tracking the movement over extended periods of time to distinguish active areas from inactive areas. This may be accomplished by GNSS tracking of (buried) reference objects (that already exist at the Hofermühle-landslide) or, although still challenging, by applying more recent technologies, such as Terrestrial or Airborne Laser Scanning, or Photogrammetry (Jaboyedoff et al., 2012; Walstra, Chandler, Dixon, & Dijkstra, 2007). Research efforts could then be focused on the identified area.

The depth of the bedrock may be determined more accurately to estimate the amount of unconsolidated (thus displaceable) rock present on the slope. A more rigorous application of DPH may resolve ambiguity in the interpretation of refusal depth (which was a major limitation of DPH in this study) and may allow the tracing of the bedrock along the slope. However, point-information may not deliver enough data for an accurate landslide hazard description. Promising options are seismic reflection and refraction technologies, which have been successfully implemented to map the bedrock (Jongmans & Garambois, 2007, pp. 6–7) Knowing the lateral extent of the endangered area as well as the depth of the bedrock, the volume of unconsolidated materials may be estimated.

However, it is far more likely that future slides occur along a failure surface that forms within the regolith, instead of the bedrock as has been the case in former landslide events at the site. Identifying potential sliding planes in the subsurface is required for an accurate estimation of the potential volume of future slides. Recent advances in modelling open up new possibilities for the determination of sliding planes in soft rocks, like the Hofermühle-landslide. In this context, the reader is referred to (Yao, Tian, & Jin, 2014), who modelled potential sliding planes on a slope similar to the Hofermühle-landslide based on information on weak structural surfaces. However, for reliable modelling results, detailed knowledge about subsurface conditions is required. Consequently, modelling may provide interesting insights for risk assessment at the Hofermühle, if enough information on subsurface conditions (i.e. weakness surfaces) and the factors that influence them (e.g. water flow, weathering, unloading, etc.) is available to be considered in the modelling process. While the evidence collected by means of PD, DPH and ERT provided too little information for such purposes (such investigations would have extended the scope of this thesis), they provide valuable information for the further investigations of subsurface conditions. Results obtained by PD and ERT suggest that weakness surfaces may occur in the form of clay-rich, impermeable layers, underlining that weathering and hydrological conditions play an important role in slope dynamics at the site. Thus, it may be expected that the analysis of the slope in terms of hydrological conditions and clay content would provide valuable results for the search of potential weakness surfaces. As demonstrated by this thesis, resistivity images are not suitable for such purposes, since in clay-rich (and water influenced) landslides, the overall conductivity comes from both electrolytic conductivity (indicative of water) and surface conductivity (indicative of clay), so that variation in clay and water cannot be assessed individually. Recently, the combined measurement of resistivity and the induced polarization effect has been proposed (Flores Orozco, Bücker, Steiner, & Malet, 2017; Gallistl, Flores-Orozco, et al., 2017; Malet, Supper, Flores-Orozco, Gautier, & Bogaard, 2017) to better characterize the subsurface materials in terms of variation in physical and hydro(geo)logical properties and to better differentiate between the effects of water and clay on the (overall) electrical resistivity. Measurements of the induced polarization effect in the subsurface are already available for the Hofermühle-landslide (see Karl, Stumvoll, Gallistl, Flores Orozco, & Glade, 2018) as well as a the Salcher-landslide in Scheibbs/Austria (Gallistl, Weigand, et al., 2017) and significantly enhanced the interpretation of these landslides. In the future, measurements on the induced polarization effect (as in ERT) may therefore be standardly applied for the investigation of clay-rich landslides in the area.

Lastly, these findings have important consequences for monitoring (and in further consequence early warning systems) at the Hofermühle-landslide (and other clay-rich landslides). As Malet et al. (2017) note, only the monitoring of subsurface parameters may provide information on the triggering of landslide before movement is measurable at the surface (other than for example early warning systems based on cameras) and that physical properties may be used as a precursor for landslide events. Consequently, a monitoring approach that focuses on the variation in water conditions together with the identification of clay-rich areas in the subsurface appears particularly promising for the Hofermühle-landslide. In combination with data from weather stations, the monitoring of variation in water conditions in the slope may help to better understand the correlation of movement and rainfall events, which are commonly identified as triggers in the area. Knowing that clay strongly influences the variation in subsurface electrical properties, potentially masking the correlation between saturation and the electrical resistivity, traditional electrical monitoring techniques, such as time-lapse resistivity measurements may not be suitable for the application in clayey conditions. Such monitoring systems are yet to be developed and tested, opening new areas of research.

9 Bibliography

Ahnert, F. (2009). *Einführung in die Geomorphologie* (4th. ed.). Stuttgart: Ulmer.

Aizebeokhai, A. (2011). 2D and 3D geoelectrical resistivity imaging: Theory and field design. *Scientific Research and Essays*, *523*, 3592–3605. Retrieved from http://eprints.covenantuniversity.edu.ng/2988/#.Wvl6X2iFM2w

Allaby, M. (Ed.). (2008). *A dictionary of earth sciences* (3rd ed.). Oxford; New York: Oxford University Press. doi: 10.1093/acref/9780199211944.001.0001

Archie, G. E., & others. (1942). The electrical resistivity log as an aid in determining some reservoir characteristics. *Transactions of the AIME*, *146*(1), 54–62. Retrieved from https://www.onepetro.org/journal-paper/SPE-942054-G

Auerswald, K., Simon, S., & Stanjek, H. (2001). Influence of soil properties on electrical conductivity under humid water regimes. *Soil Science*, *166*(6), 382–390. Retrieved from http://journals.lww.com/soilsci/Abstract/2001/06000/INFLUENCE_OF_SOIL_PROPERTIES_ON_ELECTRICAL.3.aspx

Bai, W., Kong, L.-W., & Guo, A. (2013). Effects of physical properties on electrical conductivity of compacted lateritic soil. *Journal of Rock Mechanics and Geotechnical Engineering*, *5*, 406–411. doi: 10.1016/j.jrmge.2013.07.003

Bell, R., Glade, T., Granica, K., Heiss, G., Leopold, P., Petschko, H., Pomaroli, G., Proske, H., Schweigl, J. (2011). Landslide susceptibility maps for spatial planning in Lower

Austria. In C. Margottini, P. Canuti & K. Sassa (Eds.), *Proceedings of the Second World Landslide Forum*. Rome. doi: 10.1007/978-3-642-31325-7_60

Bhattacharya, B., & Shalivahan, S. (2016). *Geoelectric Methods: Theory and Application.* New Delhi: McGraw Hill Education (India) Private Limited.

Binley, A., & Kemna, A. (2005). DC resistivity and induced polarization methods. In Y. Rubin & S. S. Hubbard (Eds.) *Hydrogeophysics* (pp. 129–156). Dordrecht: Springer. doi: 10.1007/1-4020-3102-5_5

Borgatti, L., & Soldati, M. (2010). Landslides as a geomorphological proxy for climate change: a record from the Dolomites (northern Italy). *Geomorphology*, *120*(1), 56–64. Retrieved from https://www.sciencedirect.com/science/article/pii/S0169555X09003900

Bücker, M., Lozano García, S., Ortega Guerrero, B., Caballero, M., Pérez, L., Caballero, L., Pita de la Paz, C., Sánchez-Galindo, A., Villegas, F. J., Flores Orozco, A. (2017). Geoelectrical and Electromagnetic Methods Applied to Paleolimnological Studies: Two Examples from Desiccated Lakes in the Basin of Mexico. *Boletín de La Sociedad Geológica Mexicana, 69*(2), 279–298. Retrieved from https://publik.tuwien.ac.at/files/publik_261118.pdf

BFW (2007). Digitale Bodenkarte von Österreich (eBOD). *Bundesforschungs- und Ausbildungszentrum für Wald, Naturgefahren und Landschaft.* Retrieved March 23, 2018 from https://bfw.ac.at/rz/bfwcms2.web?dok=7066

BGS. (2017). How does BGS classify landslides? *British Gelogical Society. National Environment Research Council.* Retrieved from http://www.bgs.ac.uk/landslides/how_does_bgs_classify_landslides.html

BMNT. (2015). Hydrografisches Jahrbuch von Österreich 2013. *Bundesministerium für Nachhaltigkeit und Tourismus.* Retrieved from https://www.bmlfuw.gv.at/wasser/wasser-oesterreich/wasserkreislauf/hydrographische_daten/jahrbuecher/jahrbuch2013.html

BMNT. (2018). eHYD. *Bundesministerium für Nachhaltigkeit und Tourismus.* Retrieved May 2, 2018 from http://ehyd.gv.at/

Borgatti, L., & Soldati, M. (2010). Landslides as a geomorphological proxy for climate change: a record from the Dolomites (northern Italy). *Geomorphology, 120*(1), 56–64. doi: https://doi.org/10.1016/j.geomorph.2009.09.015

Clague, J. (2013). Landslide. In P. T. Bobrowsky (Ed.), *Encyclopedia of natural hazards* (pp. 594–601). Dordrecht: Springer.

Clague, J., & Stead, D. (Eds.). (2012). *Landslides: types, mechanisms and modeling.* New York: Cambridge University Press.

Council, N. R., & others. (2005). *Contaminants in the subsurface: Source zone assessment and remediation.* National Academies Press.

Crozier, M. J. (1986). *Landslides: causes, consequences & environment.* Taylor & Francis.

Crozier, M. J. (1999). Landslides. In *Environmental Geology* (pp. 371–375). Dordrecht: Springer Netherlands. doi: http://dx.doi.org/10.1007/1-4020-4494-1_200

Cruden, D. M. (1991). A simple definition of a landslide. *Bulletin of the International Association of Engineering Geology*, *43*(1), 27–29. doi: https://doi.org/10.1007/BF02590167

Cruden, D. M., & Varnes, D. J. (1996). Landslide Types and Processes. *In: Turner, A.K., Schuster, R.L. (Eds.), Landslides: Investigation and Mitigation. National Academy Press, Washington, D.C*, *247*, 36–75.

De Blasio, F. V. (2011). Friction, Cohesion, and Slope Stability. In F. V. De Blasio (Ed.), *Introduction to the Physics of Landslides: Lecture notes on the dynamics of mass wasting* (pp. 23–52). Dordrecht: Springer Netherlands. doi: https://doi.org/10.1007/978-94-007-1122-8_2

Dikau, R., Brunsden, D., Schrott, L., & Ibsen, M.-L. (Eds.). (1996). *Landslide recognition: identification, movement, and causes.* Chichester; New York: Wiley.

Dikau, R., & Glade, T. (2002). Gefahren und Risiken durch Massenbewegungen. *Geographische Rundschau*, *54*, 38–45.

Dikau, R., & Schrott, L. (1999). The temporal stability and activity of landslides in Europe with respect to climatic change (TESLEC): main objectives and results. *Geomorphology*, *30*(1), 1–12. Retrieved from https://www.sciencedirect.com/science/article/pii/S0169555X99000409

Eißsfeldt, F. (2011). Sondierungen und deren Bewertung. In *Baugrundaufschlüsse: Planung, Ausschreibung, Durchführung, Überwachung und Interpretation.* Bau-ABC Rostrup / Bad Zwischenahn. Retrieved from https://izw.baw.de/publikationen/kolloquien/0/09-Ei%C3%9FfeldtSondierungen.pdf

Fargier, Y., Fauchard, C., Meriaux, P., Royet, P., Palma-Lopes, S., Francois, D., Cote, P., Bretar, F. (2012). Methodology Applied to the Diagnosis and Monitoring of Dikes and Dams. In Y. Luo (Ed.), *Novel Approaches and Their Applications in Risk Assessment*. InTech. Retrieved from http://www.intechopen.com/books/novel-approaches-and-their-applications-in-risk-assessment/geophysical-methods-applied-to-the-diagnosis-and-monitoring-of-earth-embankments-

Fell, R., Corominas, J., Bonnard, C., Cascini, L., Leroi, E., & Savage, W. Z. (2008). Guidelines for landslide susceptibility, hazard and risk zoning for land use planning. *Engineering Geology*, *102*(3–4), 85–98. doi: https://doi.org/10.1016/j.enggeo.2008.03.022

Flageollet, J.-C., Maquaire, O., Martin, B., & Weber, D. (1999). Landslides and climatic conditions in the Barcelonnette and Vars basins (Southern French Alps, France). *Geomorphology*, *30*(1–2), 65–78. doi: https://doi.org/10.1016/S0169-555X(99)00045-8

Flores Orozco, A., Bücker, M., Steiner, M., & Malet, J.-P. (2017). *Complex-conductivity imaging for the understanding of landslide architecture*. Manuscript submitted for publication.

Flores Orozco, A., Gallistl, J., Bücker, M., & Williams, K. H. (2017). Decay curve analysis for data error quantification in time-domain induced polarization imaging. *Geophysics*, *83*(2), 1–48. doi: https://doi.org/10.1190/geo2016-0714.1

Friedman, S. P. (2005). Soil properties influencing apparent electrical conductivity: a review. *Computers and Electronics in Agriculture*, *46*(1–3), 45–70. doi: https://doi.org/10.1016/j.compag.2004.11.001

Fukue, M., Minato, T., Horibe, H., & Taya, N. (1999). The micro-structures of clay given by resistivity measurements. *Engineering Geology*, *54*(1–2), 43–53. doi: https://doi.org/10.1016/S0013-7952(99)00060-5

Gallistl, J., Flores-Orozco, A., Ottowitz, D., Gautier, S., & Malet, J.-P. (2017). Induced polarization (IP) imaging for the improved characterization of clay-rich landslides. In *EGU General Assembly Conference Abstracts* (Vol. 19, p. 6441). Retrieved from https://meetingorganizer.copernicus.org/EGU2017/EGU2017-6441.pdf

Gallistl, J., Weigand, M., Stumvoll, M. J., Ottowitz, D., Glade, T., & Flores Orozco, A. (2017). Improved delineation of subsurface variability in clay-rich landslides through spectral induced polarization imaging and low induction number electromagnetic methods. *Engineering Geology*.

Gassner, C., Promper, C., Beguería, S., & Glade, T. (2015). Climate change impact for spatial landslide susceptibility. In *Engineering Geology for Society and Territory-Volume 1* (pp. 429–433). Springer.

Glade, T., Anderson, M., & Crozier, M. J. (Eds.). (2005). *Landslide hazard and risk*. Chichester, West Sussex, England ; Hoboken, NJ: J. Wiley.

Glade, T., Petschko, H., Bell, R., Bauer, C., Granica, K., Heiss, G., … Schweigl, J. (2012). Landslide Susceptibility Maps for Lower Austria. Methods and Challenges. In *Conference Proceedings*. Grenoble. Retrieved from http://www.interpraevent.at/palm-cms/upload_files/Publikationen/Tagungsbeitraege/2012_1_497.pdf

Highland, L. M., & Bobrowsky, P. (2008). *The Landslide Handbook - A Guide to Understanding Landslides*. Reston, Virginia. Retrieved from https://pubs.usgs.gov/circ/1325/

Hungr, O., Leroueil, S., & Picarelli, L. (2014). The Varnes classification of landslide types, an update. *Landslides*, *11*(2), 167–194. doi: https://doi.org/10.1007/s10346-013-0436-y

Hutchinson, J. N. (1968). In R. W. Fairbridge (Ed.), *Mass Movement.* (Vol. 3, pp. 688–695). Reinhold, New York.

Ishibashi, I., & Hazarika, H. (2015). *Soil mechanics fundamentals and applications* (Second edition). Boca Raton: CRC Press, Taylor & Francis Group.

Jaboyedoff, M., Oppikofer, T., Abellán, A., Derron, M.-H., Loye, A., Metzger, R., & Pedrazzini, A. (2012). Use of LIDAR in landslide investigations: a review. *Natural Hazards*, *61*(1), 5–28. doi: https://doi.org/10.1007/s11069-010-9634-2

Jakob, M., & Lambert, S. (2009). Climate change effects on landslides along the southwest coast of British Columbia. *Geomorphology*, *107*(3–4), 275–284. doi: https://doi.org/https://doi.org/10.1016/j.geomorph.2008.12.009

Jongmans, D., & Garambois, S. (2007). Geophysical investigation of landslides: a review. *Bulletin de La Société Géologique de France*, *178*(2), 101–112. doi: https://doi.org/10.2113/gssgfbull.178.2.101

Karl, C., Stumvoll, M. J., Gallistl, J., Flores Orozco, A., & Glade, T. (2018). Delineation of internal landslide structures using complex conductivity imaging and geotechnical investigations – case study Hofermühle, Lower Austria. In *Geophysical Research Abstracts* (Vol. 20). Retrieved from https://meetingorganizer.copernicus.org/EGU2018/EGU2018-13516.pdf

Keefer, D. K., & Larsen, M. C. (2007). Assessing landslide hazards. *Science*, 1136–1138. Retrieved from http://www.jstor.org/stable/20036323

Kemna, A. (2000). *Tomographic inversion of complex resistivity: theory and application*. Osnabrück: Der Andere Verlag.

Khodaparast, M., Rajabi, A. M., & Mohammadi, M. (2015). The new empirical formula based on dynamic probing test results in fine cohesive soils. *International Journal of Civil Engineering*, (2). doi: https://doi.org/10.22068/IJCE.13.2.105

Kitutu, M., Muwanga, A., Poesen, J., & Deckers, J. A. (2009). Influence of soil properties on landslide occurrences in Bududa district, Eastern Uganda. *African Journal of Agricultural Research*, *4*(7), 611–620.

Knödel, K., Krummel, H., Lange, G., & Berktold, A. (1997). *Geophysik*. Berlin ; New York: Springer.

Kottek, M., Grieser, J., Beck, C., Rudolf, B., & Rubel, F. (2006). World Map of the Köppen-Geiger climate classification updated. *Meteorologische Zeitschrift*, *15*(3), 259–263. doi: https://doi.org/10.1127/0941-2948/2006/0130

Loibl, W., Beck, A., Dorninger, M., Formayer, H., Gobiet, A., & Schöner, W. (2007). Kwiss-Programm reclip: more research for climate protection: model run evaluation. *Final Report, ARC Systems Research*. Retrieved from http://reclip.ait.ac.at/SE/projects/reclip/reports/ARC-sys-reclip_more_PJ3rep.pdf

Loke, M. (1999). Electrical imaging surveys for environmental and engineering studies. A practical guide to 2-D and 3-D surveys., *2*. Retrieved from http://pages.mtu.edu/~ctyoung/LOKENOTE.PDF

Lotter, M., & Haberle, A. (2013). *Geogene Naturgefahren - gravitative Massenbewegungen und ihre Ursachen.* (Berichte Geol. B.-A. No. 100) (p. 17). Rabenstein an der Pielach. Retrieved from https://opac.geologie.ac.at/wwwopacx/wwwopac.ashx?command=getcontent&server=images&value=BR0100_005_A.pdf

Lu, N., & Godt, J. W. (2013). *Hillslope hydrology and stability.* Cambridge; New York: Cambridge University Press.

Malet, J.-P., Supper, R., Flores-Orozco, A., Gautier, S., & Bogaard, T. (2017). High-frequency HYDRO-geophysical observations for an advanced understanding of clayey landSLIDES: the HYDROSLIDE research project. In *EGU General Assembly Conference Abstracts* (Vol. 19, p. 15434). Retrieved from https://meetingorganizer.copernicus.org/EGU2017/EGU2017-15434.pdf

Mayne, P. W., & Quental Coutinho, R. (Eds.). (2012). *Geotechnical and Geophysical Site Characterization 4: Proceedings of the Fourth International Conference on Site Characterization ISC-4, Porto de Galinhas, Pernambuco, Brasil, 17-21 September 2012.*

National Research Council. (2005). *Contaminants in the Subsurface: Source Zone Assessment and Remediation.* Washington, DC: The National Academies Press.

Retrieved from https://www.nap.edu/catalog/11146/contaminants-in-the-subsurface-source-zone-assessment-and-remediation

Ohlmacher, G. C. (2000). *The Relationship between geology and landslide hazards of Atchison, Kansas, and vicinity*. Kansas Geological Survey. Retrieved from http://www.kgs.ku.edu/Current/2000/ohlmacher/ohlmacher.pdf

Palacky, G. J. (1988). Resistivity characteristics of geologic targets. Electromagnetic Methods in *Applied Geophysics 1*, 53–129.

Patel, N. R., & Shete, D. T. (2015). Analyzing Precipitation Using Concentration Indices for North Gujarat Agro Climatic Zone, India. *Aquatic Procedia*, *4*, 917–924. doi: https://doi.org/10.1016/j.aqpro.2015.02.115

Perrone, A., Lapenna, V., & Piscitelli, S. (2014). Electrical resistivity tomography technique for landslide investigation: A review. *Earth-Science Reviews*, *135*, 65–82.

Petschko, H., Glade, T., Bell, R., Schweigl, J., & Pomaroli, G. (2010). Landslide inventories for regional landslide early warning systems. In T. Glade, J.-P. Malet, & N. Casagli (Eds.), *Mountain Risks: Bringing Science to Society* (pp. 277–282). Strasbourg: CERG Editions.

Petschko, H., Glade, T., & Brenning, A. (2012). Landslide susceptibility modeling with generalized additive models – facing the heterogeneity of large regions. In E. Eberhardt, C. Froese, A. K. Turner, & S. Leroueil (Eds.), (pp. 769–777). Canada: Taylor & Francis.

Petschko, H., Bell, R., Glade, T., & Brenning, A. (2012). Landslide susceptibility modeling with generalized additive models – facing the heterogeneity of large regions. In E.

Eberhardt, C. Froese, A. K. Turner, & S. Leroueil (Eds.), *Landslides and Engineered Slopes: Protecting Society through Improved Understanding* (pp. 769–775). Canada: Taylor & Francis. Retrieved from file:///C:/Users/Christina%20Karl/Downloads/PetschkoEtAl2012_heterogeneity.pdf

Prinz, H. (1982). *Abriß der Ingenieurgeologie.* -. Stuttgart: Enke Ferdinand.

Promper, C., Puissant, A., Malet, J.-P., & Glade, T. (2014). Analysis of land cover changes in the past and the future as contribution to landslide risk scenarios. *Applied Geography*, *53*, 11–19. doi: https://doi.org/10.1016/j.apgeog.2014.05.020

Reichenbach, P., Busca, C., Mondini, A. C., & Rossi, M. (2014). The Influence of Land Use Change on Landslide Susceptibility Zonation: The Briga Catchment Test Site (Messina, Italy). *Environmental Management*, *54*(6), 1372–1384. doi: https://doi.org/10.1007/s00267-014-0357-0

Rossi, G., Nocentini, M., Lombardi, L., Vannocci, P., Tanteri, L., Dotta, G., Bicocchi, G., Scaduto, T., Salvatici, T., Tofani, V., Moretti, S., & Casagli, N. (2016). Integration of multicopter drone measurements and ground-based data for landslide monitoring. *Landslides and Engineered Slopes. Experience, Theory and Practice, Associazione Geotecnica Italiana, Rome*, 1745–1750. Retrieved from https://s3.amazonaws.com/academia.edu.documents/46824989/206.pdf?AWSAccessKeyId=AKIAIWOWYYGZ2Y53UL3A&Expires=1526332857&Signature=uQ341dpyYrwfsvj7K72p0brhVrA%3D&response-content-

disposition=inline%3B%20filename%3DIntegration_of_multicopter_drone_measure.pdf

Rossi, G., Tanteri, L., Salvatici, T., & Casagli, N. (2017). The use of multi-copter drones for landslide investigations. Retrieved from https://flore.unifi.it/retrieve/handle/2158/1094159/256314/Farina%20et%20al%20NASL%202017.pdf

Sausgruber, T. (2013). *Hofermühlrutschung - Waidhofen/Ybbs* (No. 3491/11-2013). Innsbruck: Geologische Stelle.

Sausgruber, T. (2016). *Protokoll zum Lokalaugenschein Hangprozess Hofermühle / Hofermühlrutschung* (No. 3491/13-2016). Innsbruck.

Scheffer, F., Schachtschabel, P., Blume, H.-P., Brümmer, G., Horn, R., Kandeler, E., Kögler-Knaberer, I., Kretzschmar, R., Stahl, Karl., Wilke, B.-M., Thiele-Bruhn, S., Welp, G., & Tippkötter, R. (2010). *Lehrbuch der Bodenkunde* (16. Auflage). Heidelberg: Springer, Spektrum, Akademischer Verlag.

Schnabel, W., Krenmayr, H. G., Mandl, G. W., Nowotny, A., Roetzel, R., & Schabert, S. (2002). *Geologie der Österreichischen Bundesländer: Niederösterreich.* Wien: Geologische Bundesanstalt.

Schön, J. H. (2015). *Physical properties of rocks: Fundamentals and principles of petrophysics* (Vol. 65). Elsevier. Retrieved from https://www.elsevier.com/books/physical-properties-of-rocks/schon/978-0-08-100404-3

Schuster, R., Daurer, A., Krenmayr, H. G., Linner, M., Mandl, G. W., Pestal, G., & Reitner, J. M. (2015). *Rocky Austria: Geologie von Österreich - kurz und bunt* (4. verbesserte Aufl.). Wien: Geologische Bundesanstalt.

Schweigl, J., & Hervás, J. (2009). Landslide mapping in Austria. *JRC Scientific and Technical Reports*.

Schwenk, H., Spendlingwimmer, R., & Salzer, F. (1992). Massenbewegungen in Niederösterreich. 1953 - 1990. In *Jahrbuch der Geologischen Bundesanstalt* (Vol. 135(2), pp. 597–660). Retrieved from https://opac.geologie.ac.at/wwwopacx/wwwopac.ashx?command=getcontent&server=images&value=JB1352_597_A.pdf

Shanmugam, G., & Wang, Y. (2015). The landslide problem. *Journal of Palaeogeography*, *4*(2), 109–166. doi: https://doi.org/10.3724/SP.J.1261.2015.00071

Sharpe, C. F. S. (1938). Landslides and related phenomena: a study of mass-movements of soil and rock. Pageant Books.

Sidle, R. C. (2007). Using Weather and Climate Information for Landslide Prevention and Mitigation. In M. V. K. Sivakumar & N. Ndiang'ui (Eds.), *Climate and Land Degradation* (pp. 285–307). Berlin, Heidelberg: Springer Berlin Heidelberg. doi: https://doi.org/10.1007/978-3-540-72438-4_15

Sidle, R. C., Pearce, A. J., & O'Loughlin, C. L. (1985). Hillslope stability and land use. American Geophysical Union.

Varnes, D. J. (1958). Landslide Types and Processes. *Landslides and engineering practice*, 29(3), 20-45.

Varnes, D. J. (1978). Slope Movement Types and Processes. Special Report No. 176. In R. L. Schuster & K. J. Raymond (Eds.), *Landslides, Analysis and Control.* (pp. 11–33). Washington, D.C: National Academy of Sciences. Retrieved from http://onlinepubs.trb.org/Onlinepubs/sr/sr176/176-002.pdf

Walstra, J., Chandler, J. H., Dixon, N., & Dijkstra, T. A. (2007). Aerial photography and digital photogrammetry for landslide monitoring. *Geological Society, London, Special Publications*, *283*(1), 53–63. doi: https://doi.org/10.1144/SP283.5

Ward, S. H. (1990). Resistivity and Induced Polarization Methods. Geotechnical and Environmental Geophysics, 1, (pp. 147-189).

Wessely, G., Gangl, G., Gottschling, P., Draxler, I., Heinrich, M., Hofmann, T., Lenhardt, W., Matura, A., Pavuza, R. & Sauer, R. (2006). *Geologie der österreichischen Bundesländer. Niederösterreich*. Wien: Geologische Bundesanstalt.

WP/WLI (1993). *Multilingual landslide glossary.* The International Geotechnichal Societies' UNESCO Working Party on World Landslide Inventory Richmond, B.C., Canada: BiTech Publishers Ltd. Retrieved from http://iaeg.info/media/1454/multilingual-landslide-glossary_1993-version.pdf

Yao, A., Tian, Z., & Jin, Y. (2014). Sliding surface searching method for slopes containing a potential weak structural surface. *Journal of Rock Mechanics and Geotechnical Engineering*, *6*(3), 275–279. doi: https://doi.org/10.1016/j.jrmge.2014.03.004

ZAMG. (n.d.). Klimamittel. *Zentralanstalt für Meteorologie und Geodynamik (Central Institute for Meteorology and Geodynamics of Austria).* Retrieved May 29, 2017, from https://www.zamg.ac.at/cms/de/klima/klimauebersichten/klimamittel-1971-2000

Zung, A. B., Sorenson, C. J., & Winthers, E. (2009). Landslide Soils and Geomorphology in Bridger-Teton National Forest, Northwest Wyoming. *Physical Geography*, *30*(6), 501–516. Retrieved from https://www.tandfonline.com/doi/abs/10.2747/0272-3646.30.6.501

Appendix A. Additional Information

Table A 1. Nomenclature for the description of landslides (Cruden & Varnes, 1996).

Crown	The practically undisplaced material adjacent to the highest parts of the main scarp.
Main scarp	A steep surface on the undisturbed ground at the upper edge of the landslide caused by movement of the displaced material away from the undisturbed ground. It is the visible part of the surface of rupture.
Top	The highest point of contact between the displaced material and the main scarp.
Head	The upper parts of the landslide along the contact between the displaced material and the main scarp.
Minor scarp	A steep surface on the displaced material of the landslide produced by differential movements within the displaced material.
Main body	The part of displaced material of the landslide that overlies the surface of rupture between the main scarp and the toe of the surface of rupture.
Foot	The portion of the landslide that has moved beyond the toe of the surface if rupture and overlies the original ground surface.
Tip	The point on the toe farthest from the top of the landslide.
Toe	The lower, usually curved margin of the displaced material of a landslide, it is the most distant from the main scarp.
Surface of rupture	The surface which forms (or which has formed) the lower boundary of the displaced material below the original ground surface.
Toe of surface rupture	The intersections (usually buried) between the lower part of the surface rupture of a landslide and the original ground surface.
Surface of separation	The part of the original ground surface now covered by the foot of the landslide.
Displaced material	Material displaced from its original position on the slope by movement in the landslide. It forms both the depleted mass and the accumulation.
Zone of depletion	The area of the landslide within which the displaced material lies above the original ground surface.
Depleted mass	The volume of the displaced material which overlies the surface of rupture but underlies the original ground surface.
Accumulation	The volume of displaced material which lies above the original ground surface.
Flank	The undisplaced material adjacent to the sides of the surface of rupture.
Original ground surface	The surface of the slope that existed before the landslide took place.

Table A 2. Definitions of common properties of a landslide (Cruden & Varnes, 1996).

Width of the displaced mass, Wd	The maximum breadth of the displaced mass perpendicular to the length, Ld.
Width of the surface of rupture, Wr	The maximum width between the flanks of the landslide, perpendicular to the length, Lr.
Length of the displaced mass, Ld	The minimum distance from the tip to the top.
Length of the surface of rupture, Lr	The minimum distance from the toe of the surface of rupture to the crown.
Depth of the displaced mass, Dd	The maximum depth of the displaced mass, measured perpendicular to the plane containing Wd and Ld.
Depth of the surface of rupture, Dr	The maximum depth of the surface of rupture below the original ground surface measured perpendicular to the plane containing Wr and Lr.
Total length, L	The minimum distance from the tip of the landslide to its crown.
Length of the center line, Lcl	The distance from the crown to the tip of the landslide through points on the original ground surface equidistant from the lateral margins of the surface of rupture and the displaced material.

Table A 3. Commonly used electrical and electromagnetic methods in subsurface investigations (Knödel et al., 1997, p. 67).

Method	Frequency range	Initiation	Actual measurement parameter	Derived measurement parameter
Self-potential	DC	Natural potentials	Potential differences	
Direct current geoelectrics	DC, AC < 50 Hz	Electrodes (galvanic)	potential differences, current strength	Apparent resistivity
Mise-à-la masse	DC	One electrode of well conducting ground	potential differences, magnetic field	Apparent resistivity
Induced Polarization	10 mHz – 10 kHz	Galvanic (electrodes), inductive	Potential differences, current strength, phase difference	Chargeability, frequency dependent complex apparent resistivity (Cole-Cole-Parameter)
Electromagnetic two-coil system	100 Hz – 60 kHz	Transmitter coil (inductive)	Magnetic fields	Normalized secondary magnetic field, apparent conductivity
CSEM/CSAMT	1 Hz – 10 kHz	1-2 grounded dipoles (galvanic and inductive)	Magnetic and electric fields	Apparent resistivity, magnetotelluric impedance tensor, induction vector
VLF, VLF-R, LF, LF-R (RMT)²	15 kHz – 1 MHz	Very low frequency and low frequency transmitters (inductive)	Magnetic and electric fields	Electric and magnetic transfer functions, apparent resistivity
RIM (radio frequency imaging method)	15 kHz – 20 MHz	Antenna (inductive, capacitive)	Electromagnetic field strength	Normalized electromagnetic attenuation, normalized phase difference
GPR (ground penetrating radar)	20 MHz – 1 GHz pulse	Antenna (capacitive)	Electric field strength	Conductivity, dielectric constant, propagation speed

Table A 4. Soil Profile from the study area (BFW, 2007)

Profile number	Land use	Sea level	Relief	Inclination	Water conditions	Parent material	Soil type	-				
218031	pasture land	540 m	slope vale (depression)	15°	moderately wet	siliceous flysch, mostly weathered sandstone	rock brown earth	-				
Soil profile	Sequence of horizons	Extent of horizons	Soil moisture	Soil type	Coarse fraction	Porosity	Humus form	Humus %	Depth (cm)	Sand %	Silt %	Clay %
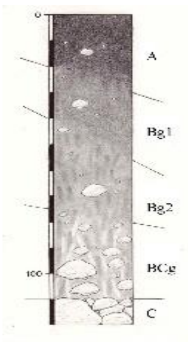	A	0-20cm	moderately moist	clayey sand	low coarse fraction (grus, 1 cm)	medium porosity	mull	rich in humus	10	44	44	12
	AB	20-45cm	moderately moist	clayey sand/sandy clay	low coarse fraction (grus, 1 – 2 cm)	medium porosity	mull	medium humus content	30	40	45	15
	Bg	45-85cm	moderately moist	Sandy clay	moderate coarse fraction (much grus, few rocks,1 – 4 cm)	medium porosity	mull	little humus	65	42	36	22
	C	85-100cm			predominantly coarse material (grus, rocks)							

Table A 5. Soil profile from the study area (BFW, 2007)

Profile number	Land use	Sea level	Relief	Inclination	Water conditions	Parent material	Soil type	-				
218028	pasture land	690 m	plane (planatation surface)	0°	moderately wet	siliceous flysch, mostly weathered sandstone	gleyey, lime-free rock brown earth	-				
Soil profile	Sequence of horizons	Extent of horizons (cm)	Soil moisture	Soil type	Coarse fraction	Porosity	Humus form	Humus %	Depth (cm)	Sand %	Silt %	Clay %
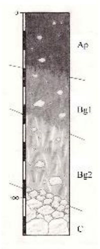	A	0 – 25	moderately moist	clayey sand	Low coarse fraction (grus, 1 – 2 cm)	medium porosity	mull	rich in humos	10	48	41	11
	ABg	25 – 45	moderately moist	sandy clay	Low coarse fraction (much grus, few rocks 1 – 4 cm)	medium porosity	mull	little humos	35	42	42	16
	Bg	45 – 90	moderately moist	clay	Moderate coarse fraction (much grus, few rocks,1 – 7 cm)	high porosity	mull	little humos	70	38	34	28
	C	90 – 100	-	-	Predominantly coarse material (grus, rocks)	-	-	-	-	-	-	-

Table A 6. Soil profile from the study area (BFW, 2007)

Profile number	Land use	Sea level	Relief	Inclination	Water conditions	Parent material	Soil type	-				
218052	pasture land	815 m	hill (hillside)	15°	moderately dry	fine and coarse siliceous alluvial material	lime-free unconsolidated sedimentary brown earth	-				
Soil profile	Sequence of horizons	Extent of horizons (cm)	Soil moisture	Soil type	Coarse fraction	Porosity	Humus form	Humus %	Depth (cm)	Sand %	Silt %	Clay %
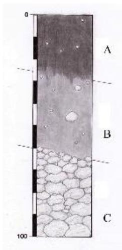	A	0 – 25	dry	clayey sand	small coarse fraction (much grus, little gravel, 1 – 2 cm)	medium proosity	mull	rich in humus	10	45	43	12
	B	25 – 60	moderately moist	sandy clay	moderate coarse fraction (much grus, little gravel, few rocks, 1 – 4 cm)	medium porosity	mull	little humus	45	42	42	16
	C	60 – 100	-	-	high coarse fraction (many rocks, little grus)	-	-	-	-	-	-	-

Appendix B. Additional Results

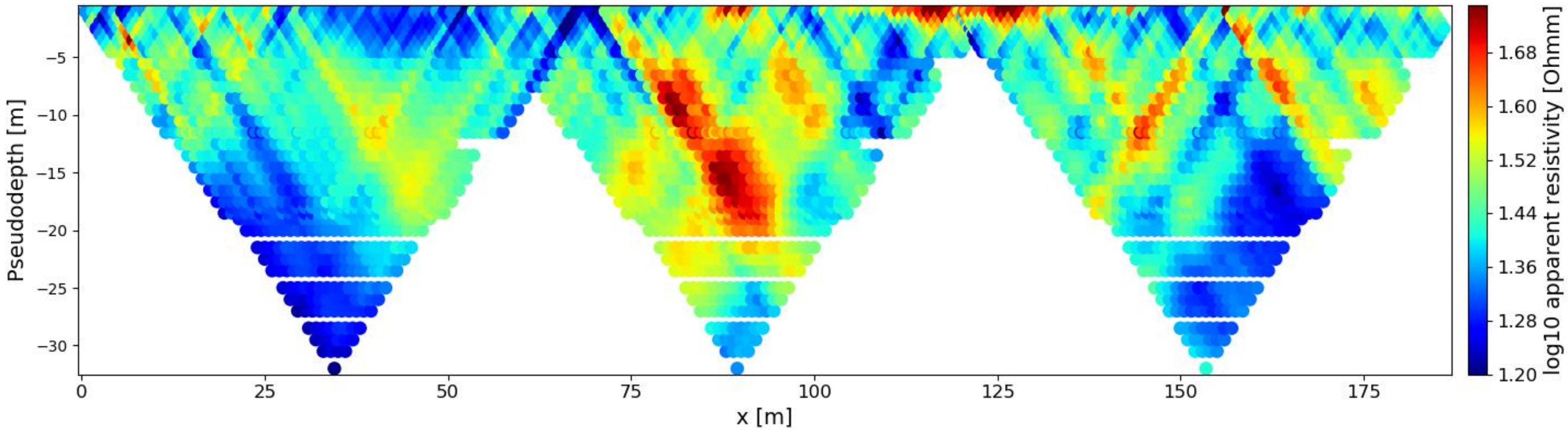

Figure B 1. Pseudosection of the resistivity for ERT profile 1

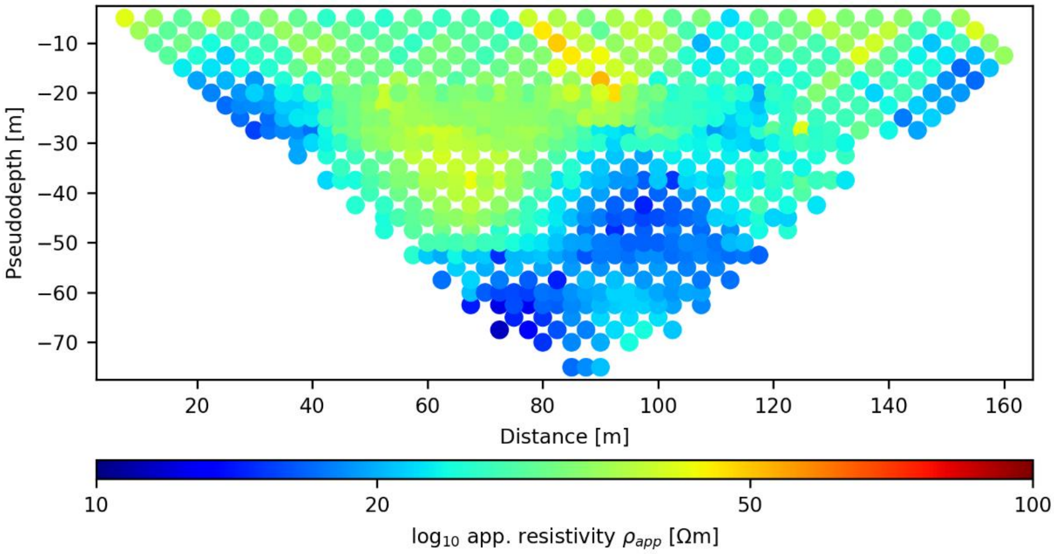

Figure B 2. Pseudosection of the resistivity for ERT profile 2

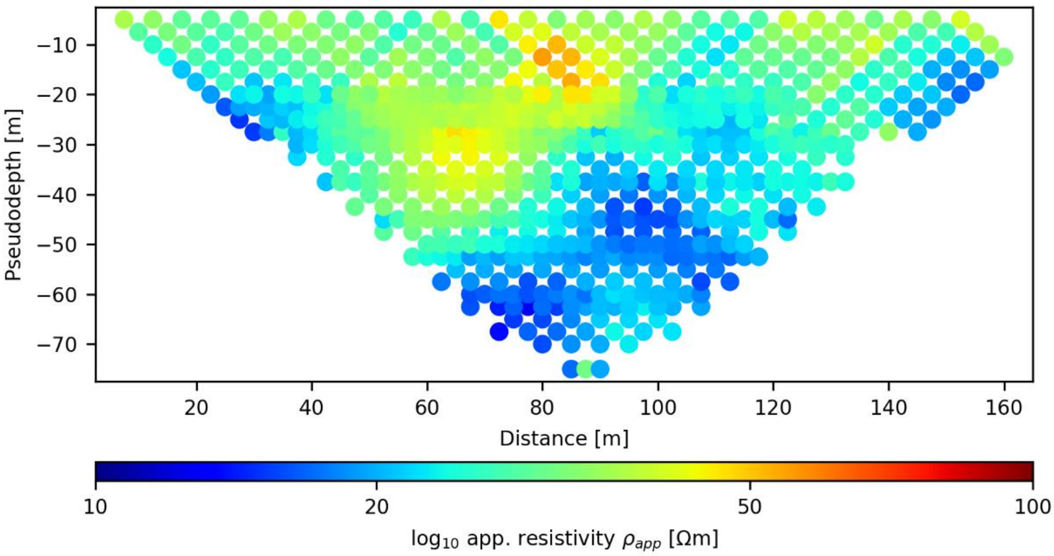

Figure B 3. Pseudosection of the resistivity for ERT profile 3

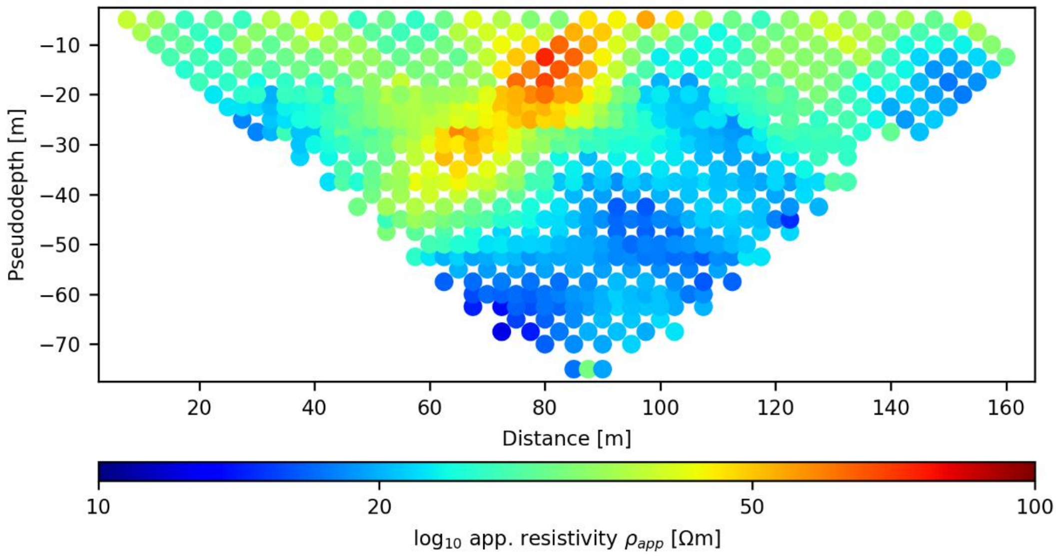

Figure B 4. Pseudosection for the resistivity for ERT profile 4

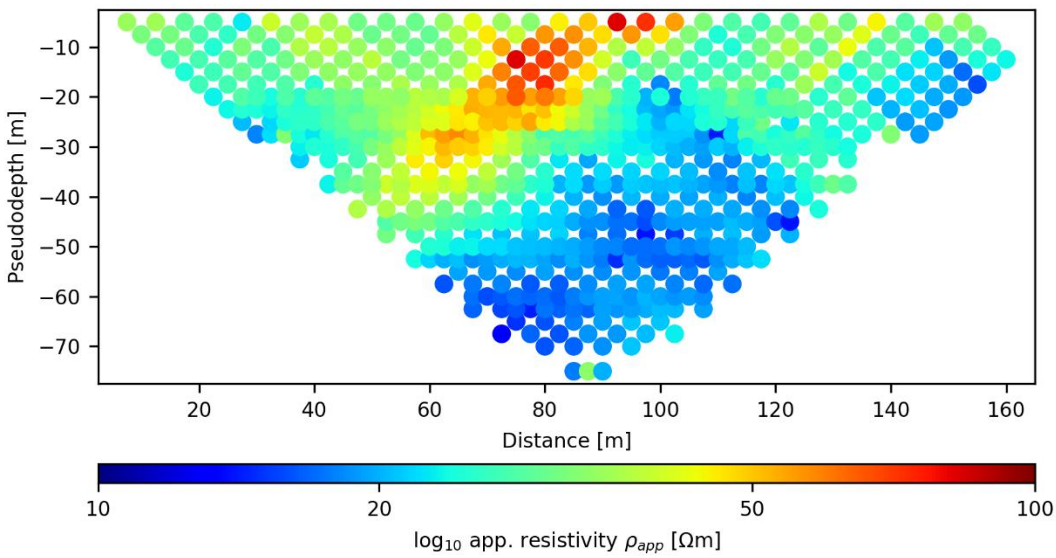

Figure B 5. Pseudosection for the resistivity for ERT profile 5

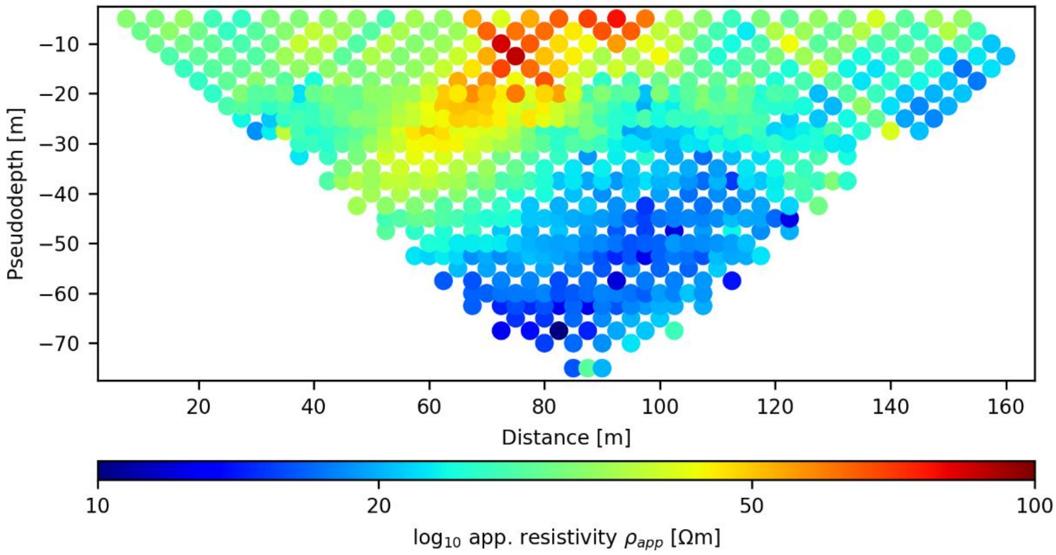

Figure B 6. Pseudosection for the resistivity for ERT profile 6

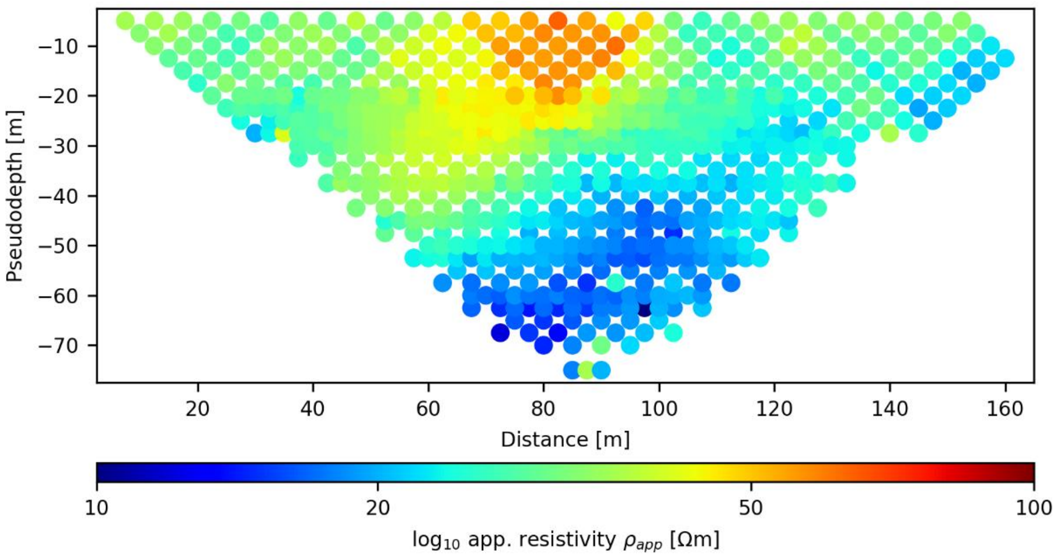

Figure B 7. Pseudosection for the resistivity for ERT profile 7

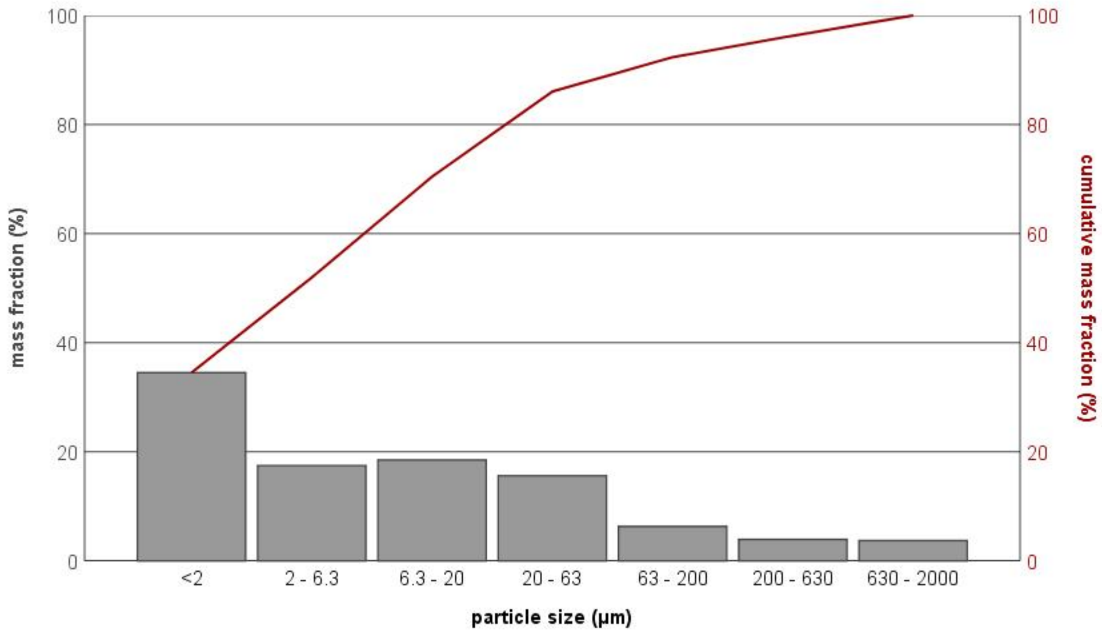

Figure B 8. Particle size distribution for PS 1

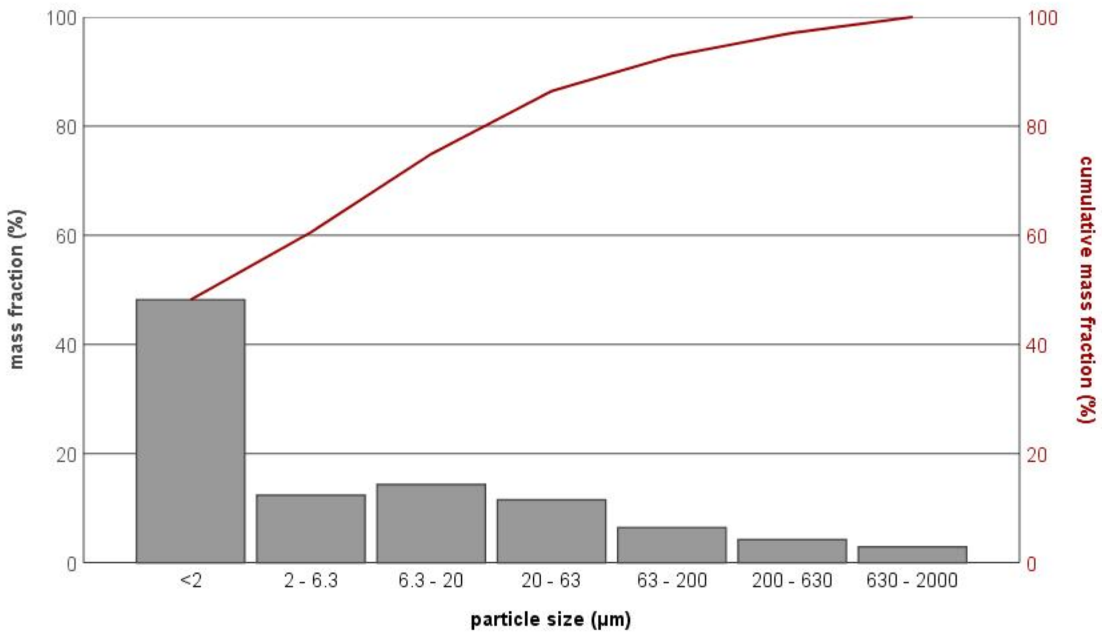

Figure B 9. Particle size distribution for PS 2

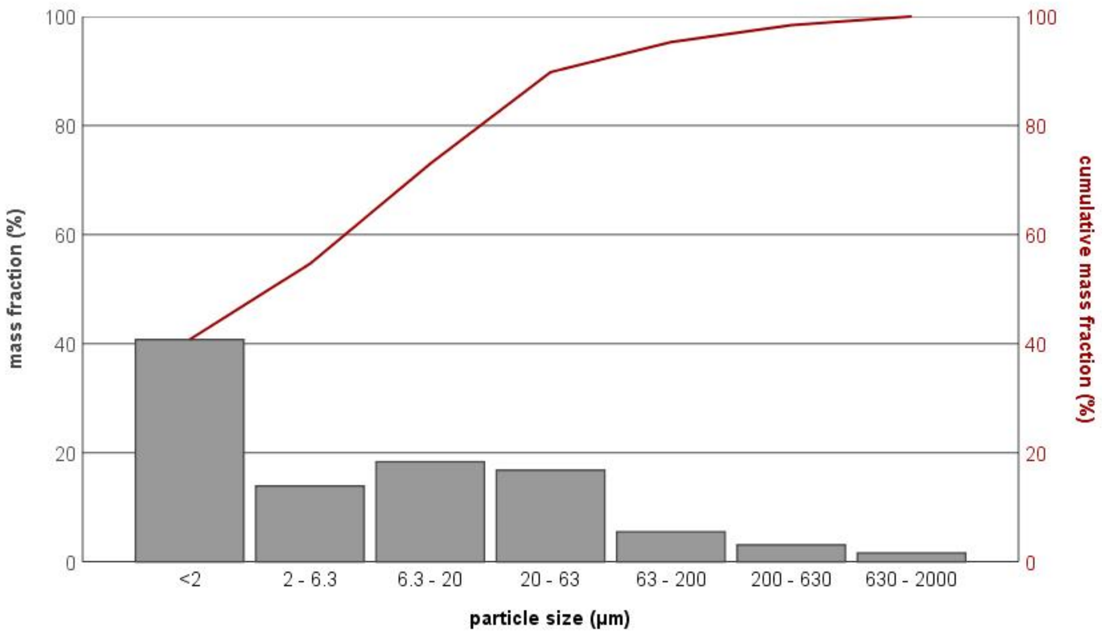

Figure B 10. Particle size distribution for PS 4

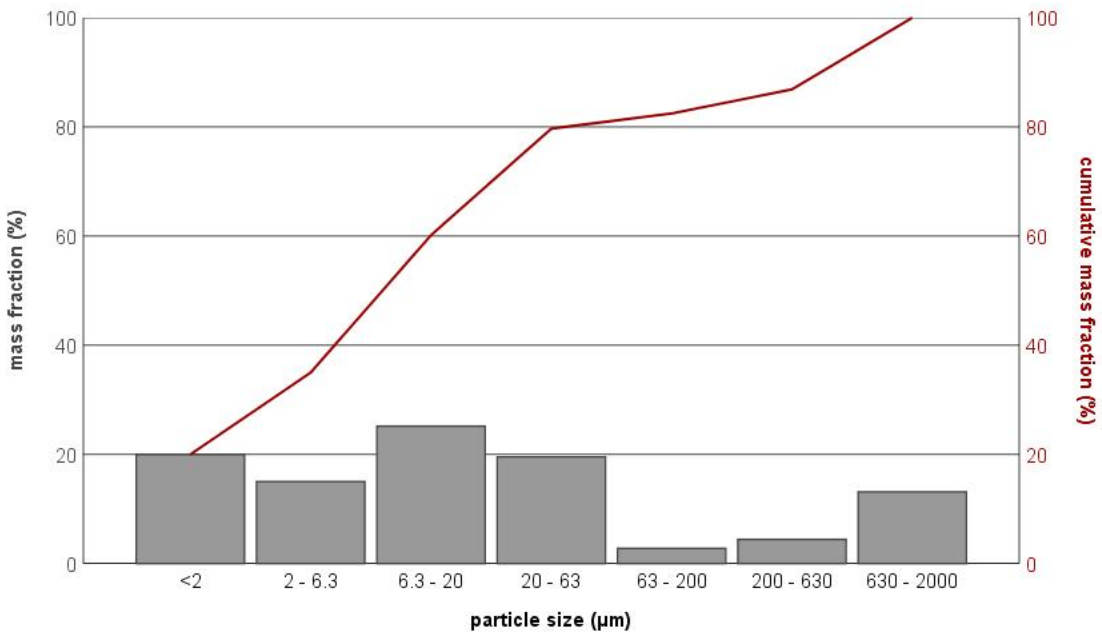

Figure B 11. Particle size distribution for PS 5

Figure B 12. Transition zone from A- to B-horizon between a depth of 40 cm to 60 cm; signs of mottling between 60 cm and 90 cm of depth

Figure B 13. Larger rocks between 90 cm and 100 cm of depth

Figure B 14. Textural transition at around 190 cm of depth.

Figure B 15. Brittle rocks at 285 cm to 300 cm of depth.

Figure B 16. Compact, dark grey material with lenses of lighter grey and coarser material between a depth of 375 cm and 400 cm.

Sample number	< 2 (%)	6 - 2 (%)	20 - 6 (%)	63 - 20 (%)	63 µm (%)	> 200 µm (%)	> 630 µm (%)	Sum %
PS 1	34,50	17,46	18,49	15,60	6,30	3,93	3,72	100,00
PS 2	48,19	12,37	14,34	11,52	6,44	4,23	2,92	100,00
PS 3	48,07	12,17	14,26	12,90	4,47	2,91	5,20	100,00
PS 4	40,75	13,90	18,35	16,80	5,50	3,10	1,60	100,00
PS 5	19,98	15,01	25,17	19,54	2,76	4,42	13,13	100,00
PS 6	14,91	15,31	22,51	14,17	2,49	5,90	24,72	100,00
PS 7	15,83	21,15	20,30	29,65	2,44	2,76	7,86	100,00
S 8	39,58	24,81	14,33	15,85	1,41	1,09	2,93	100,00

Table B 1. Particle size distribution of fine soil section (excluding gravel)

Sample number	< 2 (g)	6 - 2 (g)	20 - 6 (g)	63 - 20 (g)	63 µm (g)	> 200 µm (g)	> 630 µm (g)	>2 mm (g)
PS 1	3,34	1,69	1,79	1,51	0,61	0,38	0,36	0,32
PS 2	4,79	1,23	1,43	1,14	0,64	0,42	0,29	0,06
PS 3	4,62	1,17	1,37	1,24	0,43	0,28	0,50	0,39
PS 4	4,08	1,39	1,84	1,68	0,55	0,31	0,16	0
PS 5	1,81	1,36	2,28	1,77	0,25	0,40	1,19	0,94
PS 6	1,31	1,35	1,98	1,25	0,22	0,52	2,18	1,18
PS 7	1,49	1,99	1,91	2,79	0,23	0,26	0,74	0,59
S 8	3,65	2,28	1,32	1,46	0,13	0,10	0,27	0,79

Table B 2. Partcle size distribution

Table B 3. Data for calculation of the water content.

Sample Nr.	Depth (cm)	Mass moist (g)	Mass dry (g)	Water content (g)	Water content (%)
1	48 – 52.5	51.4	40.58	10.82	21
2	65 – 70	64.5	50.05	14.45	22
3	89.5 – 93.5	54.82	41.96	12.86	23
4	158.5 – 162.5	50.05	37.60	12.45	25
5	178.5 – 182.5	57.07	44.35	12.72	22
6	248.5 – 253	65.83	57.46	8.37	13
7	266.5 – 271	84.09	74.06	10.03	12
8	279.5 – 284.5	76.2	67.90	8.30	11
9	351 – 356	79.86	71.07	8.79	11
10	371 – 376	74.05	67.00	7.05	10
11	381 – 385.5	62.4	54.40	8.00	13

Table B 4. Measurement data fluid conductivity.

Sample Nr.	Depth (cm)	Fluid conductivity (µS/cm)	Temperature of the solution (°C)
1	43.5 – 47	23.5	22.3
2	85 – 88	29.5	22.3
3	155.5 – 158.5	30.1	22.4
4	174.5 – 178	30.7	22.5
5	253 – 255.5	70.3	22.5
6	277 – 280	91.6	22.6
7	348 – 351	184.3	22.7
8	378.5 – 382	102.6	22.7

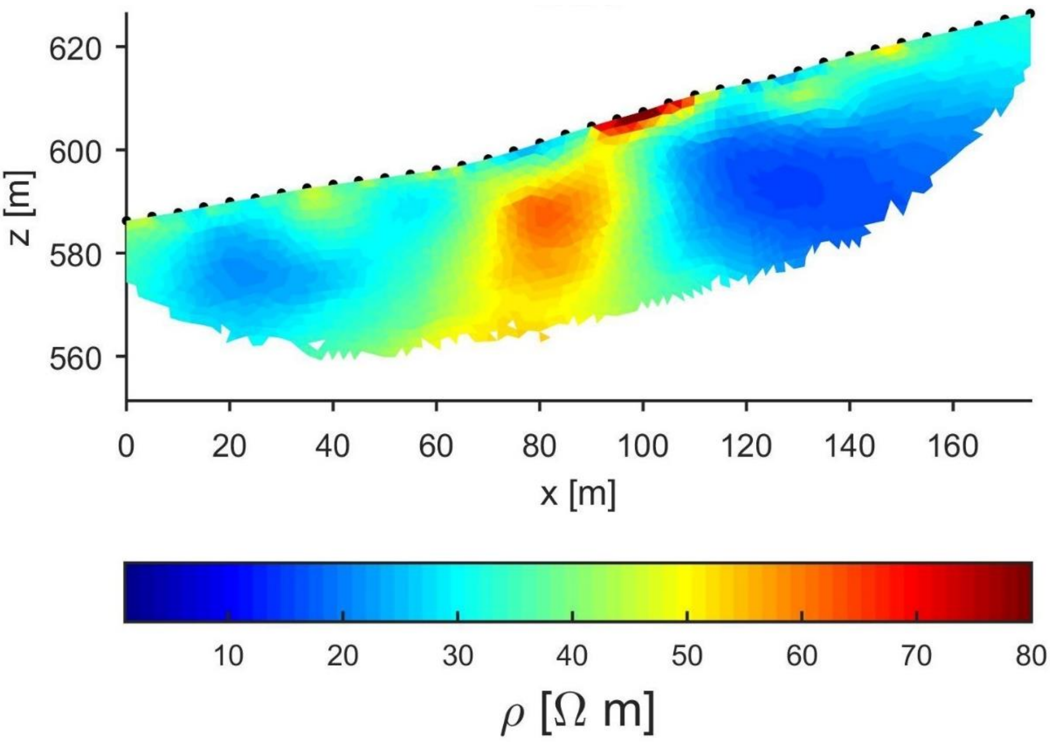

Figure B 17. ERT profile 4 (5-m electrode spacing)

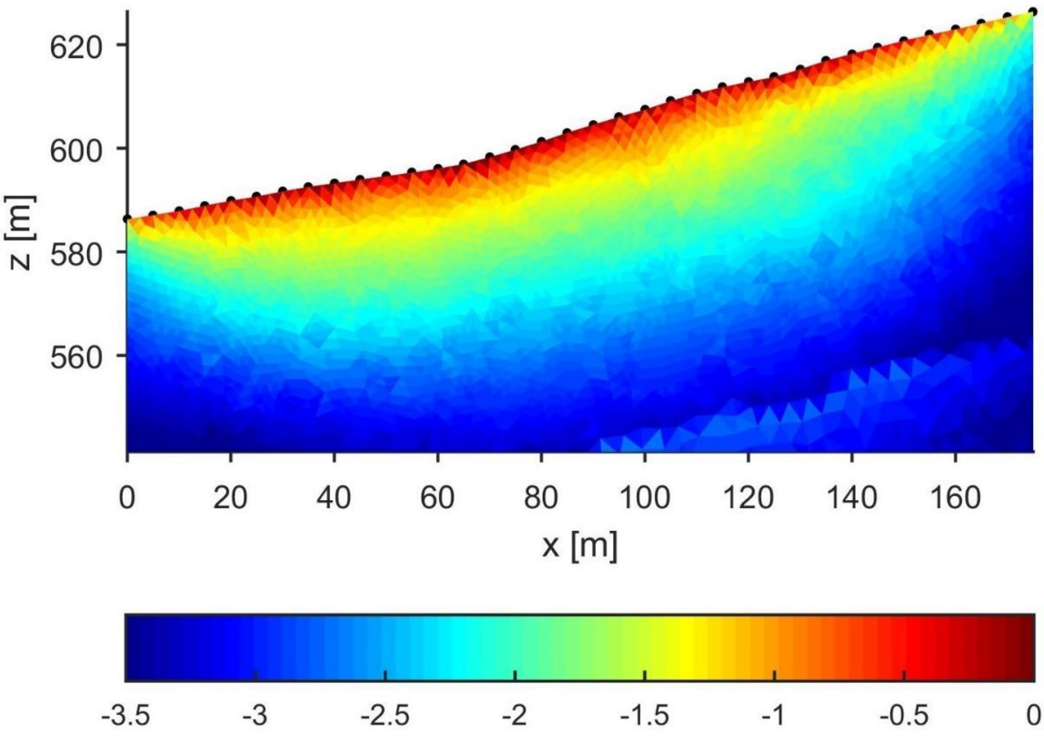

Figure B 18. Sensitivity for ERT profile 4 (5-m electrode spacing)

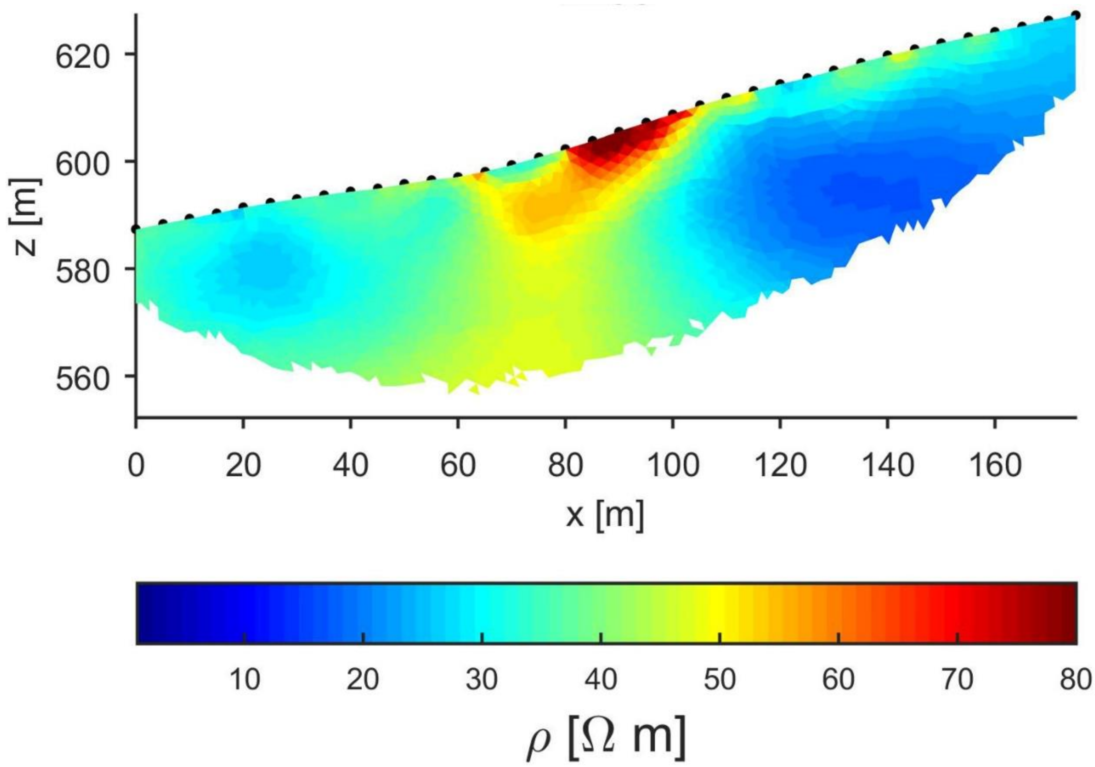

Figure B 19. ERT profile 6 (5-m electrode spacing)

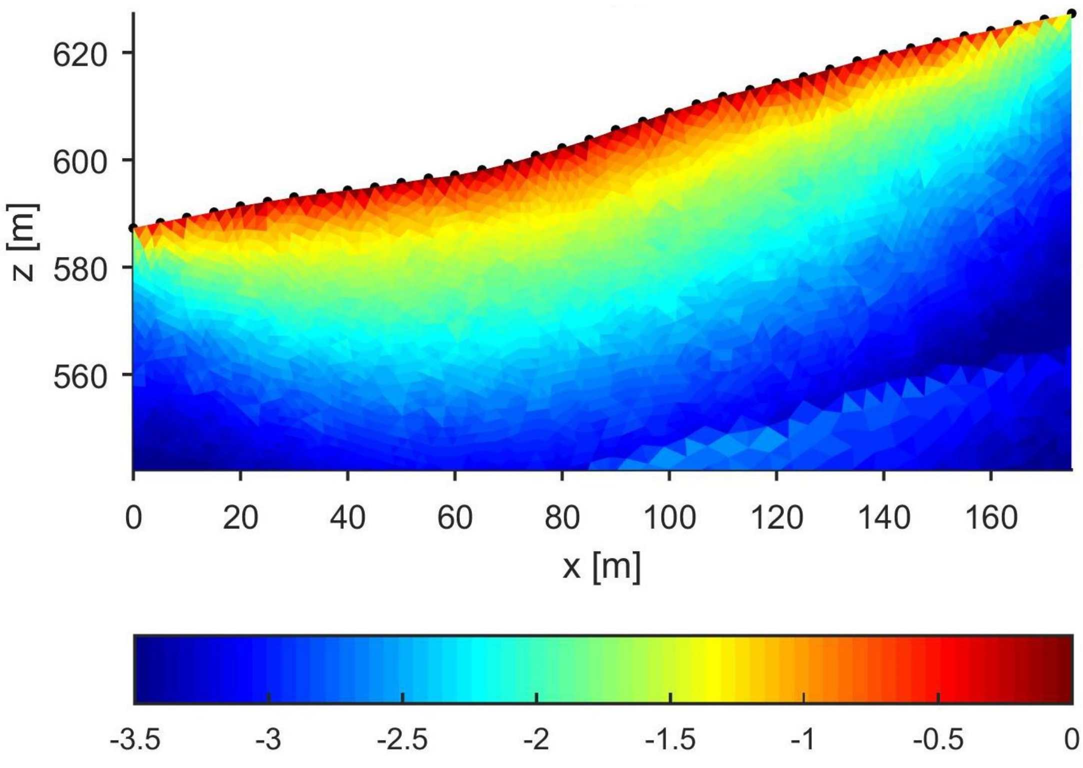

Figure B 20. Sensitivity for ERT profile 6 (5-m electrode spacing)

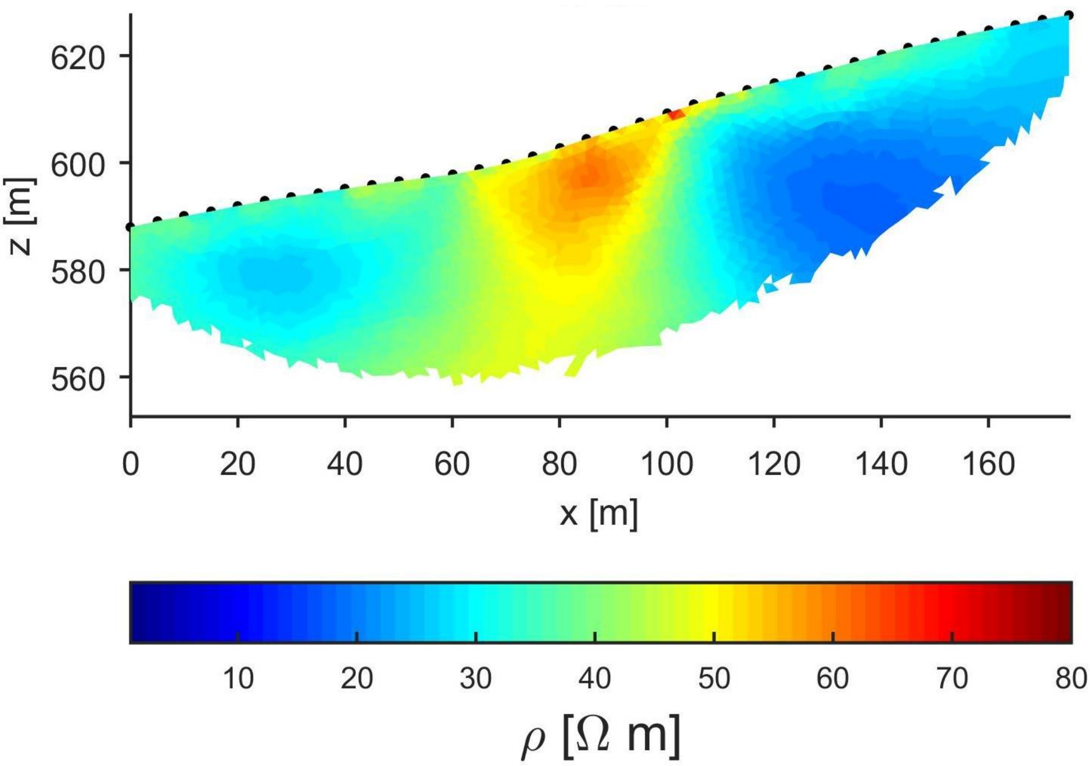

Figure B 21. ERT profile 7 (5-m electrode spacing)

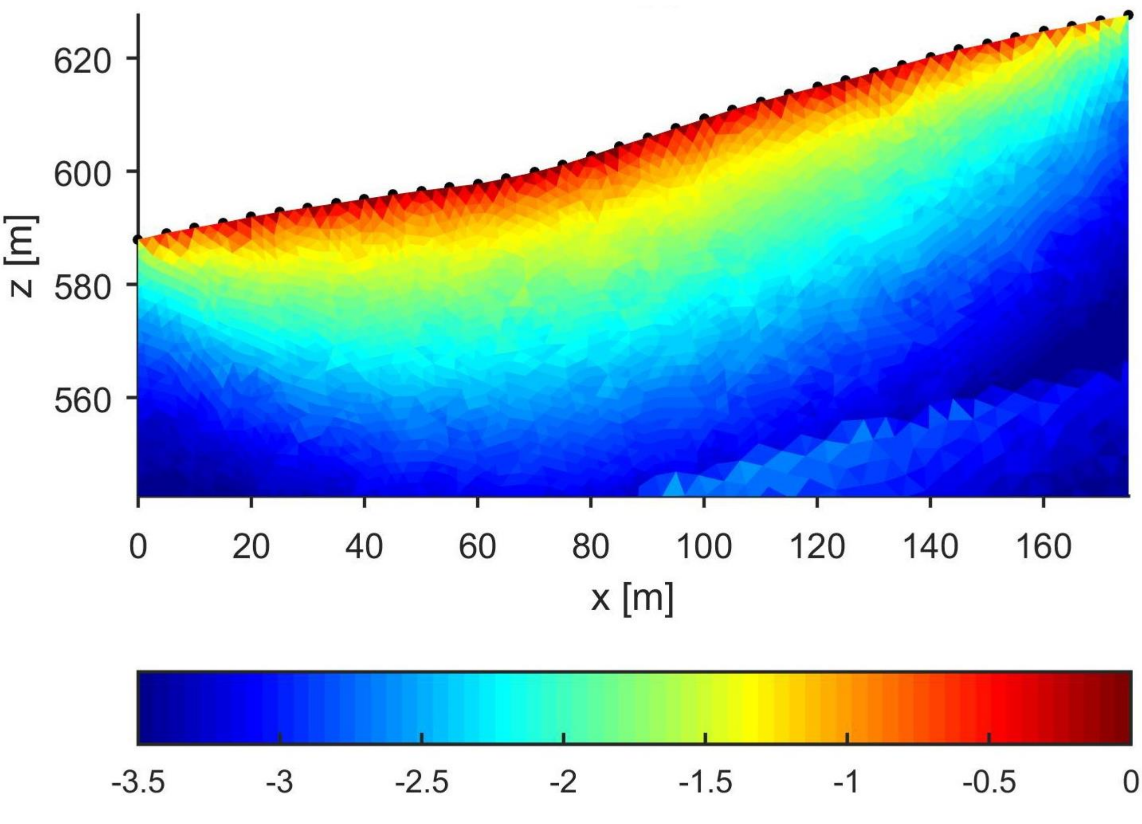

Figure B 22. Sensitivity for ERT profile 7 (5 m electrode spacing)